ROBUST COORDINATED DAMPING CONTROL OF POWER SYSTEMS WITH MULTI-TERMINAL VSC-HVDC SYSTEM AND FACTS

by

CAN LI

A thesis submitted to
The University of Birmingham
for the degree of
DOCTOR OF PHILOSOPHY

Department of Electronic,
Electrical and Systems Engineering
The University of Birmingham
June 2017

To my husband and parents

ACKNOWLEDGEMENTS

Firstly, my utmost gratitude goes towards my supervisor Professor Xiao-Ping Zhang for his dedicated and continuous support of my PhD research. With his immense knowledge and great motivation, he guided and encouraged me through my academic research and the writing of this thesis. It has been my utmost privilege and pleasure to work and study under his motivation and supervision.

My sincere thanks also goes to Dr. Dechao Kong, Dr. Xuan Yang, Dr. Suyang Zhou, Dr. Puyu Wang, Dr. Na Deng, Dr. Jianing Li, Dr. Jing Li, Dr. Zhi Wu and Dr. Ying Xue, in the Electrical Power and Control Systems group for their kind support and assistance to my PhD research.

I would also like to express my greatest appreciation to my family for their love and devotion to all my pursuits. They always have belief in me and encourage me to follow my dreams. The unconditional support and care from my family made me who I am and no words can express how grateful and blessed I feel with them as my dearest family.

Finally, I would like to thank my dear husband, Dr. Jingchao Deng, who has been my constant source of joy and inspiration throughout the years. Thank you so much for being by my side and embarking on the journey of our lives.

ABSTRACT

Power transmission systems are operating gradually closer to its limits with demand growth and aging infrastructures. Thermal, voltage, and stability limits are the often the reasons behind the constraints of transmission lines. As the advancing innovative technologies facilitate the progress of fast-responsive and highly-controllable FACTS (Flexible AC Transmission System) devices and VSC-MTDC (Voltage Sourced Converter Multi-terminal DC) systems, alternative resolutions of transmission network reinforcements are actively sought. Together with their constructive implementations, exploiting the supplementary damping control functionalities of VSC-MTDC and FACTS to enhance system small-signal stability can be beneficial to the strained ac/dc interconnected power network.

This thesis investigates the robust and coordinated design of multiple damping controllers to ameliorate the damping characteristics of a bulky power system. A new methodology is proposed in this thesis for VSC-MTDC and FACTS damping controllers based on multiple control objectives and system multi-model. The key feature of the methodology is the robust and coordinated performance of the damping controllers. The formulated BMI (Bi-linear Matrix Inequalities)-based optimization problem is solved systematically via a two-step approach. System multi-model is established in the design for the robustness of the controllers under system disturbances and changing operating conditions. The sequential design of a series of SISO (Single-Input-Signal-Output) controllers with properly selected feedback signals minimizes the negative interactions among the controllers. The approach is applied to a three-terminal VSC-MTDC embedded in a 5-area 16-machine and 68-bus power system and subsequently exerted with one terminal of VSC-MTDC and a TCSC (Thyristor Controlled Series Capacitor) to incorporate multiple devices and examine the generality and feasibility of

the design. Given the flexible internal control configuration of VSC converter, the assessment of the impact of the d-q decoupled control modes on the effectiveness and flexibility of the damping controllers is carried out. Real-Time Digital Simulator is used to examine the effectiveness and robustness of the damping controllers under various system operating conditions and disturbances.

TABLE OF CONTENTS

LIST OF FIGURES

LIST OF TABLES

LIST OF ABBREVIATIONS

AC	Alternating Current
AVR	Automatic Voltage Regulator
BMI	Bilinear Matrix Inequality
DC	Direct Current
FACTS	Flexible AC Transmission System
GB	Great Britain
HVAC	High Voltage Alternating Current
HVDC	High Voltage Direct Current
IGBT	Insulated Gate Bipolar Transistor
LCC	Line-Commutated Converters
LMI	Linear Matrix Inequality
LTI	Linear Time Invariant
MIMO	Multiple-Input and Multiple-Output
MISO	Multiple-Input and Single-Output
MMC	Modular Multilevel Converter
MTDC	Multi-Terminal Direct Current
PLL	Phase Lock Loop
PMU	Phasor Measurement Unit
PSS	Power System Stabilizer
RTDS	Real-Time Digital Simulator
SISO	Single-Input and Single-Output
SMIB	Single Machine Infinite Bus

SSSC	Static Synchronous Series Compensator
STATCOM	Static Synchronous Compensator
SVC	Static VAR Compensator
TCR	Thyristor Controlled Reactor
TCSC	Thyristor Controlled Series Compensator
TPSC	Thyristor Protected Series Compensator
TSC	Thyristor Switched Capacitor
TSR	Thyristor Switched Reactor
UPFC	Unified Power Flow Controller
VSC	Voltage Source Converter
WAMS	Wide-Area Measurement System

CHAPTER 1 INTRODUCTION

1.1 Background

Advanced electronic and electrical technologies and their intelligent controls are pivotal to smart grid implementation in many countries. Over the years, as the power system become more stressed due to increased demand for electricity, availing innovations such as semiconductor development capacitate powerful thyristors and IGBTs to be manufactured and employed in FACTS devices and HVDC, which can remarkably tackle challenging technical problems in power systems [1]. For instance, utilization of HVDC system for power transmission through long distance proves to be more favourable as it reduces power loss compared to ac transmission and is capable of connecting two separate ac grids with different operating frequencies [2]. Besides, HVDC technology can also improve system stability and increase transmission capacity with full exertion of the current electrical transmission system [3-5].

The coordinated power flow control of wide area network requires preeminent monitoring, communication, control and protection techniques [6]. A smart power transmission and distribution system with self-adaption and self-restoration capability is made possible by the advancement of power quality regulation technology [7-9]. Energy conversion technique facilitates the wide application of new energy power generation and especially wind power integration [10-12]. Meanwhile power consumers are given more choices with micro grid and

energy storage techniques [13, 14], thus creating a completely intelligent power system network embedded with high efficiency, self-cleaning and healing capability [15].

1.1.1 Power Network Interconnections and Reinforcement

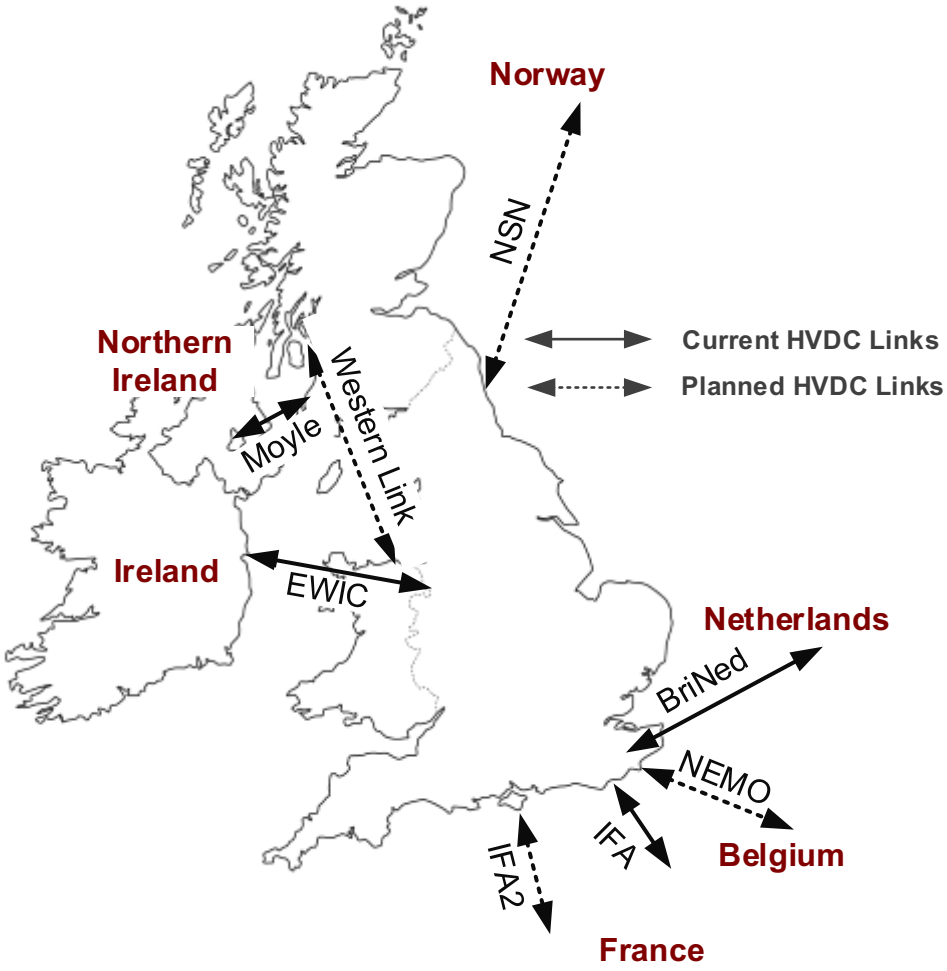

Figure 1.1 Current and planned HVDC links in the UK

Growing demand of electricity around the globe is one of the driving forces of development for electrical transmission infrastructure and a strong and stable power network. Interconnection with other countries' transmission systems by HVDC links can increase the diversity of energy sources and at the same time ensure safer operation of the power system.

By embedding HVDC systems into current ac grid as infrastructural support, the flexibly control the power exchange and busbar voltage of each ac system is achieved. In the GB system shown in Figure 1.1 reproduced from relevant materials, multiple existing interconnectors with France, Netherlands, Ireland and Northern Ireland effectively facilitate competition in the European energy market and allow integration of renewable energy generation, leading to the realization of low carbon energy sector. With the goal of achieving 10% EU interconnector capacity by the UK government, more interconnectors with VSC-HVDC and LCC-HVDC technology are being planned and some under construction [4], both shown in Table 1.1 [16]. The expected installation HVDC capacity by 2030 is 30-40 GW and the economic benefits brought by the doubled interconnection level are tremendous for the GB market and consumers [17, 18]. Such scale of network development for more interconnections needs more efficient power transmission with low costs, therefore the advantages of HVDC become more conspicuous in a practical application. The voltage threshold of the HVDC links is influenced by several aspects: the voltage threshold of semiconductors, semiconductor topology, and transmission line types. A higher voltage threshold and the ease of forming series connected topology for a semiconductor would increase the overall voltage limit of the HVDC system. Another limitation is the voltage threshold of dc cables. Dc cables with high voltage endurance would facilitate the application of HVDC links with high voltage threshold.

Table 1.1 Current and planned HVDC links

Interconnector	***Type***	***Length (km)***	***Voltage (kV)***	***Power (MW)***
IFA	LCC	70	270	2000
Moyle	LCC	63.5	250	500
BritNed	LCC	260	450	1000
EWIC	VSC	200	200	500

Western Link	LCC	414	600	2000
NEMO	VSC	130	400	1000
IFA2	VSC	230	400	1000
NSN	VSC	730	525	1400

1.1.2 VSC-HVDC Transmission System

VSC-HVDC was first introduced in the 1990s with the applications of self-commutated voltage sourced converter instead of line commutated current source converter [19]. Its enhanced flexibility and controllability have drawn great interest from academia and industry, because of its advanced capabilities such as independent control of active and reactive power. The VSC-HVDC is also free of commutation failure as found in LCC-HVDC. As the new generation of dc transmission technology, VSC-HVDC has emphasized three predominant features: full-controllable power electronics, voltage sourced converter and pulse width modulation. Therefore, it can cope with many perennial problems of the LCC-HVDC by realizing independent control of active and reactive power, competence to support passive ac networks and minimizing cost of infrastructure and space requirement [20].

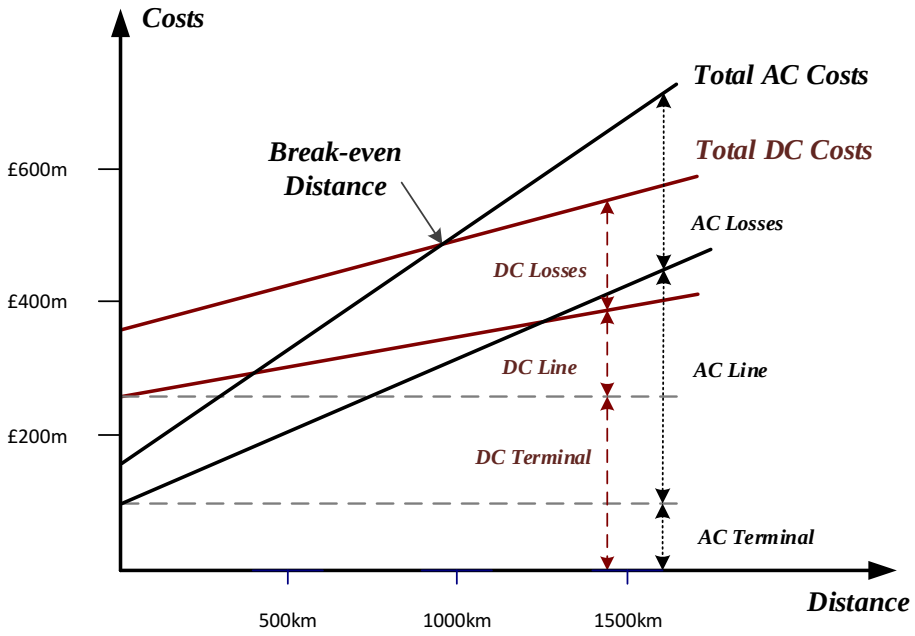

Figure 1.2 General cost-distance relationship of HVDC and HVAC system

A general cost-distance comparison with HVDC and HVAC systems is shown in Figure 1.2, which could vary depending on the type of HVDC employed, voltage ratings, environmental conditions and whether offshore platform for wind farm integration is needed [21-23]. In HVDC system, the supplementary ac/dc converter stations contribute to the higher cost of HVDC terminals and also introduce power losses within the converter station. However, the losses in HVDC cables are significantly lower than HVAC cables, as the reactance in a HVAC cable could increase the losses with alternating current.

Most of the installed commercial HVDC schemes are LCC-HVDC, including the IFA cross-channel connection with France, Moyle interconnector with Northern Ireland and BritNed interconnector with Netherlands. LCC-HVDC is thyristors based and can only maintain normal operation with successful commutation depending on the stability of ac grid environment. Additionally, the lack of reactive power control and black start ability are some of the disadvantages of LCC-HVDC schemes.

In comparison, the IGBTs in VSC-HVDC technology can be switched on and off by the instruction of an external signal, making it liberated from the zero-crossing point of the current. Both the active and reactive power can be controlled without the need of reactive power compensation in LCC-HVDC. Furthermore, the elimination of commutation failure empowers VSC-HVDC to be operated with enhanced security and reliability [24-26]. Based on the prominent advantages of VSC-HVDC, it can be applied in numerous scenarios such as wind farm integration, power transmission to an isolated island, asynchronous ac grid interconnection and multi-terminal dc power transmission. Nevertheless, the fast switching operations in reverse elevates the level of losses in converter stations, making it less economical especially with colossal power transmission. Besides, VSC-HVDC is a comparatively new technology and hasn't been applied as broadly as LCC-HVDC, so another drawback is the insufficient amount of experience in practical operation. In the foreseeable future, as electrical and electronic technology advances and cost performance of high-power full-controllable electronic devices meliorates, VSC-HVDC, with its exceptional benefits, would be the trend for dc power transmission progression.

Point to point VSC-HVDC

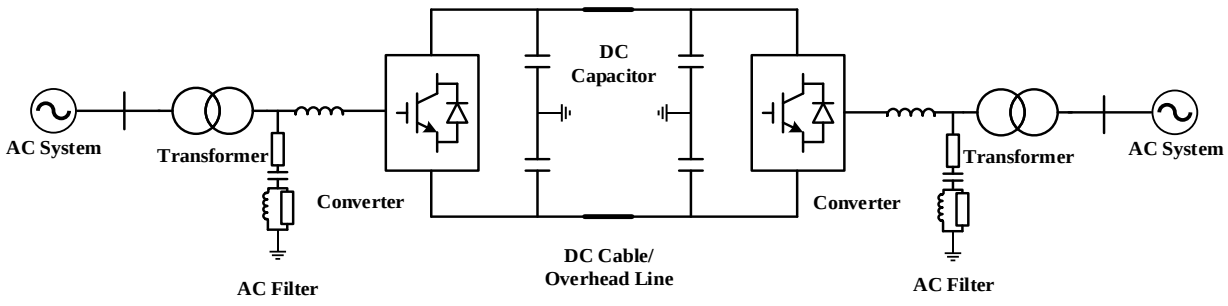

Figure 1.3 Diagram of point to point VSC-HVDC

A point to point HVDC system in Figure 1.3 can be seen as a synthetic system of two

independent STATCOMs connected by DC line. HVDC system has the capability of exchanging reactive power like STATCOM and transmitting active power because of the interconnection of VSC on the DC side. For two-level and three-level voltage topology, the amplitude and phase of reference modulation signal can be adjusted by pulse width modulation M and phase shift δ, thus modulating the amplitude and phase of the fundamental component of ac output voltage of VSC.

With PWM control technique, active and reactive power injection to the ac system through HVDC system can be both controlled [27]. From the system point of view, it mimics a generator without rotational inertia which can instantaneously adjust its output voltage and frequency. In addition, active power in the dc network must equilibrate to maintain normal operation of HVDC system. One end shall control the dc side voltage and act as active power balance inverter; the other ends shall set active power within nominal rated capacity [28].

Multi-Terminal VSC-HVDC

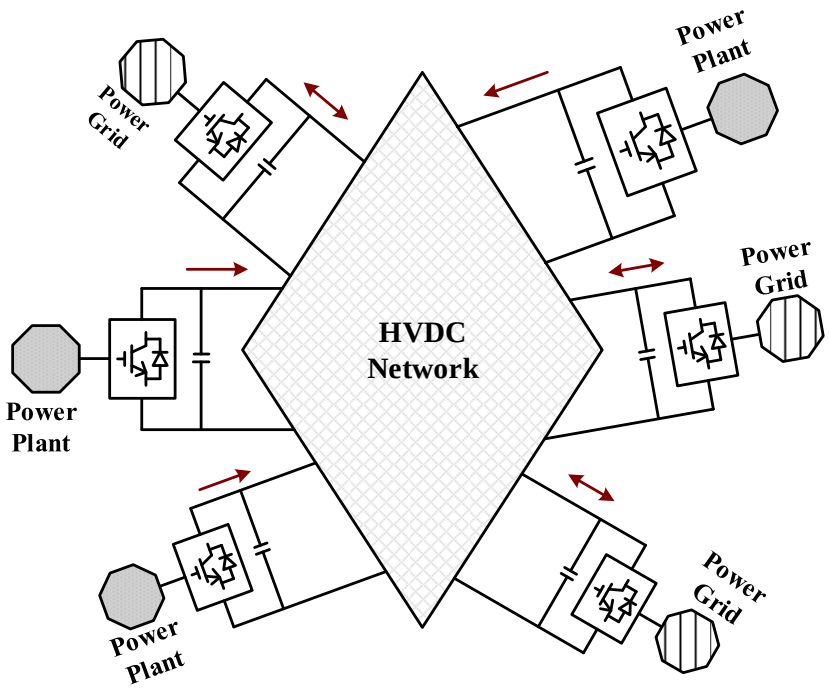

Figure 1.4 General diagram of multi-terminal VSC-HVDC

Multi-terminal VSC-HVDC comprises three or more converter stations connected by radial or meshed dc network, and can achieve interconnection between multiple power generation plants and loads [29], shown in Figure 1.4. The first VSC-MTDC project was accomplished in China to integrating multiple wind farms to the main grid [30, 31]. Table 1.2 shows the constructed voltage source based multi-terminal HVDC grids around the globe [29, 32]. The successful operation of these projects proves the feasibility and superiority of HVDC in technical and engineering aspects.

Compared to one or multiple point to point VSC-HVDC connections, multi-terminal VSC-HVDC grid can significantly reduce the number of converter stations as each station can independently input and output power depending on the system operating conditions without

Table 1.2 Current multi-terminal VSC-HVDC in the world

Multi-Terminal VSC-HVDC	*Country*	*Year*	*Number of Terminals*	*Voltage(kV)*	*Power(MW)*
Nan'ao	China	2014	4	±160	200
Zhoushan	China	2014	5	±200	1000
Super Station	US	2015	3	±345	750
South-West	Sweden-Norway	2016	3	±300	1400

influencing other stations. The interconnected topology in Figure 1.5 offers redundancy to the network so that when one line is out of service, other branches can mitigate the impact and ensure transmission reliability [29].

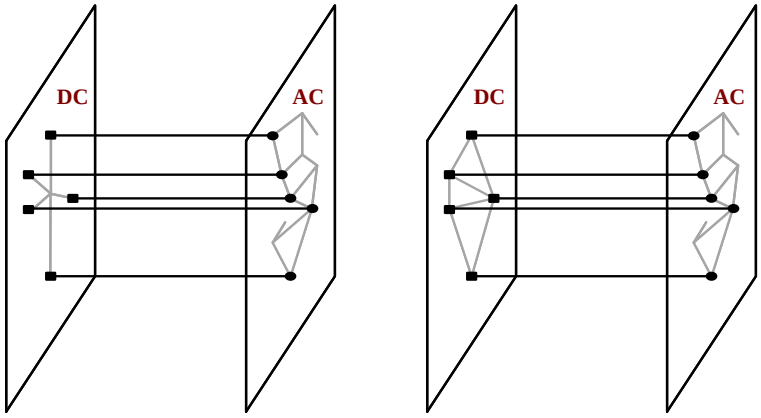

Figure 1.5 Radial (L) and Meshed (R) network topology of multi-terminal topology

1.1.3 FACTS Implementation in the Current Power System

In recent years, the power grid has become more interconnected to meet the need for low-cost energy and electricity demand. Historically, the generation sites are often located in remote locations away from the load centre and power is transferred through a long distance. Problematic issues arise such as non-optimized power flow control and resulted huge losses in transmission network. With the increasing amount of renewable energy connecting to the system, the power network faces more challenges: the increasing number of embedded solar

panels in households has led to the uncertainty of demand forecast and the installation of offshore wind farms introduces difficulty of ac/dc network integration. Under these circumstances, the emerging FACTS devices have facilitated the advancement of power systems and offered a worthy solution to the challenges in the ac grid. Without significant infrastructure reconfiguration or construction of new transmission lines, FACTS devices can be installed in strategic locations to support network stability. FACTS technology incorporates the latest development of electrical and electronic techniques such as the application of IGBTs into high voltage power transmission system and direct control of power system is realized by altering system parameters such as voltage, transmission line reactance and network topology [33-35]. It replaces conventional electromagnetic, electronic, or mechanical control mechanisms and is capable of enhancing controllability of active and reactive power and cutting down losses in ac transmission system. By setting a desired reference to the control logic and tracking the changes of system input, the error is consequently processed to set out the appropriate instructions for the device to react in situations such as system disturbance. Intelligent control of the internal electronic components to adapt rapid change of system operating conditions is what makes FACTS devices effectively and efficiently extending the operating limits of the network.

Optimizing operating conditions of transmission system

FACTS devices can establish a transmission channel and boost the unidirectional transmission capacity.. In addition, the fast and smooth control of FACTS technology facilitates proper and swift alteration of network power flow distribution. Relying on the protection circuit installed for FACTS, the impact on system operation and vulnerable appliances by short circuit and equipment malfunction can be abated [36].

Improving safety margin and transmission capacity

The B6 boundary is the significant transmission corridor between Scotland and England, shown in Figure 1.6, for power exchange of surplus wind generation at times of high renewable sources output and meeting the demand in Scotland at times of low renewable sources output.

From the Electricity Ten Year Statement analysis, the boundary capability of B6 is limited to a loading capacity of 3.5GW to secure the event when a double circuit fault occurs on one of the transmission lines the power transfer through the boundary can still be maintained, as set out in the Security and Quality of Supply Standard [18, 37]. After the planned series compensation installed in 2016, the transmission capacity increases to 4.4GW, ensuring future increment of wind generation export can be transferred to load centres in England [18, 38-40].

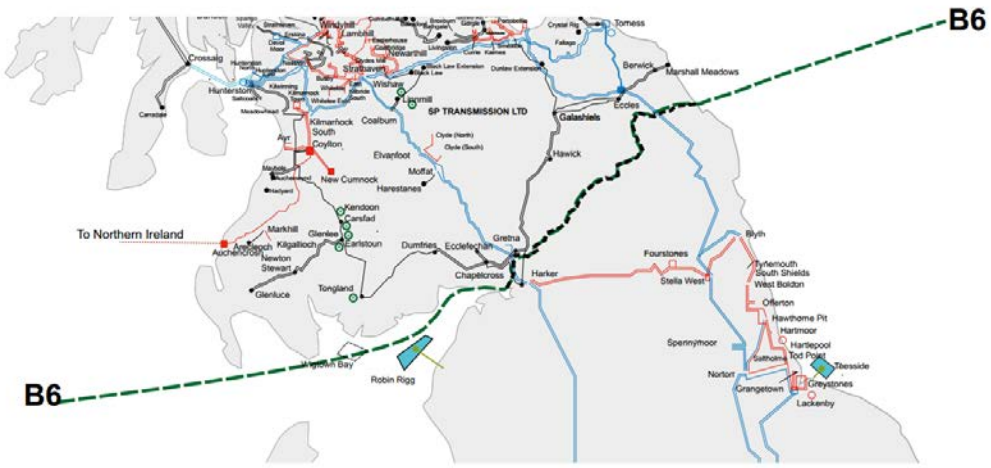

Figure 1.6 Geographic representation of boundary B6

Supplementary damping of low frequency oscillation

Low frequency oscillation often occurs when the power system is subject to a small disturbance and the oscillatory frequency varies with system capacity, network topology,

operating condition etc., usually within 0.2-2 Hz [41] [42]. Besides PSS, supplementary damping controller for FACTS devices can increase system damping ratio and inhibit low frequency oscillation in a bulk power system [43-46].

Based on the integration mode with ac grid, FACTS devices can be categorized into three clans [47]. Series connected devices can achieve real-time active power modulation, system transient stability enhancement and supress active power oscillation; shunt connected devices are more associated with tuning reactive power and in effect can sustain voltage stability and provide reactive power compensation, balancing active and reactive power on a system scale. Series-shunt devices, as its name suggests, combine the merits of both series and shunt connected devices, and UPFC is one of the advanced and powerful synthetic series-shunt connected FACTS devices. Series connected devices such as TCSC can act as a controllable capacitance in series with the transmission line, effectively reducing the overall reactance and increasing the maximum power transfer. Shunt connected devices like STATCOM can actively control its function of providing or absorbing reactive power when connected in shunt with a busbar. When the transmission line is lightly loaded, over-voltage often occurs at the end of the line. In this situation, STATCOM can absorb reactive power to decrease the voltage and maintain stability.

Another classification of FACTS devices is determined by the type of semiconductors, mainly thyristors or IGBTs. As mentioned in the section of LCC and VSC HVD comparison, thyristors are subject to controlled turn-on current and uncontrollable turn-off current. The antiparallel configuration of a couple of thyristors forms a switch to connect or short-circuit shunt or series component, which in effect composing a controlled reactor. By adjusting the firing angle, magnitude of the delayed current signal can reach minimum and maximum value.

Some of the thyristor valve based FACTS devices include TCSC and SVC. The other category of FACTS controllers utilizes ac/dc converters and VSC constitutes the basic component of these devices such as STATCOM.

1.1.4 Small-Signal Stability in the Interconnected Power System

System small-signal stability is defined as the capability to regain equilibrium after a small perturbation and the disturbance is considered to be small enough that the system can be linearized with different operating conditions for analysis [48]. Accompanying the complex interconnection of power grids, low frequency oscillation with frequency between 0.2-2.0Hz occurs more constantly and is often found in large-scale synchronously connected power networks, especially in the early stage of interconnection when interconnections between two systems are not reinforced. Local modes of the electromechanical oscillations are often more associated with a single generator station against the rest of the system and the range of the oscillatory frequency is 1-2 Hz; inter-area modes, as its name suggests, are more connected to oscillations happening between generator groups or different areas of a power system especially connected by weak ties with heavy power transfer, and the common frequency range is 0.1-1Hz [49].

In the past, there were some conspicuous incidents around the globe that triggered low frequency oscillation by disturbances and faults in the power system [42]. In some cases, the initial faults such as falling tree on the transmission line caused tripping of the line and later led to intertripping of the overloaded transmission lines and generators, transforming the structure and decreasing damping torque of the power network. Therefore, low frequency oscillations often occur in these scenarios and in turn the heavy loaded and weak links contribute to the uncontrollability of such oscillation. Besides, it’s worth to mention that

major discrepancies of power system analysis before and after the incident were identified, showing negative damping of the power system even before the fault. The possible reasons behind this phenomenon include lack of thorough understanding of the power system, inaccurate modelling of components with great contribution to system damping characteristics and system behaviour under different operating conditions. To increase damping of low frequency oscillation, various approaches regarding different aspects of the power system prove to be effective.

System topology transformation and improvement

On system topology level, strengthening systematic structure and reducing the number of over-loaded lines can expand the safety margin of operation and improve system performance in a post-fault scenario. Moreover, it is common practice to install series compensation to decrease the electrical distance of the sending and receiving ends of the line and increase the transmission capacity [39]. In the long-distance transmission lines, voltage support by reactive power compensation in the middle and at the end of the line is needed and the control system of these devices can ameliorate the system dynamic performance [50].

Operational modulation

Together with system infrastructural transformation, real-time operational adjustment bears equal importance when it comes to avoiding low frequency oscillation. Quick and accurate identification of the characteristics of the oscillation containing the information of frequency and power distribution and participation factors of generators is the foremost action that should be taken by system operators. After the oscillation pattern analysis, instructions such as re-dispatching generator and load shifting can effectively balance the system and help

regain synchronism. In extreme conditions load shedding is the last resort to avert more serious mishap like large scale blackout or system separation.

Supplementary damping control design and implementation

In addition to the structural improvements and operational modulation, supplementary control design for devices such as PSS, FACTS and HVDC can mitigate the adverse effect of low frequency oscillation and enhance system small-signal stability [51]. The implementation of the fast-acting controllers provides fast and precise response to endure any system disturbances. Without the need for additional devices, supplementary damping controllers are easily installed and maintained. Moreover, relatively low required capital and a high ratio of return on investment make these controllers more desirable.

In this thesis, investigation is carried out to design supplementary damping controllers for VSC-HVDC and FACTS devices for the enhancement of system small-signal stability. The requirements of the damping controllers are specified as robust performance with coordinated control. The detailed literature review concerning different approaches for damping controllers with various kinds of devices is introduced in section 1.2..

1.2 Literature Review

In this section, coordinated damping control design for multi-terminal HVDC and FACTS has been an important approach for enhancement of system small signal stability. It is based on accurate modelling and advanced coordination of control methodologies that have been proposed by diversified research literatures.

1.2.1 Multi-terminal VSC-HVDC Application and Control

As the new-generation dc transmission technology, the VSC-based multi-terminal direct current has offered the solutions to large-scale wind farm integration [52], power transmission to isolated islands and demand need expansion in cities [53]. As renewable generations such as wind farm, solar panels and wave power are still in the relatively early stage of development, they're often located in remote and scattered locations with limited capacity and low power quality. Research on wind farm integration with two-terminal HVDC has been done in many literatures [10, 54, 55]. Yet this method is not profitable enough because a minimum power generation to sustain acceptable benefits is not guaranteed due to the nature of the energy source. Therefore, multi-terminal VSC-HVDC is the optimal candidate in such circumstance [56]. Voltage fluctuation and flickers can be effectively suppressed and thus power quality [57] and stability can be improved. Studies on the application of VSC-MTDC on wind farm integration showed that satisfactory system performance was validated in simulations regarding wind speed variation and generation output [58]. It has been reported in [59] that a hybrid MTDC system is used for grid interconnection of wind farm and the system post-fault behaviour has been promoted.

In addition, power supply to isolated island and drilling platforms can be realized by VSC-MTDC. As it's quite challenging to merge isolated islands power system that are far away from the mainland into the unified power grid, electricity on the island is relatively expensive and less reliable. And especially for oil drilling platforms, traditional power supply utilizes diesel generators which contaminate the environment and have low power quality. Acting as interconnectors between different systems, VSC-MTDC can be utilized to supply power to these islands without system stability problems and realize linkage of asynchronous ac

systems. Besides, HVDC can achieve fast current control and thus limit the short circuit capacity of interconnected systems. Meanwhile, compared with ac lines, dc lines have the advantages of low investment, less operational costs and no need for additional compensation equipment in long distance transmission. However, there are still many issues surrounding HVDC system such as DC circuit breaker and it's not developed as fully as ac systems. In [60], hybrid MTDC with LCC and VSC converters is used to connect the ac system and VSCs are the only source of the passive network. The system exhibited strength and resilience under different disturbances with AC voltage and frequency control. Reference [61] proposes a hybrid MTDC system that is verified by simulation in EMTDC/PSCAD to be effective of supporting a weak or passive ac system without reactive power compensation.

Power grid in megalopolis faces many challenges like heavy load, short circuit current over limitation, and strict environmental constraints. With the fast rate of urbanization and expansion horizontally, overhead lines for power transmission are gradually superseded by underground cables. Hence, the transformation of city power grids can be accomplished without disturbing city landscape or electromagnetic interference, at the same time meeting the demand of electricity and preserving the environment. Suggested in [60], a multi-terminal VSC-HVDC could replace traditional HVAC in urban demand centres. As the distributed energy sources are developed further in urban areas such as solar panels, the decrease of transmission demand may lead to stranded newly built transmission infrastructures.

1.2.2 Supplementary Damping Controllers for VSC-MTDC and FACTS

The increasing demand of load centres and integration of renewable energy to the main grid lead to the stretch of operating capability limits [62]. Ac system has already been reported to be very much strained by many investigations and practical operational data [5]. Along with

the opportunities brought by the development of novel electrical and electronic technologies, challenges arise in such circumstance, especially stability problems in large interconnected power systems. As one of the key issues imposed on the expanding power networks, small-signal stability should be addressed and properly improved in systems which lack of damping where low frequency oscillation can be observed and it's categorized into local modes and inter-area modes.

Traditionally PSS are designed and installed as the feedback control of the excitation systems for synchronous generators to elevate the damping torque and consequently improve the damping ratios of local oscillatory modes [63-66]. Some research has been carried out to ameliorate the poorly-damped inter-area modes with PSS designs [67-69], yet the damping effort of PSS is much limited to local modes and has restricted impact on the damping of inter-area modes due to the local operation and tuning complications of multiple PSSs. Therefore, PSS is primarily tuned for improvement of local oscillatory modes and often uses rotor speed deviation as its feedback signal.

Inter-area oscillation is often aroused by the loss of synchronism of synchronous machines in different areas [42]. Compared to the local modes, inter-area modes are better tackled with the modulation of bus voltage, active power and reactive power on properly selected busbars and transmission lines [70-72].In the light of the scenarios presented above, supplementary damping control for the enhancement of small-signal stability utilizing a wide range of fast-switching and controllable devices has been proven to be effective in many literatures [73-75].

Point-to-Point and Multi-Terminal VSC-HVDC Based Damping Control

The proliferating HVDC projects around the world cater to the need of low-loss and

economical way for long distance system interconnection and renewable energy integration. With its highly controllable flexibility, the supplementary control capability of VSC-HVDC for small-signal stability enhancement can also be exploited. Different control modes of the VSC converter stations allow us to modulate the reference input of the outer control loop dynamically with a supplementary damping signal provided by the feedback controller. For instance, in Figure 1.7, the d-axis outer control loop is modulating active power transferred through the converter with the pre-set reference value P_{ref} and with the supplementary signal P_{damp}, it can actively damp the inter-area oscillations in power systems.

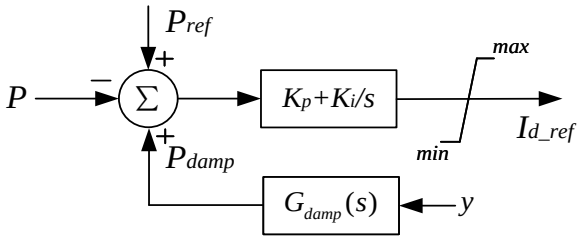

Figure 1.7 Active power control with supplementary damping signal

To conduct the damping control design using VSC-HVDC, accurate models of the synthetic ac and dc interconnected system should be established with the correct representation of system dynamic behaviours for small-signal stability analysis to guarantee valid results and the feasibility of the damping controllers to be implemented in the non-linear system. Multiple approaches to analyse the VSC-HVDC system interconnected with multi-machine ac systems have been reported in many investigations. Reference [76, 77] introduce a general modelling scheme which can be incorporated with ac systems and it is cross-compared with the detailed model in EMTDC/PSCAD. The analytical model of a five-terminal VSC-MTDC of two control modes is formulated in [28] and is verified with simulation in PSCAD which gives the comparison between the PID controller and predictive controller for inner control

loop. Reference [78] proposes the small signal stability study of VSC-MTDC based on the Cigré dc grid test system and some of the key challenges are addressed for the construction of a large-scale MTDC system. A test model for VSC-MTDC system with off-shore windfarm integration is presented in [79] and its validity is subsequently tested with time-domain simulations. Besides, the influence on stability of the system of control parameters in VSC converters is investigated by system dynamic performance in the event of small and large perturbation.

With the increasing number of VSC-HVDC projects constructed around the world, damping control based on the VSC technology has received greater interest and a variety of the control methodologies are proposed by many literatures [80-82], including decentralized controller design with homotopy approach [83, 84], model predictive control with WAMS signal [85, 86], modal linear quadratic Gaussian design [74], and linear optimal excitation control [87]. Reference [88] utilizes Lyapunov control theory to improve rotor angle stability in interconnected ac/dc systems. WAMS measurements provide the feedback signals for active power set points.

Reference [74] introduces multi-input-single-output (MISO) modal linear quadratic Gaussian (MLQG) damping controllers to damp system electromechanical oscillations by modulating the ΔP_{ref} of the active power transfer through the VSC-HVDC line. And the controller input signals are selected from wide area measurements by phasor measurement units. With the PMUs, accurate signal detection and transmission is required and could incur additional time-delays. Then in [89], the MLQG damping controllers are designed in two ways-centralized and decentralized, for two point-to-point VSC-HVDC systems embedded in a 5-area 16-machine system, and their performance is investigated and compared with probabilistic

robustness assessment. Probabilistic collocation method is proposed in [90] to tune the modal linear quadratic Gaussian controllers and improve the robustness of the controllers in a VSC-MTDC grid.

Pole placement controllers are designed for a back-to-back VSC-HVDC connected with a Single Machine Infinite Bus system in [91]. By placing the poles of the close-loop system into the desired region, the damping ratios of the corresponding modes are increased and thus the improvement of system response can be observed in MATLAB simulation. The consideration of regional pole placement as control objective alone could result in over-design and control effort optimization needs to be included as well.

In [92, 93], knowledge-based fuzzy logic control is applied to the two-area four-generator ac system with point-to-point VSC-HVDC in parallel with the ac transmission line. Without depending on the detailed system model, the fuzzy controller is based on the knowledge of rules in the form of if-then rules imitating the real-time control actions of human system operators of practical power systems. However, without knowing the detailed system model, system damping behaviours are hard to analyse and it's difficult to apply the method to more complicated power systems.

A nonlinear PWM control is proposed in [94] with pole placement technique to choose feedback gains and nonlinear model of the overall system is adopted for damping control design [95], where active and reactive power modulation is achieved by energy function control strategy approach.

Particle swam optimization of the parameter tuning of the damping controller and wide-area excitation system controller of one generator is introduced in [96] as the coordinated design to

improve power system damping. Optimal allocation of the control duty of VSC-HVDC is formed as an optimization problem to calculate the least overall control effort of a MIMO controller in [97]. The MIMO controller may face the challenges of ensuring reliable operation as the functionality of the controller could be compromised by one failing input signal. The effectiveness of real and reactive power modulation proposed in [98] is assessed in respect of the locations of renewable energy sources.

In the case of Multi-terminal VSC-HVDC damping control in a meshed ac/dc network, little research has been carried out compared to the point-to-point HVDC configuration. LMI-based H_{∞} approach framework was applied to asymmetric bipolar VSC in [99] for improving the damping performance of AC-MTDC grid. Reference [100] introduced the installation of traditional PSSs on onshore VSC stations and the simultaneous tuning of PSSs with evolutionary particle swarm optimization (EPSO) technique in MTDC system with wind farm integration could potentially provide additional damping to the inter-area electromechanical oscillations. A new decentralized control structure with dc voltage sharing for MTDC grids was presented in [101] so it maximized the controllability on each oscillatory mode and the active power modulation through the phase compensating POD controller enhanced system small-signal performance in the case of contingencies.

FACTS Damping Controller Design

FACTS devices have long been employed in the modern power systems for infrastructure reinforcement. Despite that the supplementary damping functions are often considered as secondary; the increasing number of applications have incorporated the small-signal enhancement as an essential feature in the initial design stage. Reference [102] carried out the planning and pre-specification study to increase the system transfer capacity and stability

limit in stressed areas. In this practical incident, SVC served two newly constructed transmission lines as a mutual benefit. The supplementary modulation controller of the SVC damped the inter-area oscillation in the test system. The application of a TCSC in the Brazilian North-South Interconnection was presented in [103]. The equipment and location specifications were formulated based on dynamic stability analysis and the damping function of the TCSC was tested prior to commissioning. Two types of POD controllers utilized the local line current flow as the controller input signal to modulate the reactance reference and various types of contingencies were conducted to test its effectiveness. The planned implementation of convertible static compensator in [50] was investigated for the optimal configuration with other FACTS devices for voltage, small-signal, and transient stability. Steady-state and dynamic models of the system was tested in pre- and post-fault scenarios and the weakly damped inter-area modes were addressed in the assessment process. A robust POD design for the TCSC mentioned in [103] was compared with its original approach to adapt to new challenges [104]. Reference [105] employed TCSC for transmission capacity increment and oscillatory stability enhancement in the transmission corridor between northern sea and Taiwan power grid, which was restricted by thermal limits on these transmission lines. In addition, a supplementary damping controller was designed for the TCSC to damp out the inter-area oscillations. Reference [106] presented residue approach for the identification of effective location and compensation levels for damping purposes and the input signals for the controllers were evaluated by simulations of fault scenarios.

1.2.3 Coordinated Robust Damping Control Design Approaches

As presented in the previous sections, the majority of the damping control designs are formulated upon a linearized model of power system around a specific operating point and the

mathematical model of a practical power system with constant disturbances and perennial changes of working conditions contains uncertainties. Therefore, it's required for the damping controllers to be able to function when the working environment diverge from the original state, as well as dealing with various forms of disturbances such as excitation system disturbance, line outage and generation and load variation. The robust control studies the uncertainties in the mathematical models caused by modal parameter perturbation or additive disturbances [107]. Other uncertainties such as the dynamics of the electrical components that is not modelled initially and noises from sensors could also impact the modal accuracy. Therefore, the objective of robust control theory is to maintain the expected performance even under the circumstances of uncertainties.

The H_∞ control theory proposed in the 1980s marks the rudiment of modern control theory [108]. The H_∞ norm describes the maximum gain induced by a input disturbance signal with finite energy to the output energy and H_∞ control is to minimize the peak value of the transfer function between the open-loop and close-loop response [109]. With the formulated state-space solutions [110], the H_∞ control technique was utilized for various robust damping controller designs. In [111], the a TCSC and a SVC damping controller were designed in a decentralized manner with proper selection of feedback signals from machine parameters and the system model considered multiple operating conditions, realizing the robust design approach. Riccati approach was utilized here to solve the control problem [112]. In [113], the UPFC damping controller was designed with LMI (Linear Matrix Inequality) H_∞ mixed-sensitivity approach. Unlike the Riccati approach, zero-pole cancellation was conquered with the LMI optimization technique and it had been easier to select the weights for mixed-sensitivity. Compared with root-locus approach, higher damping ratios could be achieved

given the same control effort. The advantageous LMI-optimization approach was soon applied to multiple devices in [114], where a CSC, SVC, and a CPS is investigated with different installation location in the reduced equivalent NYPS-NETS power system. The assessment of multiple feedback signals both local and global was presented in [115, 116].

Besides H_∞ approach, H_2norm [110] was also incorporated for the robust damping control design and in [75, 117], the coordinated damping control of FACTS devices and traditional HVDC system was realized by the mixed H_2/H_∞ approach. The H_∞based approach was also compatible with loop-shaping methodology [118]. For instance the robust design of a PSS was proposed in [119] and a robust damping control design was presented in [120] for TCSC with a H_∞ loop shaping approach based on LMI optimization technique. However, it's not guaranteed that the off-nominal operating conditions could still exhibit the robustness of the damping controllers.

With the ever-changing operating conditions of power systems, more research was done on the integration of multiple operating points, nominal and off-nominal. Particle swarm optimization technique [121] in reference [122] produced a low-order MISO controller with the controller objectives such as parametric optimization. In[123], similar concept was also proposed with sequential quadratic programming. Other damping control approaches with optimization techniques considering multiple operating points were also reported in [124-128]. Optimization oriented methodology has the advantage of simultaneously tuning PSS and other supplementary damping controllers, but the formulation is not as straightforward and requires more complicated design. The LMI-based approach is much more unequivocal comparing the optimization-based techniques. Reference [129] presented polytopic models to incorporate multi-model with LMI-based H_∞ approach. Other forms of the robust control

problem formulation were also reported in many literatures including parametric uncertainty[130], Kharitonov theorem [131] and polynomial based method [122, 132].

The WAM technology with PMUs offers new solutions to improve system stability [133, 134] with the expansion of feedback signal candidates. Without restricting the choice of local signals, remote signals with higher controllability and observability can be utilized in the damping control design. In [115, 116, 122, 135], MISO controller with wide-area signal for TCSC enhanced system small-signal stability and targeted inter-area oscillations. However, it's been difficult for a single device to cover all the under-damped oscillatory modes especially in a bulk power system with multiple inter-area mode that were subject for improvement. Therefore, the coordinated robust control of two or more devices had been investigated. The coordinated control approaches in [124-128] with decentralized structures were tested effective without adverse effects, but they still had the cross-coupling effect among the controllers. The sequential approach in [41] provided higher reliability and independence in improving the system's damping characteristics.

1.3 Contributions

This research presents the robust coordinated design methodology and its application on two types of devices: VSC-MTDC and FACTS. The objective of the research is the design of supplementary damping controllers for VSC-MTDC and FACTS in a coordinated way with robustness of enhancing system small signal stability under different system conditions as well as in respect to various system disturbances.

The detailed focuses and contributions are listed in the following sections.

1.3.1 Robust Coordinated Damping Design Methodology

With the linearized system model and identified weakly damped modes, the effective and efficient way of enhancing system small-signal stability remains to be sought. The primary design requirements are to ensure each damping controller can improve the weakly damped modes to a satisfactory level individually and in coordination with other controllers under various system operating conditions as well as diverse disturbances. The new methodology proposed in this thesis is the BMI-based multi-objective multi-model approach with sequential design. The main features of this approach include:

[1] Multiple control objectives can be simultaneously considered in the design stage: regional pole placement specifies the desired range of damping ratio to which the poorly damped poles should be moved; control effort optimization with H_2 norm can avoid over-design so that the actual ratings of the devices are conformed to.

[2] The structured system uncertainty is formulated with the incorporation of multiple operating conditions when the system model is linearized, which contributes to the robustness of the controllers. Unstructured uncertainties are also included to improve the resilience of the system when undergoing such scenarios.

[3] Mode shapes, participation factor and modal residue analysis are systematically carried out to select proper feedback signals for each controller and the optimal allocation of control effort.

[4] The sequential approach feature allows each damping controller to be designed as a SISO controller without coupling effect between feedback signals and increases the reliability of the overall design.

1.3.2 Power System Modelling with VSC-MTDC and FACTS

To establish a well-rounded and precise model of power system integration with VSC-MTDC and FACTS regarding its different control modes for accurate small-signal stability analysis is the foremost and crucial step for supplementary damping control design. And the integration of VSC-MTDC and FACTS devices to the test system makes the state-space representation much more complicated and it should be dealt with care. In this study, detailed modelling of electrical power components is carried out and lays the foundation for eigenvalue analysis of system damping behaviour. Besides, different control modes of VSC-MTDC are considered in system modelling stage for assessment of the impact of control modes on damping controller performance.

1.3.3 Robust Coordinated Damping Design of VSC-MTDC and FACTS

The application of the damping control methodology also extends to multiple devices that are often installed in a bulk power system for system capability and stability reinforcements. In this study, the coordinated design of damping controllers for VSC-MTDC system and FACTS devices is investigated. With the additional device, the controllability and observability of the weakly damped modes have been expanded and it offers more opportunities for the selection of feedback signals and these decentralized controllers can improve the reliability of the system. Similar design process as presented in the previous section is undertaken for VSC-MTDC system and FACTS device.

With the variations of control mode of the VSC converters, the impact of the control modes towards the selection of feedback signals and control effort allocation is reflected in each sequential control loop since the fundamental state-space representation of the whole system

diverges greatly. Comprehensive studies of the mode shapes and modal residues for the system models conclude the differences of the controllability and observability in each case. The methodology of synthesis BMI-based optimization considering regional pole placement and control effort optimization for a multi-model system is implemented with the different d-q decouple control mode and the damping control performance for different configurations of VSC-MTDC is assessed by both linear system performance and real-time simulations in RTDS.

1.4 Thesis Outline

This thesis is organised as follows:

Chapter 2 This chapter presents the modelling of the complete power system with VSC-MTDC and FACTS. Linearization of the system model is carried out in respect of different operating points, formulating multi-model system for robustness design.

Chapter 3 Methodology for robust coordinated design is explained in detail, including mixed-sensitivity multi-objective BMI-based control optimization formulation and solution, feedback signal selection, sequential design approach and the step by step explanation of the overall control design procedure.

Chapter 4 In this chapter, the methodology proposed in Chapter 3 is applied on a VSC-based multi-terminal HVDC embedded in a 5-area 16-machine system. Damping controllers are designed for each terminal of the VSC-MTDC and their effectiveness is verified through linear system performance and real-time simulations in RTDS.

Chapter 5 Supplementary damping controllers for VSC-MTDC and TCSC in a 5-area 16-

machine system are designed sequentially for enhancement of system small-signal stability.

Chapter 6 Based on different control modes of VSC-MTDC, assessment of the design and performance of supplementary damping controller is carried out.

Chapter 7 A summary of the conclusions drawn from the results and studies in the previous chapters is presented along with possible future work on this research topic.

CHAPTER 2 SMALL-SIGNAL MODELLING OF POWER SYSTEM WITH VSC-MTDC AND FACTS

2.1 Introduction

In small signal stability study and control design, the modelling of power system apparatus such as generators, excitation systems of generators, governors, PSSs, FACTS devices, and HVDC systems is essential to understand their performance and impact on system stability characteristics and vital for the design of supplementary damping controllers for VSC-HVDC and FACTS devices. In the system modelling process, dynamic behaviour will be represented by a series of non-linear differential algebraic equations (DAE) which will be linearized around different operating points to obtain a linearized model of the system for future robust control design.

In this chapter, the models of individual power system component with different configurations and internal control methods are introduced with state-space matrices and a combined multi-model system including all the components is shown. Synchronous generator is represented by subtransient level differential equations and its excitation system is modelled with detailed dynamics. The 3rd order power system stabilizer is introduced with corresponding parameters. In addition, this Chapter focuses on the modelling of VSC-HVDC

and its integration to the ac network. The dynamics of TCSC is illustrated with direct reactance control for future coordinated design of multiple devices.

2.2 Power System Modelling

In this section, the dynamics of generator and its excitations system, stator algebraic equations and network power flow equations are presented in state-space matrix formulation. The final differential algebraic equations are consistently derived.

2.2.1 Generators

In a multi-machine system, proper scaling of machine data and variables is accomplished by selecting general power base and voltage bases according to nominal transformer ratings. Necessary simplifications of generator dynamics for system stability studies including neglecting stator transients and the effect of speed deviations. In this study, synchronous generator model in the order of six is adopted with dynamics down to subtransient level [48].

The linearized 6th-order generator differential equation is represented by

$$\Delta \dot{x} = A_1 \Delta x + B_1 \Delta I + B_2 \Delta V + E_1 \Delta u \tag{2.1}$$

$$\Delta x = \begin{bmatrix} \Delta\delta \\ \Delta\omega \\ \Delta E'_q \\ \Delta E'_d \\ \Delta\varphi_{1d} \\ \Delta\varphi_{2q} \end{bmatrix}, \Delta I = \begin{bmatrix} \Delta I_d \\ \Delta I_q \end{bmatrix}, \Delta V = \begin{bmatrix} \Delta\theta \\ \Delta V \end{bmatrix}, \Delta u = \begin{bmatrix} \Delta T_M \\ \Delta V_{ref} \end{bmatrix} \tag{2.2}$$

ω rotor speed

δ rotor angle

E'_d, E'_q induced transient electromagnetic force

$\varphi_{1d}, \varphi_{2q}$ subtransient induced electromagnetic force

I_d, I_q stator current

T_M mechanical torque input

Stator algebraic equations are expressed as:

$$0 = C_1 \Delta x + D_1 \Delta I_g + D_2 \Delta V_g \tag{2.3}$$

2.2.2 Excitation System

The excitation system adopted in this thesis is the static AC excitation system and its dynamic is shown in equation (2.4).

$$\Delta E_{fd} = -\frac{1}{T_A} \Delta E_{fd} + \frac{K_A}{T_A} (\Delta V_{ref} + \Delta V_{pss} - \Delta V_t) \tag{2.4}$$

where

V_{ref} voltage reference

T_A time constant

K_A transient gain

V_{pss} Output from PSS

2.2.3 Power System Stabilizer

The PSS shown in Figure 2.1 indicates the installation location and transfer function. The common structure of PSS usually comprises a gain, a high-pass wash-out filter, and phase compensation filter.

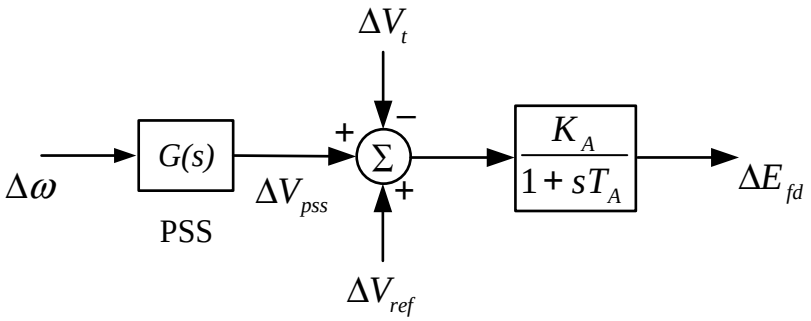

Figure 2.1 Exciter with PSS

The lead-lag transfer function of PSS is expressed as:

$$G(s) = K_p \frac{T_{WO}}{1+sT_{WO}} \frac{1+sT_1}{1+sT_2} \frac{1+sT_3}{1+sT_4} \tag{2.5}$$

where

K_p stabilizer gain

T_{WO} time constant of the wash out block

T_{1-4} time constant of phase compensation block

2.2.4 Power Flow Model

The system power flow model can be categorized into generator PV buses and non-generator PQ buses. Power balance models are utilized in this study in the following forms.

The network power flow equations for generator buses are expressed as:

$$V_i e^{j\theta_i}(I_{di} - jI_{qi})e^{-j(\delta_i - \frac{\pi}{2})} + P_{Li} + jQ_{Li} = V_i e^{j\theta_i}\sum_{k=1}^{n} V_k e^{-j\theta_k}(G_{ik} - jB_{ik})$$
$$\text{for } i = 1,...,m \tag{2.6}$$

The network power flow equations for non-generator buses are expressed as:

$$P_{Li} + jQ_{Li} = V_i e^{j\theta_i}\sum_{k=1}^{n} V_k e^{-j\theta_k}(G_{ik} - jB_{ik})$$
$$\text{for } i = m+1,...,n \tag{2.7}$$

where

m	number of generators
n	total number of buses
G_{ik}	conductance between bus i and k
B_{ik}	susceptance between bus i and k

2.3 VSC-HVDC Modelling

As a new emerging technology for power transmission with dc current, VSC-HVDC consists of converter stations and dc links. Figure 2.2 is a single line diagram of the basic topology of a multi-terminal VSC-HVDC, including three converter stations and three dc links. In VSC-HVDC, power flow is bi-directional and either converter station can act as both rectifier and inverter; the power sending end is in rectifier mode and the receiving end in inverter mode [136].

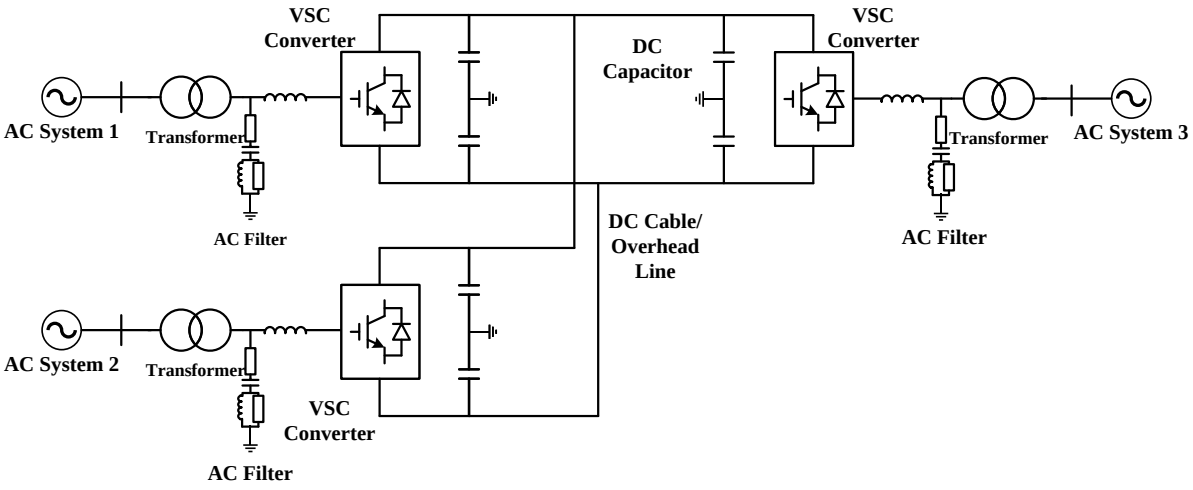

Figure 2.2 Detailed Topology of Multi-Termial VSC-HVDC

In a VSC-HVDC topology, the main apparatus includes ac filters, phase reactors, dc capacitors, dc cables or overhead lines and converters. In this thesis, three-phase two-level six-pulse converter is utilized to carry out the damping control study.

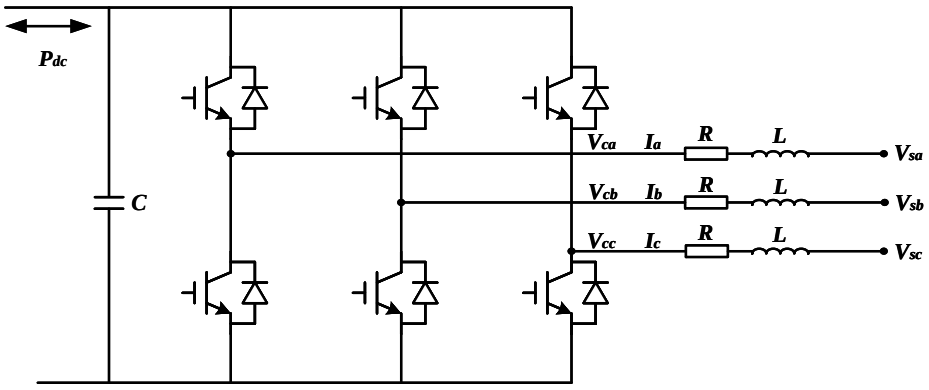

Figure 2.3 Internal Structure of one terminal of VSC-HVDC

Detailed structure of one terminal of VSC-HVDC is shown in Figure 2.3, where V_{ca}, V_{cb}, V_{cc} are the converter side voltage; V_{sa}, V_{sb}, V_{sc} are the voltage of the connecting ac system terminal; R and L represents resistance and inductance of the transformer; C is the dc capacitor and P_{dc} indicates power exchange from this terminal end to the dc network.

The three-phase differential equations for converter station can be expressed as (2.8)

$$\begin{aligned} L\frac{di_a}{dt} &= V_{sa} - V_{ca} - Ri_a \\ L\frac{di_b}{dt} &= V_{sb} - V_{cb} - Ri_b \\ L\frac{di_c}{dt} &= V_{sc} - V_{cc} - Ri_c \end{aligned} \tag{2.8}$$

Through park transformation from *abc* static three-phase coordinates to *dq* rotary two-phase coordinates, equation (2.8) is transformed into (2.9)

$$\begin{aligned} \frac{di_d}{dt} &= \frac{V_{sd} - V_{cd}}{L} - \frac{R}{L}i_d + \omega i_q \\ \frac{di_q}{dt} &= \frac{V_{sq} - V_{cq}}{L} - \frac{R}{L}i_d - \omega i_d \end{aligned} \tag{2.9}$$

where i_d, i_q are the *d, q* component of the current of the converter station; V_{cd}, V_{cq} are the *d, q* component of the converter side voltage; V_{sd}, V_{sq} are the *d, q* component of the ac system terminal voltage.

2.3.1 Internal Control Model

The control diagram for one terminal direct current VSC control is shown in Figure 2.4. The direct current control methods can be divided by inner control loop and outer control loop and the common outer control loop usually embraces dc voltage control, ac voltage control, active power control, reactive power control and frequency control. In the outer control loop, $A_{reference}$ indicates a controlled variable with active power characteristic, for instance, dc voltage and active power, meanwhile the variable controlled through $B_{reference}$ falls into reactive power category and ac voltage and reactive power are usually used as the input of q-

axis control. The inner current control realizes direct control of waveform and phase of converter ac side current, to fast track reference current. The other control component in Figure 2.4 is phase-locked loop, synchronizing converter control with line voltage.

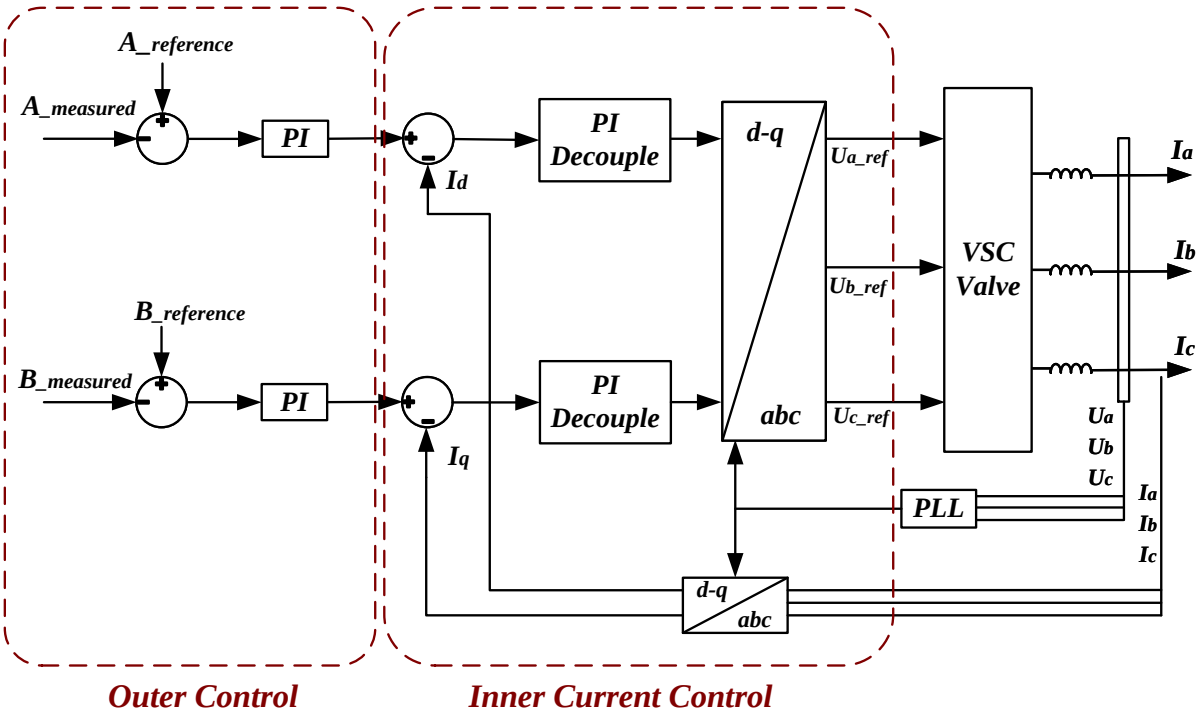

Figure 2.4 Direct current control of VSC converter station

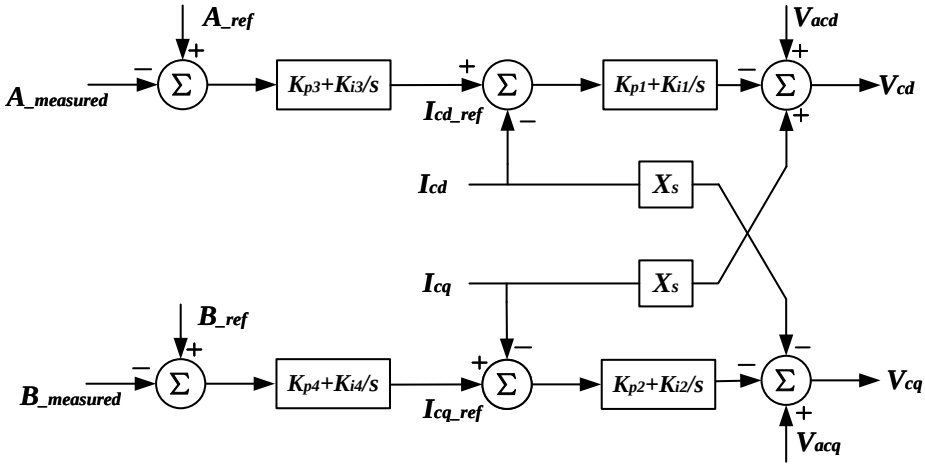

Figure 2.5 d-q axis control with parameter assignment

The choices of K_p and K_i for the outer and inner control are analysed by taking the parameters from benchmark models into simulation for sensitivity studies for improved performance. PI parameter selection and optimization can also be achieved through various techniques [137]. The particle swarm optimization technique has simple implementation and few algorithm parameters but it can suffer from partial optimism [138]. PI parameter calculation can also determine the parameter values based on the whole knowledge of system dynamics, which potentially can be more complex for large and interconnected systems [139].

With the assigned parameters of PI controller and internal control state variables, the d-q axis control equations can be expressed in the following categories: dc voltage control, ac voltage control, active power control and reactive power control.

Constant dc voltage control mode

In converter stations that employ constant dc voltage control, active power is balanced and dc side voltage is maintained. Unbalanced active power in ac and dc side of the converter leads to dc voltage fluctuation and at the moment ac current will charge or discharge dc capacitor until dc voltage stabilizes to the reference value. Thus the designated dc voltage value is effectively an active power balance point.

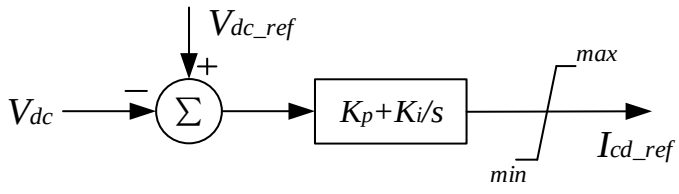

Figure 2.6 Constant dc voltage control

Figure 2.6 shows the diagram of constant dc voltage control, where the error between

measured and reference dc voltage is fed into PI controller and modulated as the reference value for d-axis component of ac current.

Mathematical expression of constant dc voltage control:

$$\begin{cases} \Delta V_{dc\_ref} - \Delta V_{dc} = \Delta x_{c3} \\ K_{p3}\Delta x_{c3} + K_{i3}\Delta x_{c3} - \Delta I_{cd} = \Delta x_{c1} \\ -(K_{p1}\Delta x_{c1} + K_{i1}\Delta x_{c1}) + \Delta V_{acd} + X_s \Delta I_{cq} = \Delta V_{cd} \end{cases} \tag{2.10}$$

Constant ac voltage control mode

As ac voltage fluctuation mainly depends on reactive component of system power flow, constant ac voltage control must be adopted to sustain ac busbar voltage, which fundamentally is realized through adjustment of reactive power.

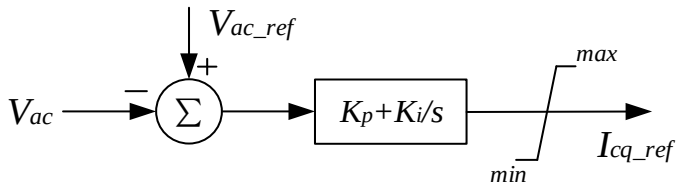

Figure 2.7 Constant ac voltage control

Mathematical expression for ac voltage control is:

$$\begin{cases} \Delta V_{ac\_ref} - \Delta V_{ac} = \Delta x_{c4} \\ K_{p4}\Delta x_{c4} + K_{i4}\Delta x_{c4} - \Delta I_{cq} = \Delta x_{c2} \\ -(K_{p2}\Delta x_{c2} + K_{i2}\Delta x_{c2}) + V_{acq} - X_s \Delta I_d = \Delta V_{cq} \end{cases} \tag{2.11}$$

Active and reactive power control mode

Active and reactive power exchange between converter and ac system can be expressed in dq

coordinates as the following equations:

$$P = V_{sd} I_{sd} + V_{sq} I_{sq}$$
$$Q = V_{sd} I_{sq} - V_{sq} I_{sd} \quad (2.12)$$

When d axis is set as the direction of ac voltage of point of common coupling, it is assumed that $V_{sd} = V_s$ and $V_{sq} = 0$, therefore equation (2.12) is transformed into:

$$P = V_{sd} I_{sd}$$
$$Q = V_{sd} I_{sq} \quad (2.13)$$

From equation (2.13), P and Q can be controlled through d q component of ac current. In Figure 2.8, the error between measured value and reference value is transformed to references for I_d and I_q through proportional and integral controller modulation.

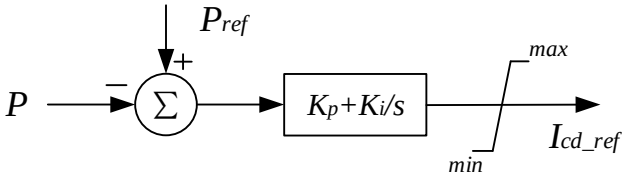

Figure 2.8 Active power control

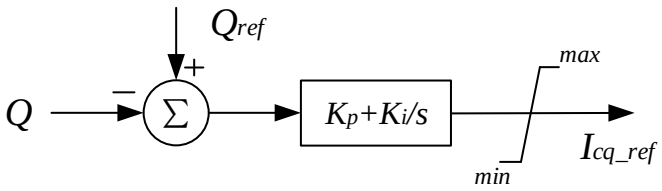

Figure 2.9 Reactive power control

Mathematical expression of active power control mode is:

$$\begin{cases} \Delta P_{ref} - \Delta P = \Delta x_{c3} \\ K_{p3}\Delta x_{c3} + K_{i3}\Delta x_{c3} - \Delta I_{cd} = \Delta x_{c1} \\ -(K_{p1}\Delta x_{c1} + K_{i1}\Delta x_{c1}) + \Delta V_{acd} + X_s \Delta I_{cq} = \Delta V_{cd} \end{cases} \tag{2.14}$$

$$\begin{cases} \Delta Q_{ref} - \Delta Q = \Delta x_{c4} \\ K_{p4}\Delta x_{c4} + K_{i4}\Delta x_{c4} - \Delta I_{cq} = \Delta x_{c2} \\ -(K_{p2}\Delta x_{c2} + K_{i2}\Delta x_{c2}) + V_{acq} - X_s \Delta I_{cd} = \Delta V_{cq} \end{cases} \tag{2.15}$$

2.3.2 d-q to D-Q transformation

In the d-q decoupling control of converter station, ac voltage of the point of common coupling is taken as the d-axis reference direction, yet the dynamic and static behaviours of the ac network components such as synchronous generators, excitation system and PSS are modelled with a common reference D-Q. Therefore, necessary transformation from d-q coordinates to D-Q reference is needed to incorporate the dynamic equation of VSC-HVDC converters into ac system. d-q to D-Q transformation is shown in Figure 2.10.

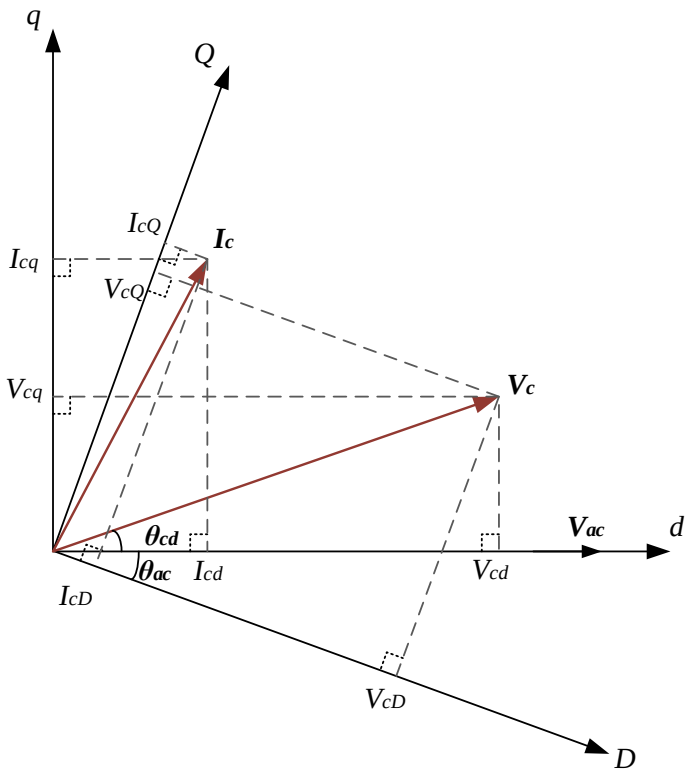

Figure 2.10 d-q to D-Q transformation

As d-axis takes ac voltage direction as reference, the phase angle of converter voltage in respect to d-q axis and D-Q axis has the relationship in equation (2.16)

$$\theta_{cD} = \theta_{ac} + \theta_{cd} \tag{2.16}$$

Thus the d-q and D-Q components can be expressed as:

$$\begin{aligned} V_{cD} + jV_{cQ} &= V_c(\cos(\theta_{ac} + \theta_{cd}) + j\sin(\theta_{ac} + \theta_{cd})) \\ I_{cd} + jV_{cq} &= I_c(\cos(\theta_{cD} - \theta_{cd}) + j\sin(\theta_{cD} - \theta_{cd})) \end{aligned} \tag{2.17}$$

Hence converter voltage and current are transformed from d-q axis to D-Q axis and then can be merged into ac system dynamics.

$$
\begin{aligned}
V_{cD} &= V_{cd}\cos\theta_{ac} - V_{cq}\sin\theta_{ac} \\
V_{cQ} &= V_{cq}\cos\theta_{ac} + V_{cd}\sin\theta_{ac} \\
I_{cd} &= I_{cD}\cos\theta_{ac} + I_{cQ}\sin\theta_{ac} \\
I_{cq} &= I_{cQ}\cos\theta_{ac} - I_{cD}\sin\theta_{ac}
\end{aligned}
\tag{2.18}
$$

2.3.3 Transformer Model

The voltage-current relationship at the transformer is given in the following equation:

$$
\boldsymbol{V_{ac}} - \boldsymbol{V_{cd}} = \boldsymbol{I_{cd}} \times jX_s \tag{2.19}
$$

X_s is the reactance of the transformer.

Real and imaginary part of the equation is derived as:

$$
\begin{cases}
V_{ac}\cos\theta_{ac} - V_c\cos\theta_{cD} = -I_{cQ}X_s \\
V_{ac}\sin\theta_{ac} - V_c\sin\theta_{cD} = I_{cD}X_s
\end{cases}
\tag{2.20}
$$

Linearization of the above equation is shown in equation (2.21)

$$
\begin{cases}
\cos\theta_{ac}\Delta V_{ac} - V_{ac}\sin\theta_{ac}\Delta\theta_{ac} - \Delta V_{cD} = -X_c\Delta I_{cQ} \\
\sin\theta_{ac}\Delta V_{ac} + V_{ac}\cos\theta_{ac}\Delta\theta_{ac} - \Delta V_{cQ} = X_c\Delta I_{cD}
\end{cases}
\tag{2.21}
$$

2.3.4 DC Network and Dynamics

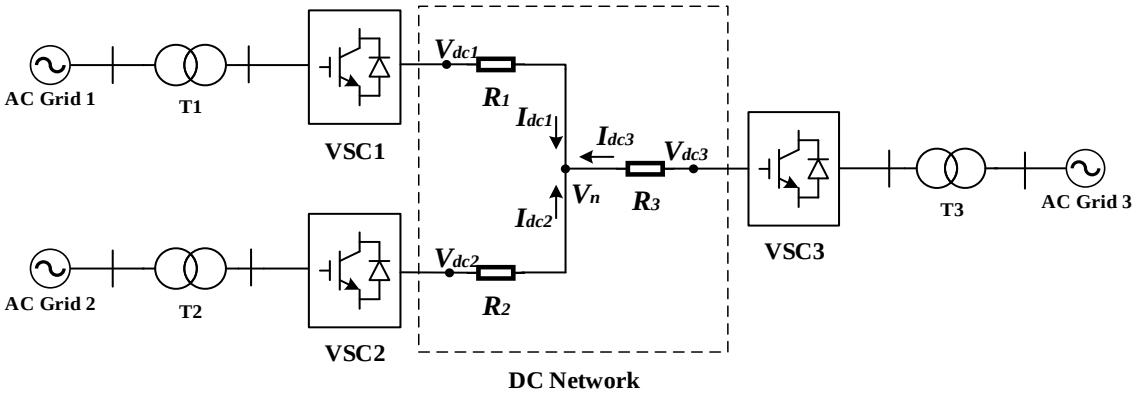

Figure 2.11 DC power flow in Multi-terminal VSC-HVDC

The multi-terminal VSC-HVDC dc network is illustrated in Figure 2.11, where star connection is employed and the directions of current are all set as from the converter into the dc network.

Based on kirchhoff's law, the relationship among dc voltages at each converter station V_{dc1} V_{dc2} V_{dc3} and network common point $V_{n.}$ is shown in equation (2.22).

$$\frac{V_{dc1}-V_n}{R_1}+\frac{V_{dc2}-V_n}{R_2}+\frac{V_{dc3}-V_n}{R_3}=0 \tag{2.22}$$

Power balance of the converter station gives that the power charging the capacitor and power going into the dc transmission line equal power in converters imported from ac system.

$$P_{converter}=P_{capcitor}+P_{line} \tag{2.23}$$

$$\begin{cases} P_{converter}=V_{cD}I_{cD}+V_{cQ}I_{cQ}\Rightarrow V_{cD}I_{cD}+V_{cQ}I_{cQ}=V_{dc1}C_{\mu F}\dfrac{dV_{dc}}{dt}+V_{dc}\dfrac{V_{dc}-V_n}{R} \\ P_{capcitor}=V_{dc1}C_{\mu F}\dfrac{dV_{dc}}{dt} \\ P_{line}=V_{dc}\dfrac{V_{dc}-V_n}{R} \end{cases} \tag{2.24}$$

Equation (2.24) shows the active power in converter station, dc capacitor and dc transmission line. Then the dynamics of dc voltage of each terminal are shown in equation (2.25).

$$\begin{cases} \dfrac{dV_{dc1}}{dt} = C_{pu1}\dfrac{V_{cD1}I_{cD1}+V_{cQ1}I_{cQ1}}{V_{dc1}} - C_{pu1}\dfrac{V_{dc1}-V_n}{R_1} \\ \dfrac{dV_{dc2}}{dt} = C_{pu2}\dfrac{V_{cD2}I_{cD2}+V_{cQ2}I_{cQ2}}{V_{dc2}} - C_{pu2}\dfrac{V_{dc2}-V_n}{R_2} \\ \dfrac{dV_{dc3}}{dt} = C_{pu3}\dfrac{V_{cD3}I_{cD3}+V_{cQ3}I_{cQ3}}{V_{dc3}} - C_{pu3}\dfrac{V_{dc3}-V_n}{R_3} \end{cases} \tag{2.25}$$

Linearize the above equation to the following format:

$$\begin{cases} \Delta V_{dc1} = C_{pu1}[-(V_{cD1}I_{cD1}+V_{cQ1}I_{cQ1})\dfrac{1}{V_{dc1}^2} - \dfrac{R_2+R_3}{R_1R_2+R_1R_3+R_2R_3}]\Delta V_{dc1} + C_{pu1}\dfrac{R_3\Delta V_{dc2}+R_2\Delta V_{dc3}}{R_1R_2+R_1R_3+R_2R_3} \\ \qquad + C_{pu1}\dfrac{1}{V_{dc1}}(V_{cD1}\Delta I_{cD1}+V_{cQ1}\Delta I_{cQ1}+I_{cD1}\Delta V_{cD1}+I_{cQ1}\Delta V_{cQ1}) \\ \Delta V_{dc2} = C_{pu2}[-(V_{cD2}I_{cD2}+V_{cQ2}I_{cQ2})\dfrac{1}{V_{dc2}^2} - \dfrac{R_1+R_3}{R_1R_2+R_1R_3+R_2R_3}]\Delta V_{dc2} + C_{pu2}\dfrac{R_3\Delta V_{dc1}+R_1\Delta V_{dc3}}{R_1R_2+R_1R_3+R_2R_3} \\ \qquad + C_{pu2}\dfrac{1}{V_{dc}}(V_{cD2}\Delta I_{cD2}+V_{cQ2}\Delta I_{cQ2}+I_{cD2}\Delta V_{cD2}+I_{cQ2}\Delta V_{cQ2}) \\ \Delta V_{dc3} = C_{pu3}[-(V_{cD3}I_{cD3}+V_{cQ3}I_{cQ3})\dfrac{1}{V_{dc1}^2} - \dfrac{R_1+R_2}{R_1R_2+R_1R_3+R_2R_3}]\Delta V_{dc3} + C_{pu3}\dfrac{R_2\Delta V_{dc1}+R_1\Delta V_{dc2}}{R_1R_2+R_1R_3+R_2R_3} \\ \qquad + C_{pu3}\dfrac{1}{V_{dc3}}(V_{cD3}\Delta I_{cD3}+V_{cQ3}\Delta I_{cQ3}+I_{cD3}\Delta V_{cD3}+I_{cQ3}\Delta V_{cQ3}) \end{cases} \tag{2.26}$$

2.3.5 Power Injection Model

The embedded VSC-HVDC system in ac network is constantly altering the transmission line power flow, changing the power flow model. Thus, the equivalent power injection model representing the power modulation effect should be established.

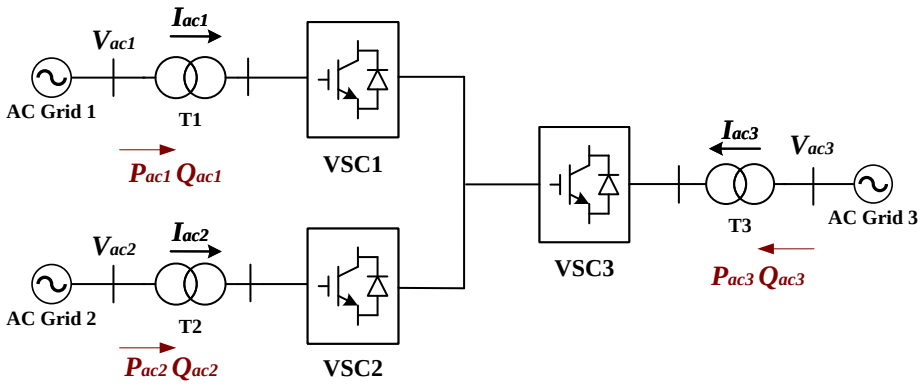

Figure 2.12 Power flow model of MTDC

The power injection model is expressed as equation (2.27).

$$P_{ac} + jQ_{ac} = \boldsymbol{V_{ac}} \boldsymbol{I_{ac}^{*}} \tag{2.27}$$

Taking the common reference as power exporting from ac grid into each converter, active and reactive power can be expressed regarding to D-Q coordinates as:

$$\begin{aligned} P_{ac} &= V_{ac} cos\theta_{ac} I_{cD} + V_{ac} sin\theta_{ac} I_{cQ} \\ Q_{ac} &= V_{ac} sin\theta_{ac} I_{cD} - V_{ac} cos\theta_{ac} I_{cQ} \end{aligned} \tag{2.28}$$

2.4 FACTS Modelling

In a complex power system, FACTS devices are often installed in various locations for multiple purposes of system enhancement such as maintaining voltage stability and increasing power transfer capability [36]. Exploiting the supplementary damping functions of these FACTS devices and incorporating into the coordinated design can be beneficial to strengthen system damping characteristics. In this study, TCSC is utilized and modelled for supplementary damping controller design.

2.4.1 TCSC

In a TCSC model, a TCR and a fixed series capacitor is connected in parallel. The TCSC is seen as a controllable reactance and it's configured as a capacitive reactance to reduce the equivalent electrical distance between buses and increase active power transfer capability of the transmission line. Figure 2.13 represents the structure of TCSC. By adding supplementary damping controller, TCSC can actively modulate power flow to damp out inter-area oscillations.

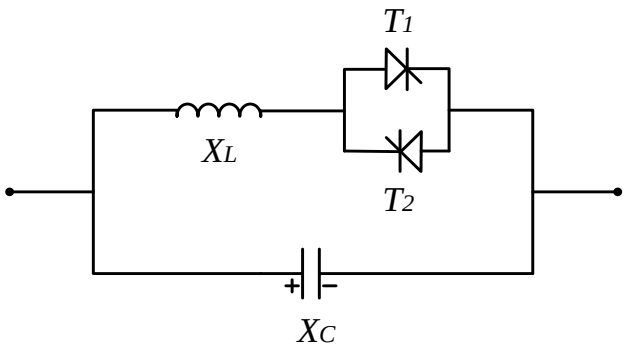

Figure 2.13 Block diagram of TCSC

Open-loop reactance control as one of the basic control modes of TCSC for power flow modulation for TCSC is adopted in this study. It is, as shown in Figure 2.14. The desirable steady state series compensation level or line power transfer is sent to the controller as reactance reference and the controller is simulated by a time delay block with a typical time constant of 15ms. Then the controller outputs an instruction signal for TCSC reactance. The firing angle can be obtained by linearization of the instruction signal and transmitted to trigger generator, which finally leads to the desirable value of reactance.

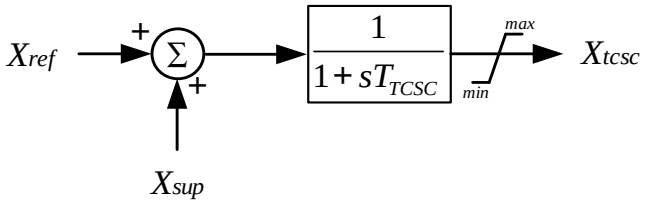

Figure 2.14 Dynamic model of TCSC

Differential equation of TCSC dynamics is shown below:

$$\dot{X} = -\frac{1}{T_{t\,\mathrm{csc}}}(-X + X_{ref} + X_{sup}) \tag{2.29}$$

where

X	actual reactance
X_{ref}	reference reactance
X_{sup}	supplementary damping reactance
$T_{t\,\mathrm{csc}}$	time constant of firing circuit delay

Power injection model

Similar to the VSC-HVDC, the impact of TCSC on power flow can be modelled as power injection at each series connected bus of TCSC.

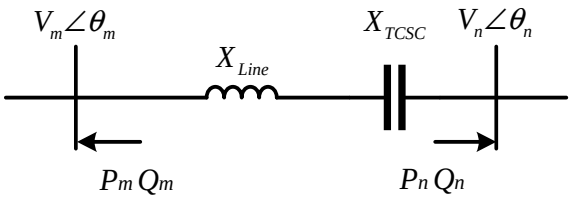

Figure 2.15 Power injection model of TCSC

The active and reactive power injection at bus *m* and bus *n* can be calculated by the following

equations:

$$P_m = \frac{X_{TCSC}}{X_{Line} - X_{TCSC}} V_m V_n B_{Line} \sin(\theta_m - \theta_n) \tag{2.30}$$

$$Q_m = \frac{X_{TCSC}}{X_{Line} - X_{TCSC}} B_{Line}[V_m^2 - V_m V_n \cos(\theta_m - \theta_n)] \tag{2.31}$$

$$P_n = \frac{X_{TCSC}}{X_{Line} - X_{TCSC}} V_m V_n B_{Line} \sin(\theta_n - \theta_m) \tag{2.32}$$

$$Q_n = \frac{X_{TCSC}}{X_{Line} - X_{TCSC}} B_{Line}[V_n^2 - V_m V_n \cos(\theta_n - \theta_m)] \tag{2.33}$$

where

X_{Line}	transmission line equivalent reactance
X_{TCSC}	TCSC effective capacitive reactance
B_{Line}	transmission line equivalent susceptance

2.5 Multi-Model System Establishment

In small signal stability studies, power system is required to be linearized around a certain operating point and reorganized as a set of differential and algebraic equations (DAE). State-space representation is shown in the following equation.

$$\Delta x = A\Delta x + B\Delta u \tag{2.34}$$

Different from a single mode system where power system is linearized around one operation point; multi-model system allows the system to be linearized around several operating points which greatly increases the robustness of the damping controller, making it more effective

under different system operating conditions. A series of linearized system models are integrated together to form the multi-model system.

2.6 Summary

The small-signal models of power system components are modelled in detail as the foundation for future damping control studies. As inter-area oscillation is often induced by the loss of synchronism among generator groups in different areas, it's crucial to model the synchronous generators to the sub-transient level with 6^{th}-order differential equations. The dynamics of static ac excitation system and power system stabilizer utilized in the study was modelled in detail. The general d-q decoupled VSC converter control was shown with d-axis active power control and dc voltage control as well as q-axis reactive power control and ac voltage control. Each outer control loop can be integrated with inner current control loop, forming the complete d-q decoupled control model. Furthermore, the dc capacitor dynamics and multi-terminal dc network were investigated to conclude the VSC-MTDC modelling. In addition, the TCSC model with direct reactance control mode was presented along with the power injection models which represented the effects of the installation of the device on original system power flow. Finally, with the combined system dynamics including synchronous generator and its excitation system, PSS, VSC-MTDC, and FACTS devices, the system was linearized around multiple operating conditions to lay the foundation of robust design against structured uncertainties.

CHAPTER 3 ROBUST COORDINATED DAMPING CONTROL METHODOLOGY

3.1 Introduction

Low frequency oscillation has posed great challenges on the development of modern power grids and restrained the power transmission capability. To improve system small signal stability, various devices has been employed to dynamically modulate system parameters such as active and reactive power to mitigate the impact of the oscillation and facilitate power system to quickly regain synchronism under disturbances. Besides, as the application of PMU and WAMS technology in the modern power network, it is made possible to choose remote signals as feedback signal to the damping controller. The coordination between damping controllers of different devices e.g. PSS, FACTS and HVDC needs to be considered in the design stage to avoid adverse interactive effects on system performance.

In this chapter, the methodology of coordinated and robust supplementary damping control design for multiple devices is introduced. In the following sections, the damping control optimization is formulated with BMI-based mixed-sensitivity approach of synthetic control objectives. The optimization problem is then solved in a two-step approach. Additionally, feedback signal selection for the controller is determined by the analysis of participation

factor and modal residue analysis, identifying system oscillatory modes and sensitivity between feedback signal candidates and oscillatory modes. Then the system order is reduced with balanced truncation method for the practicality of controller design. With balanced realization technique, the states of the original system are partitioned into most significant states with high controllability and observability and lease significant states with low controllability and observability. The balanced truncation method offers many important characteristics compared to modal truncation and residualization and better accuracy [41]. Besides, balanced truncation system reduction can preserve stability in the low-order system [140]. The coordinated design is realized by sequentially devising each damping controller for individual device with minimal coupling effort. Finally, controller design procedure is summarized in detailed steps incorporating the design methods above.

3.2 BMI-Based Damping Control Approach on Multi-Model System

3.2.1 Control Objectives

Designing supplementary damping controllers requires careful assessment of control objectives regarding disturbance rejection, control effort optimization and regional pole placement and then these objectives are described with matrix inequalities forming a BMI-based synthetic optimization problem.

Regional Pole Placement

Consider a set of system models linearized under different operating points in (3.1).

$$x = A_k x + B_k u$$
$$y = C_k x + D_k u \tag{3.1}$$

The eigenvalues are determined by state matrix A_k and poles of the system are given by the roots of equation (3.2).

$$\det(s\mathbf{I} - \mathbf{A}) = 0 \tag{3.2}$$

When all of the poles have negative real parts, the system is considered as asymptotically stable. A pair of conjugate complex eigenvalues corresponds to an oscillatory mode with frequency f and damping ratio ζ. And a real eigenvalue indicates non-oscillatory mode.

Suppose a pair of conjugate complex eigenvalue in the form

$$\lambda = \sigma \pm j\omega \tag{3.3}$$

where ω is the oscillation frequency given in rad/s:

$$\omega = 2\pi f \tag{3.4}$$

And damping ratio is determined by the real part of the eigenvalue:

$$\zeta = \frac{-\sigma}{\sqrt{\sigma^2 + \omega^2}} \tag{3.5}$$

The poles in the complex plane is shown in Figure 3.1. A pair of complex conjugate poles are located in the left side of the plane.

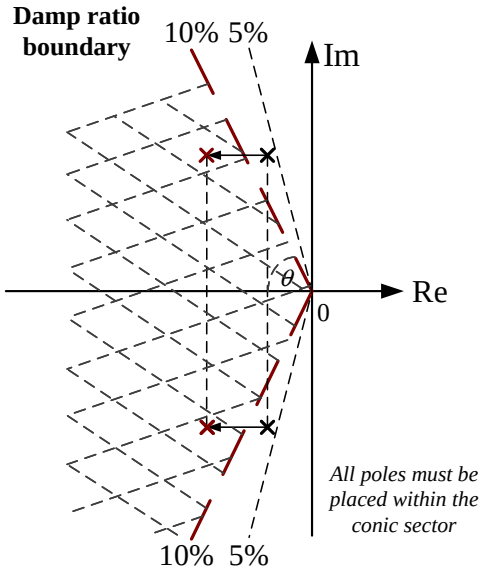

Figure 3.1 Regional Pole Placement

The rate of decay is indicated by the magnitude of damping ratio and in respect to the location of the eigenvalue pairs on the complex plane, it can be deduced that by moving the poles in the opposite direction of the real axis, meaning to increase the absolute value of the real part, damping ratio of a particular mode can be increased. Therefore, regional pole placement can be utilized to improve system damping ratios and the boundary of such a conic area can be defined with angle θ, bearing the relationship with damping ratio ζ in equation (3.6).

$$\theta = \cos^{-1}(\zeta) \tag{3.6}$$

LMI Definition of Regional Pole Placement

Define *R* a subset of the left complex plane and a dynamic system is *D* stable if all the poles are located in *R*. It can be expressed as a LMI region in (3.7) if there exists symmetric

matrices a and b such that [141]:

$$R=\left\{z\in C: f_R(\mathrm{z})=a+\mathrm{z}b+\bar{\mathrm{z}}b^T<0\right\} \tag{3.7}$$

In Figure 3.1, the LMI expression is transformed into (3.8)

$$R=\left\{z\in C: f_R(\mathrm{z})=a+\mathrm{z}b+\bar{\mathrm{z}}b^T<0\right\}$$
$$a=0 \;\&\; b=\begin{bmatrix}\sin\theta & -\cos\theta\\ \cos\theta & \sin\theta\end{bmatrix} \tag{3.8}$$

State matrix A is considered stable if and only if there exists a positive symmetric matrix Z satisfying

$$A^TZ+ZA<0 \tag{3.9}$$

The close-loop system with state matrix A is R- stable if and only if there exists a symmetric matrix Z such that:

$$a\otimes Z+b\otimes(ZA)+b^T\otimes(A^TZ)<0$$
$$Z>0 \tag{3.10}$$

where "$\otimes$" denotes the Kronecker product of two matrices.

3.2.2 System Uncertainty Formulation

Disturbances such as load variation, line outage and excitation system disturbance could often cause low frequency oscillation in the system. Thus the primary objective of the damping controllers is to diminish the impact of the disturbances and meanwhile control effort in the design process should be optimized in accordance with the actual ratings of actuators to avoid

over-design.

The mixed H_2 / H_∞ synthesis output feedback control is adopted to quantify these two objectives: disturbance rejection and control effort optimization. Figure 3.2 shows the mixed-sensitivity system formulation where system plant is the open-loop model and feedback controller K is to be designed. The sensitivity between disturbance $w(s)$ and system output $y(s)$ is defined by transfer function $G_{wy}(s)$ and sensitivity between disturbance $w(s)$ and controller output $u(s)$ is defined as $G_{wu}(s)$. Weights w_y and w_u are carefully selected as a low pass filter and a high pass filter respectively.

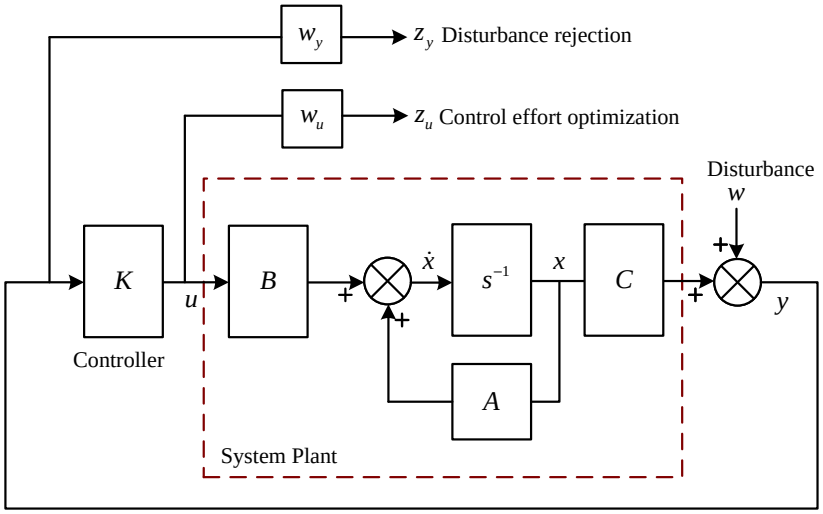

Figure 3.2 Mixed-sensitivity multi-objective synthesis system formulation

From Figure 3.2, the relationships are summarized in the following equations:

$$\begin{aligned} x &= Ax + Bu \\ z_y &= Cx + w \\ z_u &= u \\ y &= Cx + w \end{aligned} \tag{3.11}$$

where

x	system state variable
w	disturbance input
u	control input (output of the FACTS or VSC-MTDC controller)
y	measured system output
z	augmented outputs

Incorporating the controller K gives the close-loop system:

$$\begin{aligned} x_{cl} &= A_{cl}x_{cl} + B_{cl}w \\ z_y &= C_{cly}x_{cl} + D_{cly}w \\ z_u &= C_{clu}x_{cl} + D_{clu}w \end{aligned} \tag{3.12}$$

where

x_{cl}	close-loop system state variable

H_2 *and* H_∞ *norm*

The H_2 norm measures the overall energy relating input disturbance w and output response z_u, numerically given in (3.13)

$$\|G_{wu}(s)\|_2 = \sqrt{tr\left(C_{clu}JC_{clu}^T\right)} \tag{3.13}$$

where

tr	sum of the elements on the main diagonal of matrix

J is the Lyapunov matrix which satisfies:

$$A_{cl}J + JA_{cl}^T + B_{cl}B_{cl}^T < 0 \tag{3.14}$$

The H_2 control design problem can be summarized as finding a symmetric positive definite matrix J that satisfies:

$$Trace(C_{cl2}JC_{cl2}^T) < \nu \tag{3.15}$$

$$A_{cl}J + JA_{cl}^T + B_{cl}B_{cl}^T < 0 \tag{3.16}$$

(3.16) can be rewritten into the following matrix inequalities:

$$\begin{bmatrix} JA_{cl} + A_{cl}^T J & JB_{cl} \\ B_{cl}^T J & -I \end{bmatrix} < 0 \tag{3.17}$$

$$\begin{bmatrix} L & C_{cl2} \\ C_{cl2}^T & J \end{bmatrix} > 0 \tag{3.18}$$

$$Trace(L) < \nu \tag{3.19}$$

where L is an auxiliary matrix.

The H_∞ norm denotes the peak value of the magnitude of the transfer function over the whole frequency range and the numerical expression is given in (3.20)

$$\left\| G_{wy}(s) \right\|_\infty = \max_\omega \left| G_{wy}(j\omega) \right| \tag{3.20}$$

To minimize the peak value to be less than a certain criterion that satisfies $\left\| G_{wy}(s) \right\|_\infty < \gamma$, it is required to find a symmetric Lyapunov matrix J such that:

$$\begin{bmatrix} JA_{cl} + A_{cl}^T J & JB_{cl} & C_{cl1}^T \\ B_{cl}^T J & -\gamma I & D_{cl}^T \\ C_{cl1} & D_{cl1} & -\gamma I \end{bmatrix} < 0 \tag{3.21}$$

3.2.3 Synthesis BMI Optimization Problem Formulation

Combining the control objectives introduced in section 3.2.1 and 3.2.2, regional pole placement, control effort optimization and disturbance rejection can be formulated as the following expressions:

$$\min\left[\alpha_1 Trace(L) + \alpha_2 \gamma\right]$$

$$s.t. \quad \begin{cases} \alpha \otimes J + \beta \otimes (JA_{cl}) + \beta^T \otimes (A_{cl}^T J) < 0 \\ \begin{bmatrix} JA_{cl} + A_{cl}^T J & JB_{cl} & C_{cl1}^T \\ * & -\gamma I & D_{cl1}^T \\ * & * & -\gamma I \end{bmatrix} < 0 \\ \begin{bmatrix} L & C_{cl2} \\ * & J \end{bmatrix} > 0 \\ Trace(J) < \nu \end{cases} \tag{3.22}$$

where

$\alpha_1\ \alpha_2$ weights of H_2 and H_∞ performance

"$*$" the transpose of its symmetry element in the matrix

It's important to mention that the above different optimization specifications should be solved simultaneously for one Lyapunov matrix *J* as a joint convex optimization problem.

3.2.4 Solution to the BMI-Based Optimization Problem

The combined optimization problem considering multi-model is represented as:

$$\min\left[\alpha_1 Trace(L)+\alpha_2\gamma\right]$$

$$s.t.\quad \begin{cases} \alpha\otimes J+\beta\otimes\left(J\begin{bmatrix}A_i & B_iC_c\\ B_cC_i & A_c\end{bmatrix}\right)+\beta^T\otimes\left(\begin{bmatrix}A_i & B_iC_c\\ B_cC_i & A_c\end{bmatrix}^T J\right)<0 \\ \begin{bmatrix} J\begin{bmatrix}A_i & B_iC_c\\ B_cC_i & A_c\end{bmatrix}+\left(J\begin{bmatrix}A_i & B_iC_c\\ B_cC_i & A_c\end{bmatrix}\right)^T & J\begin{bmatrix}0\\ B_c\end{bmatrix} & \begin{bmatrix}C_i^T\\ 0\end{bmatrix} \\ * & -\gamma I & I \\ * & * & -\gamma I\end{bmatrix}<0 \\ \begin{bmatrix}Q & \begin{bmatrix}0 & C_c\end{bmatrix}\\ * & J\end{bmatrix}>0 \\ Trace(J)<\nu \end{cases} \tag{3.23}$$

$$i=1,2,\quad ,P$$

The objectives of the above synthesis optimization problem can be concluded as finding a common feedback controller with variables $(A_c,\ B_c,\ C_c)$ in accordance to the BMI constraints. Furthermore, the other criterion is that the solution to all constraints should result in a common symmetric Lyapunov matrix J. The bilinear optimization problem is solved through a two-step approach to deal with the difficulties which are brought by the varying system matrices A_i, B_i, C_i in respect of different operating points[142].

Step 1: Find a state-feedback controller with the representation of $u = Kx$ such that the control objectives can be met by the close-loop system formed by the state-feedback controller under the operating points considered in the structured uncertainties.

Step 2: Find an output-feedback controller with the pre-determination of the controller variable from step 1 (i.e. $C_c = K$) such that the control objectives are met with the close-loop system under all considered operating points.

3.3 Feedback Signal Selection

Proper selection of system output as the controller feedback signal is needed for effective and robust design. In the eigenvalue analysis of the system damping characteristics, valuable information can be obtained such as mode shape, sensitivity and modal residue.

3.3.1 Participation Factor

After identifying the weakly damped modes in power system, it is important to distinguish the contribution of each generator to each mode. Participation factor is defined as dimensionless measure of the product of the right and left eigenvector and the normalized participation factor is scaled to 1.0.

The general form of participation factor is given in (3.24) [48]

$$P_{ki} = \frac{|v_{ik}||w_{ki}|}{\sum_{k=1}^{n}|v_{ik}||w_{ki}|} \tag{3.24}$$

where

P_{ki} participation factor relating the k^{th} state to i^{th} eigenvalue

v_{ik} right eigenvector relating the i^{th} mode to the k^{th} state variable

w_{ki} left eigenvector relating the k^{th} state variable to the i^{th} mode

Participation factor can be used to choose the feedback signal for controller design and the state with the highest normalized participation factor can be a good tool to determine the installation location and control signal of PSS in a power system with multiple generators. It has been reported in [66, 143] that participation factors are used for optimized control effort in damping controller design. However, this practice is not as realistic in damping controller design for VSC-MTDC and FACTS, which focuses on inter-area modes involving groups of generators in different locations. One generator state has relatively low sensitivity to the inter-area oscillatory mode. Nevertheless, participation factor analysis can provide crucial information about the generator involvement in a particular mode and facilitates installation location of these devices.

3.3.2 Modal Residue Analysis

As stated from the previous section, participation factor can only show the correlation between state variables and oscillatory mode, unable to incorporate the sensitivity of system input and output, so it's not sufficient to determine feedback signal for VSC-MTDC and FACTS devices only on the basis of participation factor. Therefore, in this section, modal residue analysis is introduced to analyse controllability and observability of each input to each oscillatory mode.

Modal residue R_k is given in the following equation:

$$G(s) = C(sI - A)^{-1}B = \sum_{i=1}^{i=n} \frac{Cv_i w_i B}{s - \lambda_i} = \sum_{i=1}^{i=n} \frac{R_i}{s - \lambda_i} \tag{3.25}$$

where

$G(s)$	system transfer function
R_i	modal residue
Cv_i	modal observability
$w_i B$	modal controllability
λ_i	eigenvalue

From the above equation (3.25), it's clear that the modal observability is calculated with matrix C, which is determined by the choice of feedback signal; modal controllability is calculated with matrix B, whose variation depends on input signal and installation location of the devices. To maximize the economic benefit when implementing the controllers in practical design, both controllability and observability must be taken into consideration. Some of the criteria that restrict choices of feedback signal include high sensitivity on the designated swing mode, which means that after the damping controller of a certain device is set to suppress a particular swing mode, it should have a high level of sensitivity in the frequency range so that the mode is observable. In addition, it should have low or no degree of sensitivity to other swing modes and its own controller output, to minimize adverse controller interactions and preserve valuable control effort.

In the modal residue analysis, the magnitude of residue R_i is the indicator for the amount of control effort needed for suppressing swing mode i with a certain feedback signal: the higher the magnitude means the lower the required control effort. When calculating the scaled residues of different feedback signals, the comparison must be made within the same type of the signal and not against each other.

As the locations of VSC-MTDC and FACTS devices are mostly decided by its primary functions such as series compensation, voltage support or wind farm integration, the modal controllability is considered to be fixed. In this situation, feedback signal candidates for these devices are evaluated with the differences of their observability. Some categories of possible candidates as feedback signal include generator output power, line power flow, line current machine speed and angle, etc. Furthermore, while local signals are conveniently measurable for the ease of practical implementation, some remote signals may bear higher sensitivity to the swing modes with less control effort. Therefore, the signal location should also be taken into careful consideration.

3.4 System Order Reduction

In Chapter 2, the linearized system model is derived as the basis of the damping control design. It shows clear correlation of system order with a number of factors e.g. the number and level modelling complexity of generators, number of PSSs and the installed VSC-MTDC and FACTS devices. Typically, in a bulk system, the system order can go up to hundreds of states. Therefore, simplification of the system model is a necessary step for the ease of controller design and computational effort and avoiding complexity of the desired controller. It is required that the equivalent system retains the information within the frequency range for inter-area oscillations i.e. 0.1-1Hz for inter-area oscillation mode and 1-2Hz for local mode so that it's a good approximation of the full-order original open-loop system. The balanced truncation method offers many important characteristics compared to modal truncation and residualization and better accuracy[41].

The model reduction problem as be expressed as the n^{th}-order original system with transfer

function $G_n(s)$ can be approximated as a m^{th}-order reduced system $G_m(s)$ such that

$$\| G_n(s) - G_m(s) \|_\infty < \gamma \tag{3.26}$$

where γ is sufficiently small

In this study, balanced truncation model reduction is applied for system order reduction [144]. With balanced realization technique, the states of the original system are partitioned into most significant states with high controllability and observability and lease significant states with low controllability and observability. Then the dynamics of the least significant states are ignored to reduce the system order. Equation (3.26) is transformed into (3.27)

$$\| G_n(s) - G_m(s) \|_\infty < 2 \sum_{i=k+1}^{n} \chi_i \tag{3.27}$$

where

χ_i Hankel singular values of the system $G_n(s)$

It's worthy to mention that in multi-model approach, the states of linearized system models under multiple operating points are identical with the same sequences. However, by reducing the system order with balanced modal truncation, state sequences for low-order systems won't be the same. This will result in failure of finding a common feedback controller in the first step of the two-step approach of solving the BMI based optimization problem. Therefore, it is necessary to transform the reduced system into a controllable canonical form [145].

For a system with transfer function expressed as:

$$G_n(s) = \frac{\beta_0 s^n + \beta_1 s^{n-1} + \quad \beta_{n-1} s + \beta_n}{s^n + \alpha_1 s^{n-1} + \quad + \alpha_{n-1} s + \alpha_n} \tag{3.28}$$

The canonical form is expressed as

$$\begin{bmatrix} x_1 \\ x_2 \\ \\ x_{n-1} \\ x_n \end{bmatrix} = \begin{bmatrix} 0 & 1 & 0 & 0 \\ 0 & 0 & 1 & 0 \\ & & & \\ 0 & 0 & 0 & 1 \\ -\alpha_n & -\alpha_{n-1} & -\alpha_{n-2} & -\alpha_1 \end{bmatrix} \begin{bmatrix} x_1 \\ x_2 \\ \\ x_{n-1} \\ x_n \end{bmatrix} + \begin{bmatrix} 0 \\ 0 \\ \\ 0 \\ 1 \end{bmatrix} u$$

$$y = \begin{bmatrix} \beta_n - \alpha_n \beta_0 & \beta_{n-1} - \alpha_{n-1} \beta_0 & \beta_2 - \alpha_2 \beta_0 & \beta_1 - \alpha_1 \beta_0 \end{bmatrix} \begin{bmatrix} x_1 \\ x_2 \\ \\ x_{n-1} \\ x_n \end{bmatrix} + \beta_0 u \tag{3.29}$$

3.5 Sequential Approach for Coordinated Design

When designing supplementary damping controllers for multiple devices or multi-terminals of VSC-MTDC, it is required that no adverse interactions between these controllers should occur.

A series of decentralized damping controllers for each terminal/device is designed sequentially to minimize the coupling effect and preventing adverse interactions among the controllers. Damping controller for the first device/terminal is designed and the first loop is closed, then the close-loop system is treated as the new open-loop system for damping controller design for the second terminal/device.

In Figure 3.3, the system state-space representation is depicted as $A\ B\ C\ D$, and supplementary damping controllers $i = 1 \cdots n$ are represented by $A_{Ki}\ B_{Ki}\ C_{Ki}\ D_{Ki}$. Each controller is designed based on mixed-sensitivity multi-objective BMI optimization technique

and its feedback signal is carefully selected considering participation factor and modal residue analysis. With each loop closure, the new close-loop system order increases with addition of feedback controller and system order reduction is carried out in each loop.

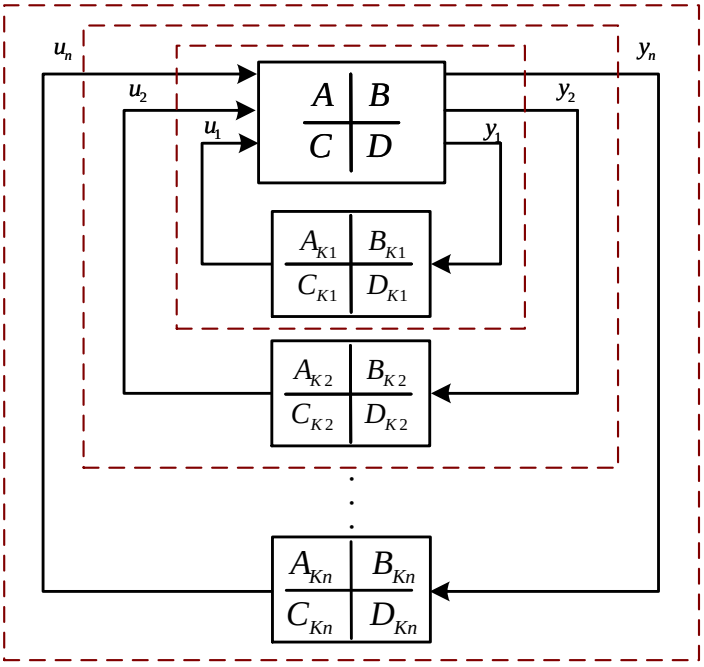

Figure 3.3 Sequential design approach

3.6 Real-Time Simulation on RTDS

Real time digital simulator is used in this study for validate the effectiveness of the controllers. Compared with other off-line types of simulation software, the RTDS has the real-time feature which enables simulation time to be in real time frame of the actual events [146]. Besides, with the expandable hardware, the simulation limitation can be pushed further to condition more detailed and larger scale modelling with exceptional simulation speed and accuracy. Furthermore, the hardware in loop testing feature can interface control devices such as relays to the panel of RTDS for performance evaluation in real-world conditions [147].

3.7 Controller Design Procedure

A summary of the complete coordinated robust design procedure is listed as follows:

Step 1. Establish system small-signal multi-model with state-space representation linearized under various operating points.

Step 2. Analyse system eigenvalue characteristics and isolate poorly damped oscillatory modes of the original open-loop system.

Step 3. Damping controller design for one terminal/device

a. Appropriately reduce the original system to decrease the complexity of the original system to facilitate the control design.

b. Choose system output signal as controller input by participation factor analysis and modal residue analysis of mode shape and sensitivity.

c. Define pole placement target region D and LMI expressions in accordance with damping ratio requirements.

d. Set H_2 and H_∞ augmented outputs with proper weight selection.

e. Formulate synthesis multi-objective mixed-sensitivity BMI control problem.

f. Solve the optimization problem with the two-step approach and obtain the controller mathematical representation, forming a close-loop system.

Step 4. Damping controller design for the second terminal/device: repeat **Step 3** for another terminal/device and achieve loop closure for the second time.

Step 5. Evaluate the effectiveness of the controllers with linear system performance

analysis and compare eigenvalue properties of the open-loop and close-loop system.

Step 6. Non-linear system performance validation is carried out in RTDS to check system performance.

3.8 Summary

In this chapter, the robust coordinated design methodology for damping controllers was introduced. The control constraints were summarized as mixed-sensitivity multi-objective BMI-based synthesis optimization problem for multi-model system, in which regional pole placement, disturbance rejection and control effort optimization are simultaneously considered and solved via the two-step approach. Choices of feedback signal were evaluated with participation analysis and modal residue analysis. This allowed the effectiveness of the feedback signal to be taken into account to prevent wasting valuable control effort. The order-reduced system was sought by balanced modal truncation, retaining the key information for the interested frequency range, facilitating the practicality of the controller design. Sequential design of each SISO controller with multiple loop closure incorporated multiple devices of concern. The effectiveness of the controllers will be tested by real-time digital simulation in RTDS under diverse operating scenarios and disturbances.

CHAPTER 4 ROBUST COORDINATED DAMPING CONTROL DESIGN OF VSC-MTDC

4.1 Introduction

The methodology of robust and coordinated control has highlighted the main features of the design procedure and it's crucial to select appropriate test system and devices for the implementation of the damping control theory and experiment with the effectiveness and robustness of the obtained controllers. Test systems with apparent under-damped inter-area oscillatory modes as well as proper-damped local modes are deemed suitable for small-signal damping control studies and based on the test system, electrical and electronic devices such as FACTS and HVDC can offer the platform for supplementary damping controller design with their smart and flexible control of system parameters like power flow and bus voltage.

In this chapter, robust supplementary damping controllers for a 3-terminal VSC-HVDC embedded in the 5-area 16-generator equivalent NYPS-NETS power system are designed in a coordinated way to avoid any adverse interactions between the controllers. The VSC-MTDC is connected in radial pattern and the control modes for all three terminals are d-axis dc voltage control and q-axis ac voltage control. The formulated synthesis BMI-based multi-objective multi-model control problem is solved via a two-step approach. By incorporating

multiple operating points in the design stage, damping controllers can exhibit great robustness when system operating conditions vary, which often is the case for a practical power system with perennial changes of load, generation and transmission line power flow. Such controllers will be tested with linear system analysis to check system eigenvalue characteristic numerically for a clear picture of the degree of improvement of each under-damped oscillatory mode. In addition, real-time simulation of the test system will provide further confirmation of the validity of the controllers and also its adaptability to the alterations of system operating conditions.

4.2 VSC-MTDC V_{dc}-V_{ac} Control Mode Configuration

The configuration of d-axis dc voltage control and q-axis ac voltage control is illustrated in Figure 4.1, where the supplementary damping control signal V_{ac_damp} for the dynamic control of ac voltage reference is to be designed with the control procedures presented in Chapter 3. The d-axis controls dc voltage through tracking the reference level given by upper system level control and similarly q-axis regulates ac voltage with the ac voltage reference value. Both references are set to be a constant value and not subject to change under disturbances, hence they cannot provide damping to oscillations and minimize the settling time. Therefore, a supplementary damping signal acts as the dynamic regulation of the reference so that it can actively modulate the corresponding system parameter such as ac voltage to cater to the need of supplementary damping to the insufficiently damped modes in the event of disturbances.

PI controllers with the parameters K_p and K_I are used in both inner and outer control loops for processing the error between actual measured value and the reference value into a correction based on the proportional and integral terms.

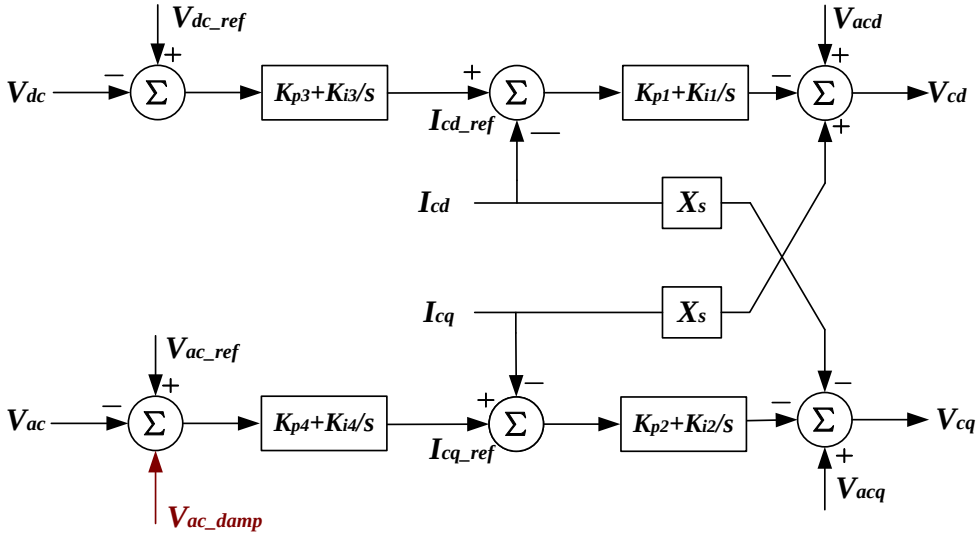

Figure 4.1 V_{dc}-V_{ac} control mode configuration with supplementary control signal

The mathematical representation of the dynamics of the control mode can be expressed in (6.1)-(6.2).

d-axis dc voltage control mode:

$$\begin{cases} \Delta V_{dc\_ref} - \Delta V_{dc} = \Delta x_{c3} \\ K_{p3}\Delta x_{c3} + K_{i3}\Delta x_{c3} - \Delta I_{cd} = \Delta x_{c1} \\ -(K_{p1}\Delta x_{c1} + K_{i1}\Delta x_{c1}) + \Delta V_{acd} + X_s \Delta I_{cq} = \Delta V_{cd} \end{cases} \tag{4.1}$$

q-axis ac voltage control mode:

$$\begin{cases} \Delta V_{ac\_ref} - \Delta V_{ac} = \Delta x_{c4} \\ K_{p4}\Delta x_{c4} + K_{i4}\Delta x_{c4} - \Delta I_{cq} = \Delta x_{c2} \\ -(K_{p2}\Delta x_{c2} + K_{i2}\Delta x_{c2}) + V_{acq} - X_s \Delta I_d = \Delta V_{cq} \end{cases} \tag{4.2}$$

where $\Delta x_{ci1}, \Delta x_{ci2}, \Delta x_{ci3}, \Delta x_{ci4}$ are internal states.

With all three terminals in $V_{dc} - V_{ac}$ control mode, the following state-space representation of

the dynamics of the VSC-MTDC can be expressed as (4.3).

$$\Delta x_c = A_c \Delta x_c + B_c \Delta V + D_c \Delta U_c \tag{4.3}$$

where

$$\Delta x_c \qquad \left[\Delta x_{c1} \quad \Delta x_{c2} \quad \Delta x_{c3}\right]^T$$

$$\Delta x_{c1} \qquad \left[\Delta V_{dc1} \quad \Delta x_{c11} \quad \Delta x_{c12} \quad \Delta x_{c13} \quad \Delta x_{c14}\right]^T$$

$$\Delta x_{c2} \qquad \left[\Delta V_{dc2} \quad \Delta x_{c21} \quad \Delta x_{c22} \quad \Delta x_{c23} \quad \Delta x_{c24}\right]^T$$

$$\Delta x_{c3} \qquad \left[\Delta V_{dc3} \quad \Delta x_{c31} \quad \Delta x_{c32} \quad \Delta x_{c33} \quad \Delta x_{c34}\right]^T$$

$$\Delta V_c \qquad \left[\Delta \theta_{s1} \quad \Delta V_{s1} \quad \Delta \theta_{s2} \quad \Delta V_{s2} \quad \Delta \theta_{s3} \quad \Delta V_{s3}\right]^T$$

$$\Delta U_c \qquad \left[\Delta V_{dc1\_ref} \quad \Delta V_{ac1\_ref} \quad \Delta V_{dc2\_ref} \quad \Delta V_{ac2\_ref} \quad \Delta V_{dc3\_ref} \quad \Delta V_{ac3\_ref}\right]^T$$

Note: $A_c \in 15\times15$, $B_c \in 15\times6$ and $D_c \in 15\times6$

4.3 Robust Coordinated Damping Controller Design for VSC-MTDC

4.3.1 Test System Small-Signal Modelling and Eigenvalue Analysis

The test system used in this study is the reduced order equivalent of the interconnected New York Power System and New England Test System[148]. It consists of 5 areas, 16 synchronous generators and 68 buses. Generators 1-9 represent the New England Test system and Generators 10-13 represent the New York Power System, whereas the neighbouring power system areas are represented by Generators 14-16. Figure 4.2 shows the single-line representation of the test system. Power system stabilisers are installed on generator 1-12 to

provide damping to local oscillations and as generators 13-16 are area equivalents, it's not practical to install PSS on these generators.

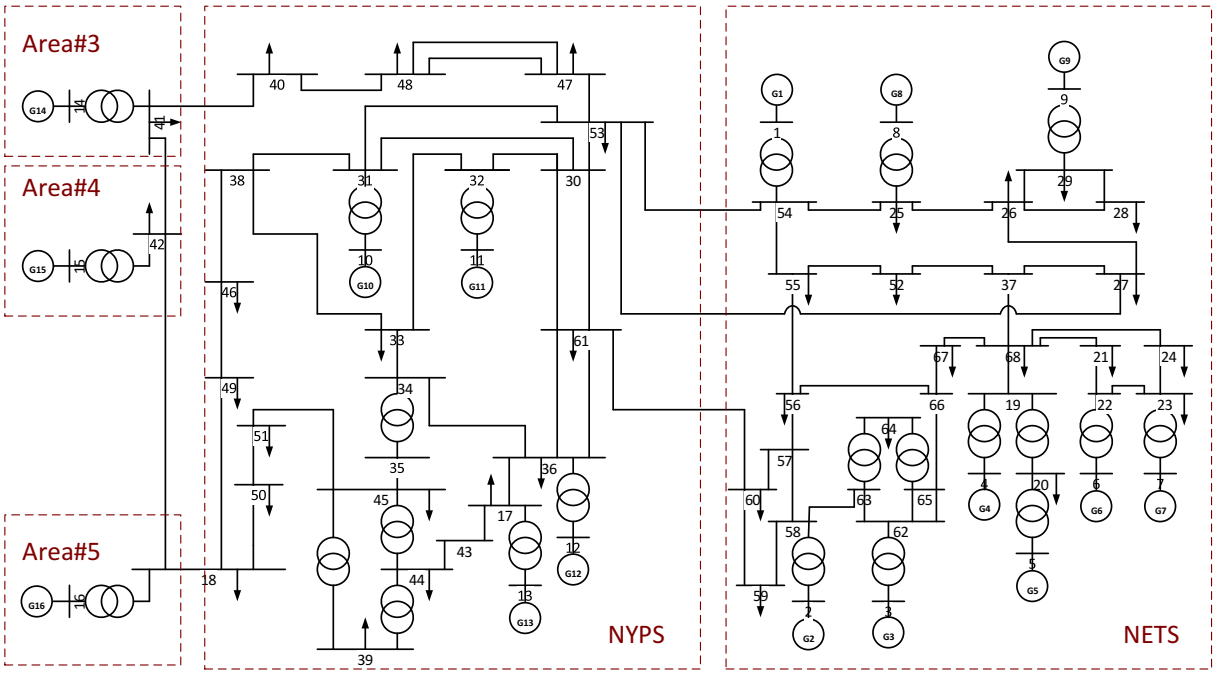

Figure 4.2 Reduced equivalent NYPS-NETS power system

Power flow pattern in this test system is that the NYPS is importing power from Area #3-#5 and power is transmitted from NETS to NYPS through 3 major corridors. Table 4.1 shows the steady-state power exchanges on major transmission corridors among the areas.

Table 4.1 Steady-state power exchange on transmission corridors in test system

Power Exchange (MW)	*From*	*To*
1500	Area 5 Bus 18	NYPS Bus 50
330	Area 5 Bus 18	NYPS Bus 49
580	Area 3 Bus 41	NYPS Bus 40
400	NETS Bus 54	NYPS Bus 53
27	NETS Bus 27	NYPS Bus 53
275	NETS Bus 60	NYPS Bus 61

The operating points for multi-model approach are selected by changing power transfer on

one of the major transmission corridors, which can be achieved with load variation in related areas. Table 4.2 lists the operating points for multi-model formulation.

Table 4.2 Operating points selection

Operating Points	*Load 18(MW)*
1	2470
2	2570
3	2670
4	2770

Eigenvalue analysis shows the poorly damped inter-area modes in Table 4.3, Table 4.4, Table 4.5 and Table 4.6. Four modes are identified with damping ratios less than 10%, among which mode 1, 2 and 4 with frequency 0.40Hz, 0.55Hz and 0.80Hz are significantly lack of damping and although mode 3 has a better degree of damping, it can still be improved.

Table 4.3 Damping ratio, frequency and Eigenvalues of Mode 1

Operating points	*Mode 2*		
	ζ	f (Hz)	*Eigenvalue*
1	6.4%	0.406	-0.163262±2.552482i
2	6.4%	0.406	-0.163563±2.551184i
3	6.4%	0.407	-0.165051±2.558563i
4	6.4%	0.407	-0.165072±2.556574i

Table 4.4 Damping ratio, frequency and Eigenvalues of Mode 2

Operating points	*Mode 2*		
	ζ	f (Hz)	*Eigenvalue*
1	5.1%	0.556	-0.178906±3.493549i
2	5.1%	0.555	-0.179508±3.489296i
3	5.2%	0.556	-0.180700±3.493768i
4	5.2%	0.555	-0.181214±3.489265i

Table 4.5 Damping ratio, frequency and Eigenvalues of Mode 3

Operating points	*Mode 3*		
	ζ	f (Hz)	*Eigenvalue*
1	8.6%	0.639	-0.346066±4.018540i
2	8.6%	0.639	-0.345977±4.018322i
3	8.6%	0.640	-0.346421±4.023215i
4	8.6%	0.640	-0.346137±4.021652i

Table 4.6 Damping ratio, frequency and Eigenvalues of Mode 4

Operating points	*Mode 4*		
	ζ	f (Hz)	*Eigenvalue*
1	5.1%	0.804	-0.258964±5.052409i
2	5.1%	0.804	-0.258791±5.050768i
3	5.1%	0.804	-0.258513±5.049625i
4	5.1%	0.804	-0.258422±5.049211i

Meanwhile, eigenvalues are plotted in Figure 4.3 to provide graphical intuition to the overall system Eigen-properties. With the 10% damping ratio line, it's clear to distinguish the insufficiently damped modes as the complex conjugate poles are located outside the conic area. Regional pole placement is specified as shifting these weakly damped eigenvalues into the designated area with at least 10% damping ratio.

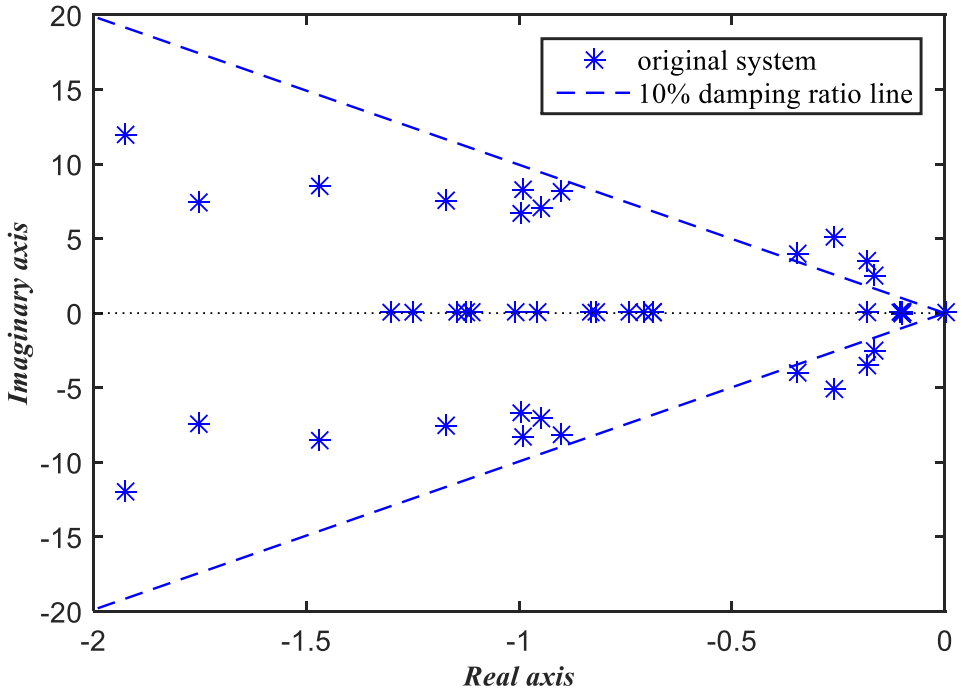

Figure 4.3 Eigenplot of the original open-loop system

From eigenvalue analysis, vital information such as mode shape can also be obtained. The right eigenvector matrix V is known to describe the mode shape which shows the

involvement of which one or groups of generator in one particular mode. In this case, the modes of interest are the four weakly damped ones and their mode shapes are illustrated in compass plot in Figure 4.4. It can be observed from the diagram that mode 1 is between generator groups in Area #1, 2 and single generator equivalent Areas#3, 4, 5; mode 2 is more asscociated with Area #3 and Area #5; mode 3 is between NYPS and NETS and mode 4 is between Area #3,5 and Area #4.

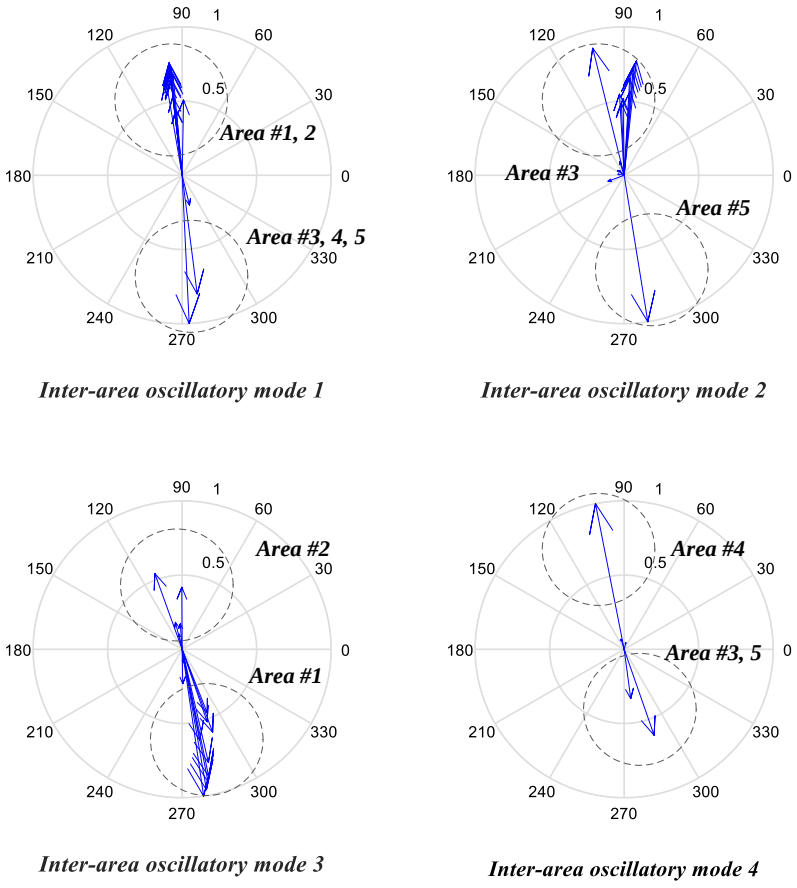

Figure 4.4 Inter-area oscillatory mode shapes

VSC-MTDC Installation Location and Control Mode

In this chapter, a 3-terminal VSC-HVDC is embedded in radial connected form in the test system. Bus 18, 50 and 49 are interconnected with the VSC-MTDC, in parallel with ac

connection between Bus 18 to Bus 49 and Bus 18 to Bus 50. It's notable that as shown in Table 4.1, a relatively large quantity of power is transferred from area 5 to the NYPS, which strains transmission corridor Line 18-50 and Line 18-49. The installation location is determined by two factors: network reinforcement and mode shape analysis of the weakly damped modes. As Area 5 has relatively high involvement in the modes due to heavy power output and weak link, VSC-HVDC could offer both network reinforcement as well as supplementary damping functions. Therefore, the VSC-MTDC should be utilized to expand transmission capacity of this area and provide supplementary damping to enhance system small-signal stability in the event of disturbances.

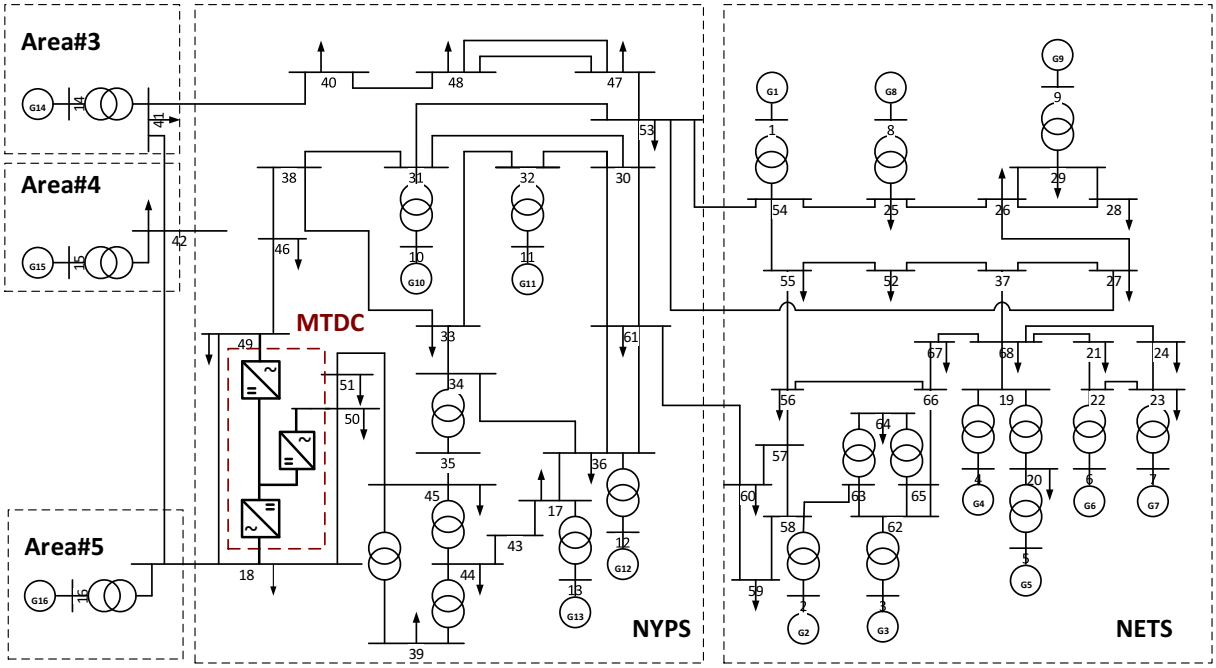

Figure 4.5 3-Terminal VSC-HVDC embedded in the test power system

The detailed diagram of the 3-terminal VSC-HVDC damping controller design is shown in Figure 4.6. There are three types of load models: constant power, constant current and constant impedance. The loads models in the system is constant power load and transmission

lines are modelled as nominal-pi model in RTDS. The dynamics of load and transmission lines are not considered in the mathematical modelling stage; however further studies can provide valuable information about the impact of dynamic modelling of load and transmission line on power damping controller design. Terminal 1 is connected with ac system Bus 18, importing power from the grid; Terminal 2 is connected with Bus 50, effectively in parallel with the ac transmission Line 18-50; Terminal 3 is connected with Bus 49, in parallel with the ac transmission Line 18-49. The adopted control modes for the three terminals are d-axis V_{dc} control mode and q-axis V_{ac} control mode, regulating dc voltage reference and ac voltage reference. Supplementary damping controllers are to be designed for Terminal 2 and Terminal 3, essentially designing a modulation signal V_{ac_damp} to dynamically change ac voltage reference and reactive power input or output. The transformers at PCC1-3 are modelled with parameters of benchmark systems and analysed with sensitivity studies for improved performance in system modelling and simulation process.

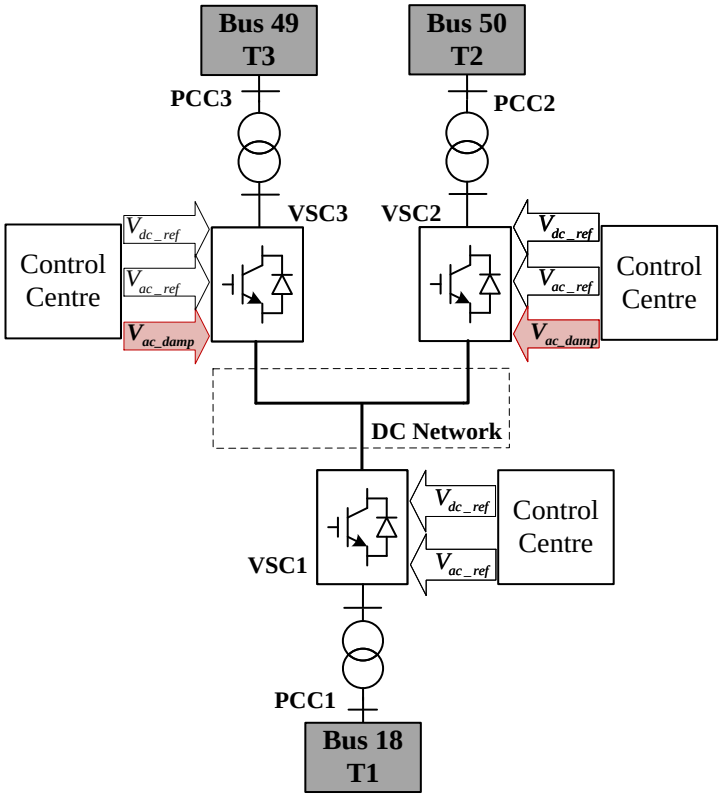

Figure 4.6 Detailed 3-terminal VSC-HVDC damping cotroller design in 68-bus test system

4.3.2 Feedback Signal Selection

Participation Factor

As mentioned in section 3.3.1, participation analysis is a great measurement for the sensitivity of an eigenvalue to a change of the diagonal element of the state matrix. It can provide ideal locations for the installation of PSSs, but without considering input and output of the system, the feedback signal candidates only lie within the state variables and thus the participation analysis alone cannot be the only criteria for choosing feedback signal for VSC-MTDC and FACTS devices. Nonetheless, the participation factor can coherently help choosing installation location of the devices.

The participation analysis in Figure 4.7 shows the involvement of each generator to each

inter-area oscillatory mode. Higher participation factor indicates that the particular generator has more influence on the weakly damped mode. It is observed in the results that inter-area oscillatory mode 1 has the contributions from generators in all the areas; mode 2 is between generator 14 and 16; mode 3 shows involvement from generators in area 1 and 2; and mode 4 is contributed by generators in area 3, 4 and 5.

As generator 14, 15 and 16 are area equivalent generators, their linkage to the other areas as single or double circuits can be seen as weak ties. In addition, these generators have relatively high power output, which further increased their participation factors in the weakly damped inter-area oscillatory modes. Whereas the rest of the generators forms NYPS and NETS areas, they have relatively low participation factors. Therefore, the VSC-MTDC connecting Area #5 and NYPS can provide efficient supplementary damping action in the vicinity as well as acting as transmission line reinforcement.

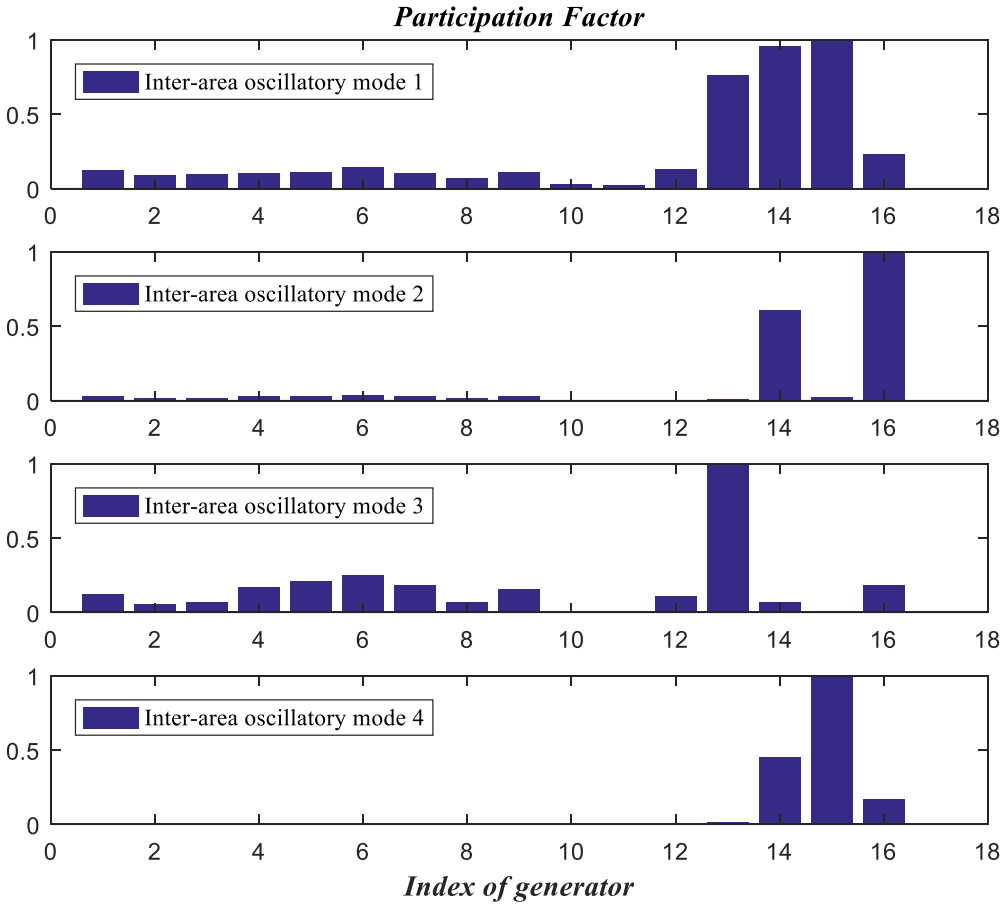

Figure 4.7 Participation factor analysis for weakly damped modes

Modal Residue Analysis

Modal residue calculation of the power flows on each transmission line is evaluated for choosing the proper feedback signal for T2 and T3 of the VSC-MTDC where supplementary controllers are located. A higher value of the modal residue means greater observability of an oscillatory mode from a power flow signal.

Figure 4.8 shows the absolute residue of system output-line power flow as feedback signal candidates for Terminal 2. It can be observed that Terminal 2 displays high residue across mode 1, 2 and 3. The modal residue analysis has the contribution of both controllability and

observability. The controllability of terminal 2 is high because it's connected with Bus 50 and the HVDC transmission line is in parallel with the heavily loaded ac transmission Line 73 (Bus 18-50), shown in Figure 4.2 in the previous section. The heavily loaded transmission line and weak links between areas are some of the key causes for weakly damped inter-area oscillation. Therefore, the VSC-HVDC link between Bus (18-50) acts as both transmission line reinforcement as well as damping controllers with high controllability.

In the state space equations, the modal observability is determined by Cv_i, varied by different system output (controller input). Therefore, the modal residue for the particular damping controller design is determined by the observability of the various system outputs. Thus finding the proper feedback signal as controller output with the balanced modal residues on the weakly damped inter-area modes is the objective of modal residue analysis.

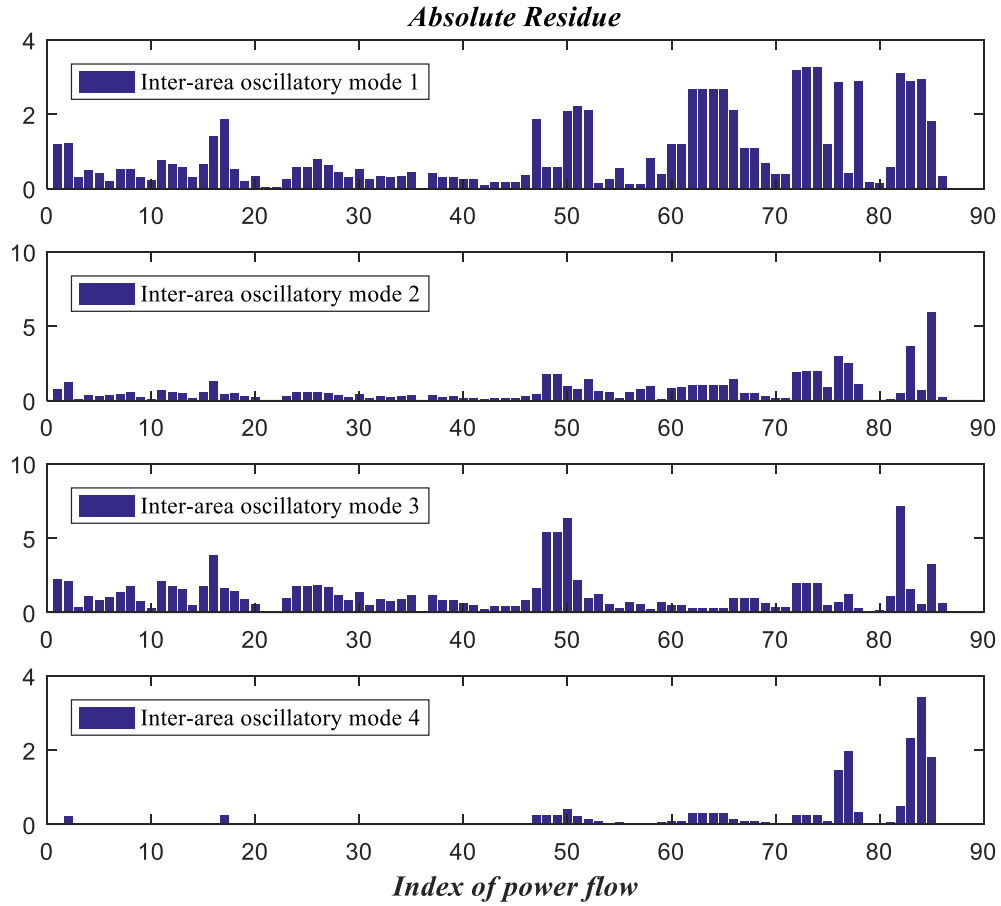

Figure 4.8 Absolute residue of line power flow for T2 damping controller

Terminal 3 bears relatively low residue compared to Terminal 2 shown in Figure 4.9, because the transmission line power flow from Bus 18 to Bus 49 is not as significant as Bus 18 to Bus 50 and Bus 49 voltage stability suffers less than that of Bus 50. However, it has great potential to provide damping to the mode 4 which not covered by the control objective of Terminal 2, since Bus 49 is more correlated with area 3 and 5.

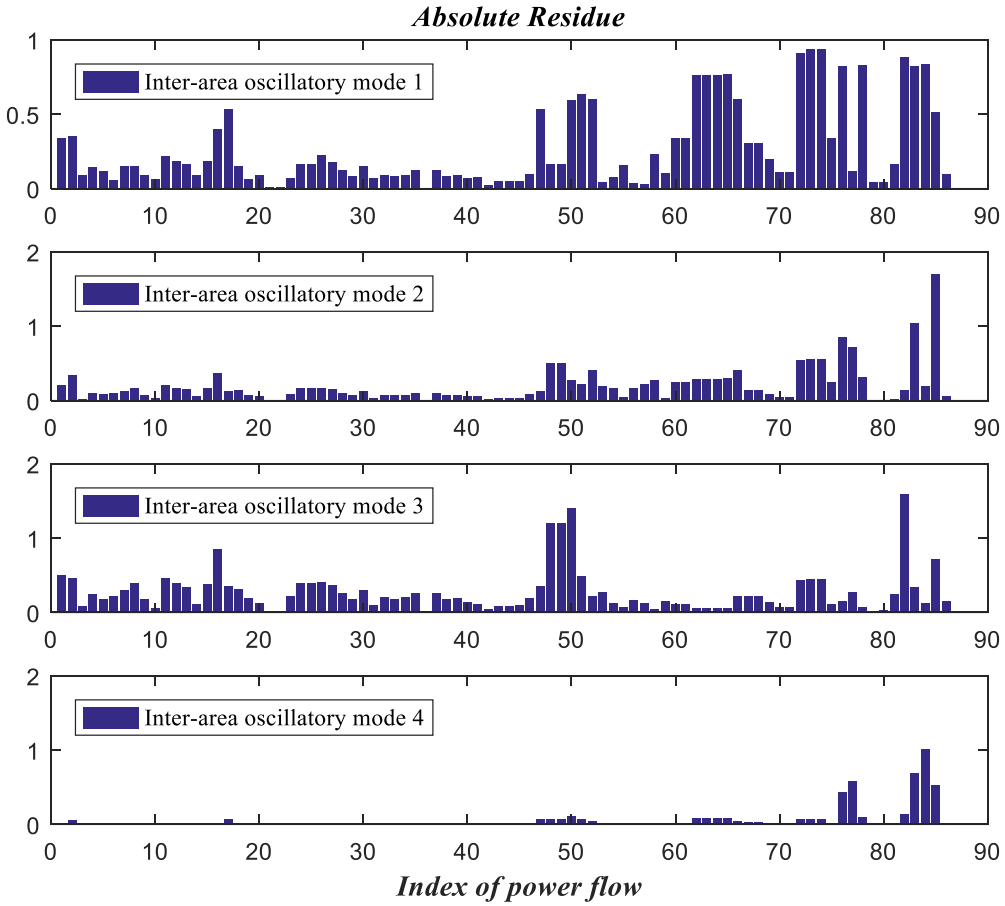

Figure 4.9 Absolute residue of line power flow for T3 damping controller

To conclude, feedback signal selection for Terminal 2 is to select a signal which has high residue on mode 1, 2 and 3 but relatively low residue on mode 4 to avoid adverse interaction between different controllers. Similarly, feedback signal for Terminal 3 should have high residue on mode 4 but little residue on the other modes.

Based on the criteria listed above, damping control signal for Terminal 2 is the power flow on Line 73 (Bus 18-50) and the feedback signal for Terminal 3 is the power flow on Line 84 (Bus 42-15), shown in Figure 4.10.

The modal residue analysis carried out in this study is focused on the magnitude of the

residues. Additional feedback signal selection criteria such as less variation of magnitude and phase angle and less sensitivity to other modes can also be introduced for a more comprehensive analysis of the feedback signal and control effort [149, 150].

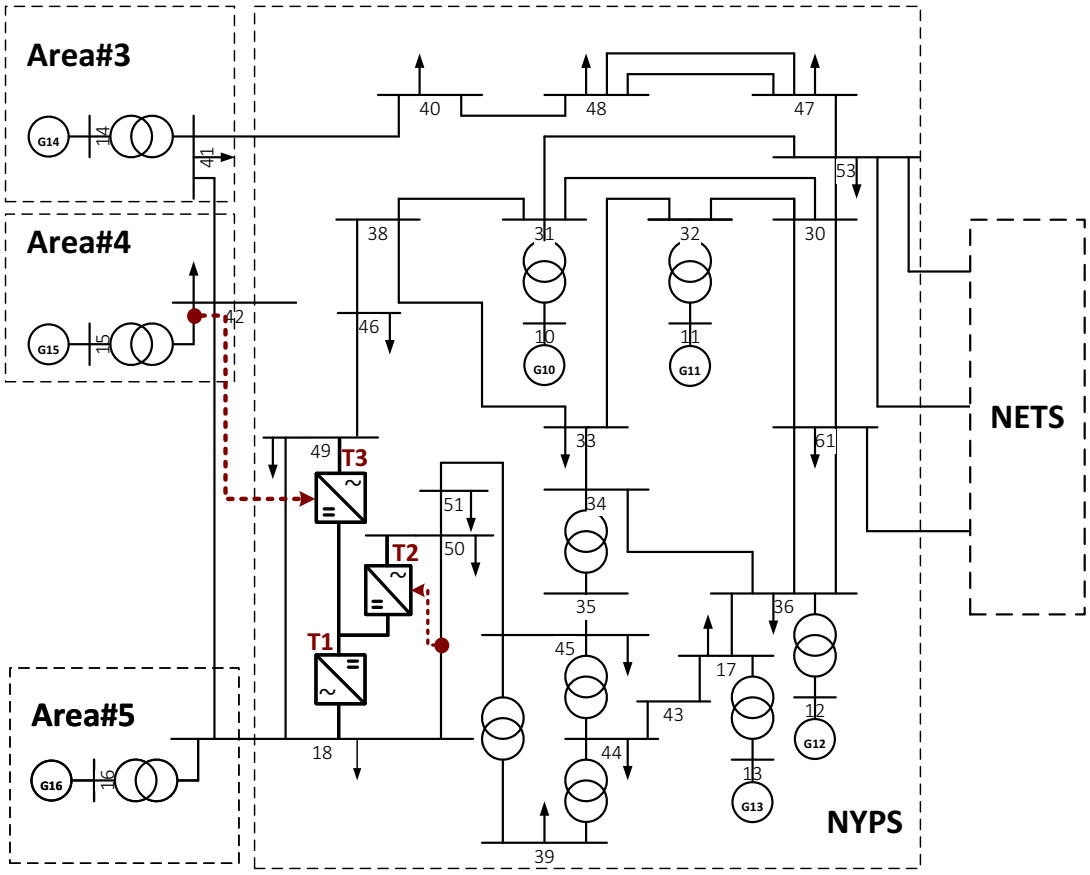

Figure 4.10 Feedback signal locations for Terminal 2 and 3

4.3.3 Damping Controller Design for T2 of VSC-MTDC

Supplementary damping controller for Terminal 2 in the NYPS-NETS power system is firstly designed with the sequential design approach. In the sequential design, the first loop closure is formulated by designing the damping controller T2 and the next damping controller would be based on the close-loop system and treat it as the new open-loop system for the next design.

System Order Reduction

System model formulation results in the order of the original system to be 163 and if unreduced, the damping controller design and controller order will be over-complex and impractical to be implemented in power systems. Thus it's mandatory to reduce the system order to a manageable level and in the meantime the reduced system should retain vital information of the original system and be a good approximation of the original system in the frequency range of interest. Balanced modal truncation system reduction is carried out to reduce the system order to 7.

Table 4.7 lists the eigenvalues corresponding mode 1, 2 and 3 with their damping ratios and oscillation frequency. For comparison, the eigenvalues of the original full-order system are shown in Table 4.8.

Table 4.7 Eigenvalue analysis of reduced 7th order system

Mode Index	*Eigenvalues*	ζ	f *(Hz)*
1	-0.166681±2.554124i	6.5%	0.407
2	-0.194058±3.506565i	5.5%	0.558
3	-0.293981±3.961732i	7.4%	0.631
/	-16.050958	/	/

Table 4.8 Eigenvalue analysis of the original full-order system

Mode Index	*Eigenvalues*	ζ	f *(Hz)*
1	-0.163563±2.551184i	6.4%	0.406
2	-0.179508±3.489296i	5.1%	0.555
3	-0.345977±4.018322i	8.6%	0.640

Since Terminal 2 has relatively low observability to mode 4, the reduced system only preserves the first three modes and mode 4 is removed for damping control design. Frequency response of the original system and reduced system in Figure 4.11 clearly shows the system reduced to be valid since bode diagram of the reduced and original system are almost identical

with few disparities, as the balanced truncation model retained the most significant states with high controllability and observability [41].

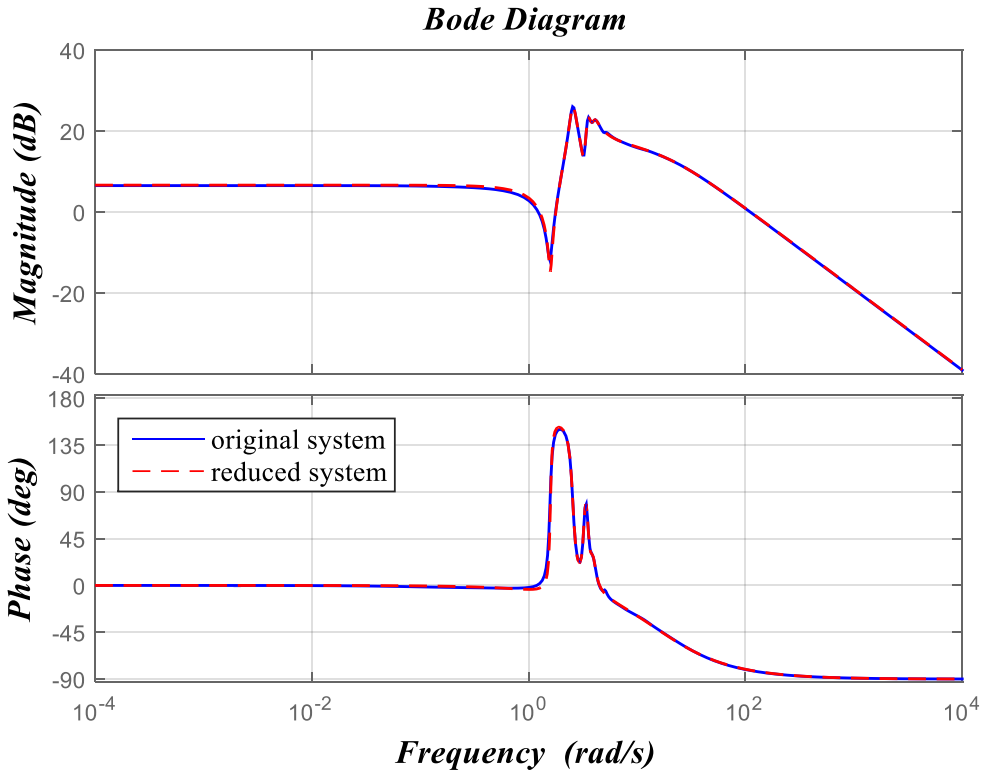

Figure 4.11 Bode diagram comparison

Control Objective Specification and State-Space Realization

Regional pole placement boundary is set to be 10% to ensure satisfactory settling time of the power system under disturbances, as it often set in many operational guidelines. Additionally, control effort optimization is include to ensure practical design [41]. The state-space realization is represented by:

$$
\begin{aligned}
&x = A_i x + B_i u \\
&z_2 = u \\
&y = C_i x + w \\
&i = 1, 2, 3, 4.
\end{aligned}
\tag{4.4}
$$

Controller State-Space Representation and Transfer Function

By solving the optimization problem through the two-step approach, controller state-space representation is given with the following matrices:

$$
A_{T2} = \begin{bmatrix}
242.83 & 117.34 & 6539.40 & 2344.30 & 47042.21 & 1768.45 & 61177.65 \\
58.76 & 26.16 & 1254.20 & -291.13 & 4326.92 & -6970.14 & -20020.46 \\
-19.31 & -15.06 & -507.41 & -186.44 & -3442.3 & 74.85 & -3376.87 \\
-2.85 & -0.75 & -56.33 & 32.79 & -111.46 & 478.96 & 1489.33 \\
1.34 & 1.01 & 34.51 & 10.23 & 220.16 & -32.74 & 137.85 \\
0.11 & -0.02 & 1.82 & -2.99 & -4.29 & -31.36 & -103.02 \\
-0.07 & -0.04 & -1.84 & -0.11 & -10.66 & 5.46 & -0.65
\end{bmatrix}
\tag{4.5}
$$

$$
B_{T2} = \begin{bmatrix} -2.42 & -0.84 & 0.20 & 0.46 & -0.014 & -0.0022 & 0.00088 \end{bmatrix}
$$

$$
C_{T2} = \begin{bmatrix} -0.99 & -17.21 & -41.80 & -382.20 & -318.07 & -1898.23 & 36.0839 \end{bmatrix}
$$

Transfer function for Terminal 2 controller is

$$
T_{T2}(s) = \frac{0.059(s^2 + 23.441s + 97.469)(s^2 + 2.040s + 3.972)(s^2 + 1.209s + 3.095)}{(s + 9.868)(s^2 + 1.496s + 3.904)(s^2 + 0.934s + 3.162)(s^2 + 5.196s + 2.021)}
\tag{4.6}
$$

4.3.4 Damping Controller Design for T3 of VSC-MTDC

The first close-loop is formed with Terminal 2 controller in (4.6) and the updated system order is increased to 170 with the original system order 163 and T2 damping controller order 7. The first close-loop system is regarded as the new open-loop system for Terminal 3

damping controller design. Similar procedures such as system order reduction, control objective specification and state-space formulation are taken to solve the optimization problem and produce the controller for Terminal 3.

System Order Reduction

Balanced modal truncation is used to reduce the system order from 170 to 7. Eigenvalue analysis is carried out to check the poles of the reduced system, shown in Table 4.9. It's clear to see that mode 1, 3 and 4 can be observed in Terminal 3 damping controller design. The damping ratio of mode 1 has been greatly improved to 14.5% with the previous implementation of Terminal 2 damping controller, as the improved modes in damping controller 1 design are mode 1, 2 and 3. The eigenvalues of the original full-order system are listed in Table 4.10 for comparison with the reduced system.

Table 4.9 Eigenvalue analysis of reduced 7th order system

Mode Index	*Eigenvalues*	ζ	f *(Hz)*
1	-0.359867±2.514570i	14.2%	0.400
/	-2.831526	/	/
3	-0.296361±3.770227i	7.8%	0.600
4	-0.256082±5.042180i	5.1%	0.802

Table 4.10 Eigenvalue analysis of the original full-order system

Mode Index	*Eigenvalues*	ζ	f *(Hz)*
1	-0.309486±2.477115i	12.4%	0.349
3	-0.327012±3.452014i	9.4%	0.549
4	-0.264863±5.053595i	5.2%	0.804

Frequency response of the original system and reduced system in Figure 4.12 clearly shows the system reduced to be valid since bode diagram of the reduced and original system are almost identical with few disparities, as the balanced truncation model retained the most significant states with high controllability and observability [41].

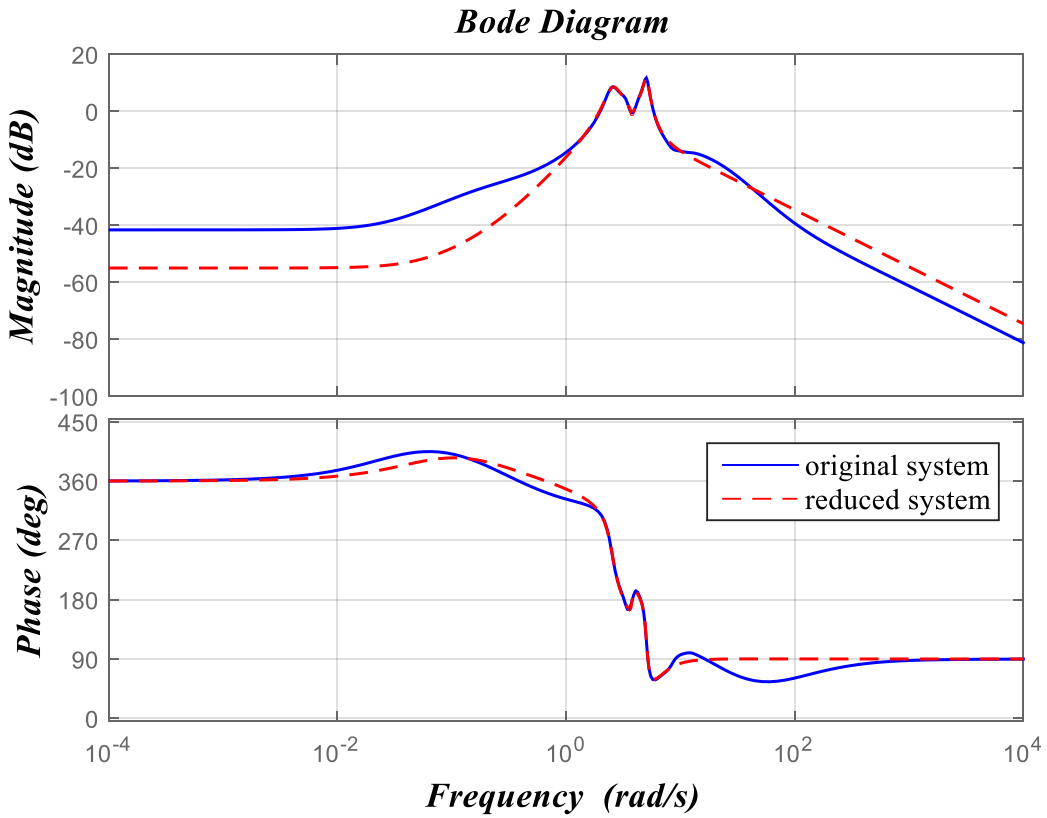

Figure 4.12 Bode diagram comparison

Control Objective Specification and State-Space Realization

Similar to the control objectives specified in Terminal 2 damping controller design, regional pole placement and control effort optimization are defined and solved via a two-step method.

Controller State-Space Representation and Transfer Function

$$A_{T3} = \begin{bmatrix} -2.672 & -35.97 & -74.88 & -466.17 & -806.14 & -2235.50 & -3918.20 \\ -0.211 & -9.428 & -74.34 & -180.20 & -863.61 & -482.25 & -1240.62 \\ -0.101 & 0.1171 & -5.33 & -19.43 & -63.26 & -89.63 & -160.03 \\ 0.0712 & 0.5614 & 5.349 & 10.85 & 50.52 & 30.61 & 74.67 \\ 0.0019 & 0.0310 & 0.1311 & 1.79 & 2.01 & 4.75 & 8.95 \\ -0.0045 & -0.035 & -0.27 & -0.70 & -2.21 & -2.13 & -5.19 \\ -0.00018 & -0.00034 & 0.0068 & -0.018 & 0.04 & 0.79 & -0.282 \end{bmatrix} \quad (4.7)$$

$$B_{T3} = [0.6634 \quad -0.6049 \quad -0.0131 \quad 0.0342 \quad -0.000709 \quad -0.0020 \quad 0.000135]$$

$$C_{T3} = [-0.9975 \quad -4.2209 \quad -27.3267 \quad -91.7726 \quad -148.92 \quad -294.805 \quad 29.972]$$

Transfer function for Terminal 3 controller is

$$T_{T3}(s) = \frac{0.157(s^2 - 7.685s - 27.874)(s^2 + 0.954s + 3.372)(s^2 + 0.719s + 2.548)}{(s + 2.810)(s^2 + 2.278s + 5.218)(s^2 + 1.090s + 3.690)(s^2 + 0.804s + 2.487)} \tag{4.8}$$

4.3.5 Linear Eigenvalue Evaluations

Linear eigenvalue analysis is carried out on three different scenarios: T2 controller close-loop system, T3 controller close-loop system and both T2 and T3 controller close-loop system. As T2 and T3 damping controllers are designed with different sensitivities to the inter-area modes, such improvement for the pre-designed modes can be observed in the eigenvalue characteristics below. And for the close-loop system with both controllers installed, the synthetic control effort can ameliorate the damping ratios across all four modes.

Table 4.11 lists the damping ratio and frequencies of four inter-area modes under four operating points with T2 damping controller in place. It can be observed that mode 1, 2 and 3 are improved into the more desirable damping ratio zone and since mode 4 is neglected in this design stage, it remains under-damped. In general, T2 VSC-MTDC damping controller exhibits great control effort across the first 3 modes, proving the controller's controllability and the selected feedback signal's observability on these modes to be effective.

Table 4.11 System performance with T2 VSC-MTDC damping controller

Operating points	*Mode 1*		*Mode 2*		*Mode 3*		*Mode 4*	
	ζ	f (Hz)	ζ	f (Hz)	ζ	f (Hz)	ζ	f (Hz)
1	**12.6%**	0.394	**9.5%**	0.550	**11.6%**	0.641	5.2%	0.805

2	**12.4%**	0.394	**9.5%**	0.549	**11.5%**	0.642	5.2%	0.804
3	**12.1%**	0.396	**9.4%**	0.551	**11.3%**	0.641	5.2%	0.804
4	**12.0%**	0.396	**9.6%**	0.550	**11.2%**	0.640	5.2%	0.804

Another scenario is that only T3 VSC-MTDC damping controller is installed in the system. Although the T3 damping controller is designed based on the close-loop system formed by T2 damping controller and the open-loop system, it still can be implemented alone and possesses the capability of enhance system small-signal stability by itself. Shown in Table 4.12, T3 damping controller focuses its control effort on inter-area mode 4, uplifting its damping ratio from 5.2% to more than 10%. The results are consistent with the alterations of different operating point, demonstrating the controller's robustness against changes of operating conditions.

Table 4.12 System performance with T3 VSC-MTDC damping controllers

Operating points	*Mode 1*		*Mode 2*		*Mode 3*		*Mode 4*	
	ζ	f (Hz)	ζ	f (Hz)	ζ	f (Hz)	ζ	f (Hz)
1	6.38%	0.40	5.10%	0.55	8.60%	0.64	**10.8%**	0.82
2	6.40%	0.40	5.14%	0.56	8.58%	0.64	**10.8%**	0.82
3	6.40%	0.41	5.21%	0.56	8.63%	0.64	**10.8%**	0.81
4	6.41%	0.41	5.20%	0.55	8.61%	0.64	**10.6%**	0.81

Lastly, both controllers are installed on the original open-loop system, forming a close-loop system of 177th order. The combined control effort enables all the modes to be adequately damped and the system small-signal stability is properly enhanced.

Table 4.13 System performance with both T2 and T3 VSC-MTDC damping controllers

Operating points	*Mode 1*		*Mode 2*		*Mode 3*		*Mode 4*	
	ζ	f (Hz)	ζ	f (Hz)	ζ	f (Hz)	ζ	f (Hz)
1	**11.9%**	0.39	**9.5%**	0.55	**10.0%**	0.64	**11.0%**	0.82
2	**11.8%**	0.40	**9.6%**	0.55	**10.0%**	0.64	**11.1%**	0.82
3	**11.1%**	0.40	**9.5%**	0.56	**10.0%**	0.64	**11.1%**	0.81
4	**11.7%**	0.40	**9.4%**	0.55	**10.0%**	0.64	**11.0%**	0.81

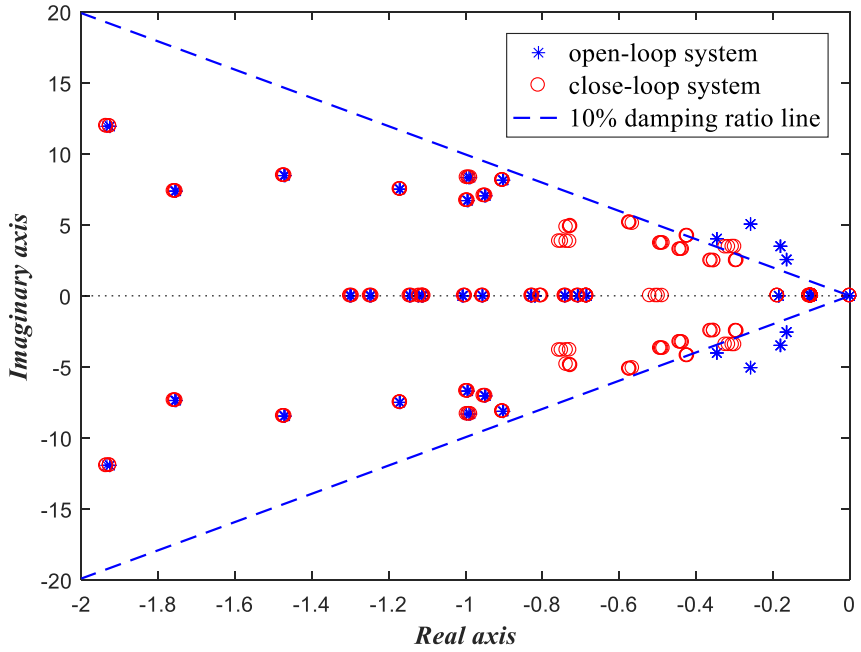

Figure 4.13 Eigenplot under all operating points

By plotting the poles onto the complex plane, the system damping characteristics comparison between the original open-loop system and close-loop system with both controllers installed can validate the effectiveness of the design in respect of the linear system performance.

4.3.6 Real-Time Simulation Case Studies

With the powerful real-time digital simulator facility, system disturbance case studies can be conducted on the platform for detailed and accurate real-time simulation of the specific test system and the designed supplementary damping controllers. By setting different scenarios of system disturbances, the validity of the controllers is examined by their capability to suppress inter-area oscillations. Original and close-loop system performances under the same operating condition and disturbance are plotted onto the same diagram with clear contrast. A series of the diagrams are made with the changing of operating conditions, as well as in respect of types of disturbances. The disturbances introduced to the system are organized as follows: excitation system disturbance, load step change and transmission line outage. The

corresponding results and comments are shown in the following sections.

Excitation System Disturbance

The excitation system disturbance proposed in this study is induced by a step-up change of the exciter voltage reference for the G14 synchronous generator. The initial value for the voltage reference is 1.01pu and it endures an increase to 1.03 pu for 50ms. This small disturbance causes the loss of synchronism among generators and also inter-area oscillation, which can be observed on the graphs of system parameters such as line power flow in Figure 4.14. Power flow on Line 73 (Bus 18-50) is used to demonstrate the functions of the damping controllers under such circumstances. It can be observed that the active power flow goes through an oscillation with decaying magnitude and regains equilibrium after a certain period of time. As the damping controllers have improved the damping ratios of the poorly damped modes and the rate of decay is determined by the magnitude of the damping ratio, the oscillations observed in Figure 4.14 show shorter settling time compared to the original open-loop system without damping controllers.

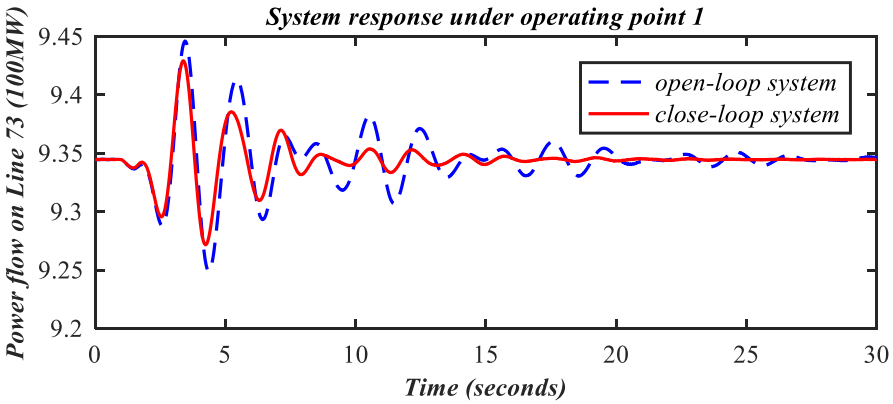

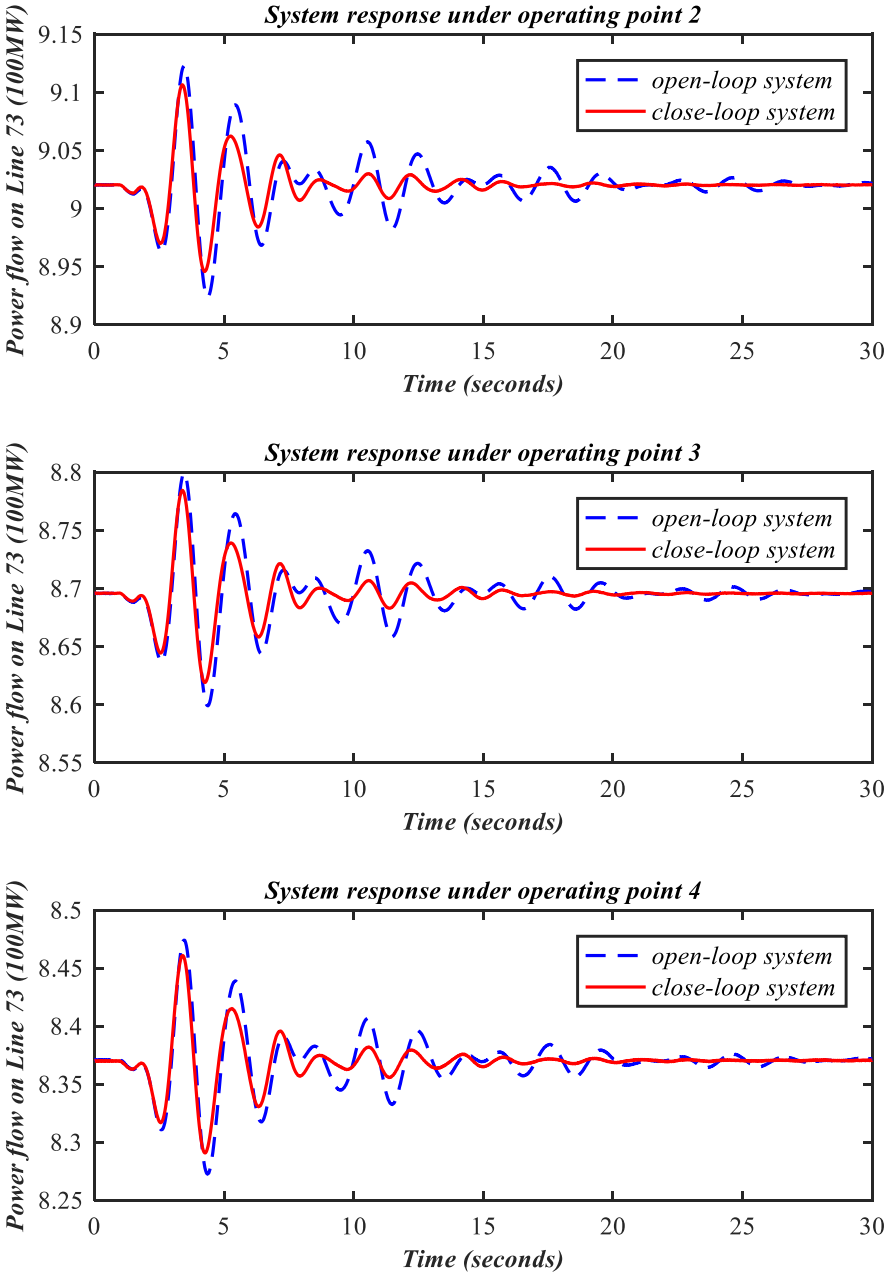

Figure 4.14 System response to excitation system disturbance on power flow of Line 73

Load Variation

Another category of disturbance is the active power variation of loads. In this particular scenario, load 41 is permanently changed from 1000MW to 800MW, which is observed by the power flow on the adjacent Line 78 (Bus 41-40). The decease of load power on the

sending terminal of Line 78 introduces the increment of active power flow on this line. Although load variation with such scale is not considered to be a small disturbance and does not fall into the small signal stability scope, it's fruitful to consider this type of disturbance in a small-signal stability study as it's essentially changing the operating points of the system and a great way to test the controller robustness. It's worthy to mention that although changing the load characteristics of the system lead to system model change, it's essential to test the controller's robustness under this varied system operating condition which is not included in the design stage. The purpose of the test is to check if the controllers can perform their functionality to improve system damping in the situations that are not previously defined in the modelling stage.

Besides, given the supplementary damping controller is primarily designed for small disturbances, its capability to enhance system stability under large disturbances further validates the controller effectiveness. The results in Figure 4.15 show that the controllers can effectively deliver sufficient damping under the new operating condition. And the decrease of system settling time indicates the faster decay rate and higher percentage of damping ratios, which are provided by the supplementary damping controllers.

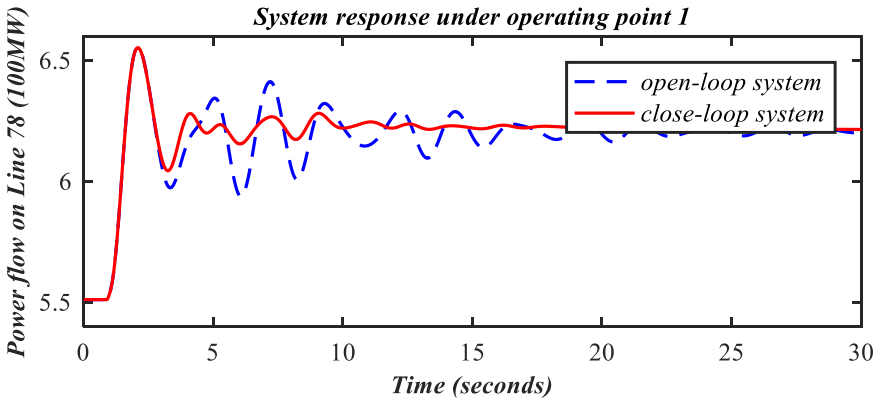

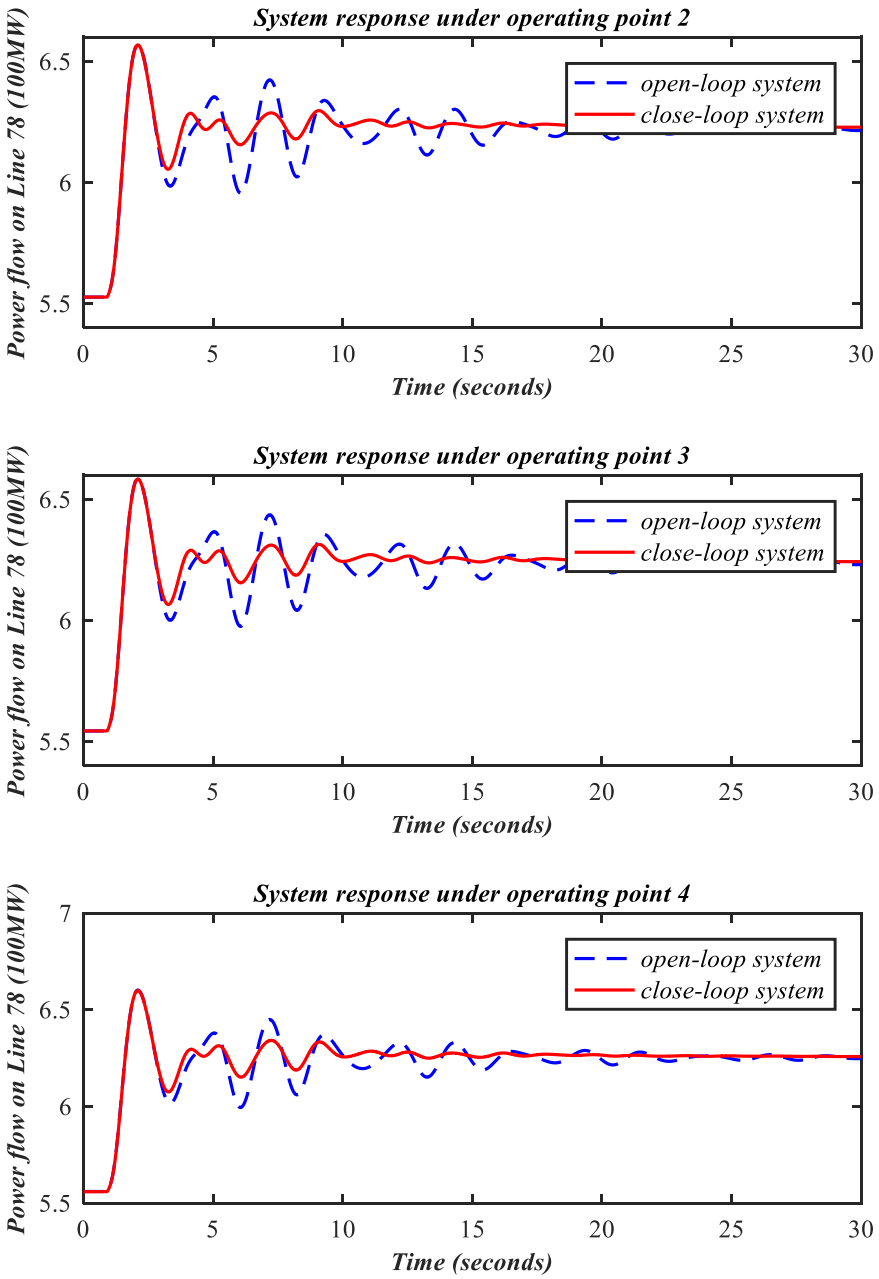

Figure 4.15 System response load variation on power flow of Line 78

Line Outage

Considering system disturbances and contingencies, outage of transmission lines, especially the ones that connect two areas, are one of the most fatal kind. Without proper pre-fault design and calculation, losing one of the transmission corridors could potentially cause overloading on the other transmission lines and jeopardize the safe and reliable operation of

power systems. Therefore, in this example of system disturbance, one of the transmission lines connecting NTPS and NETS endures a three-phase to ground fault and subsequently drops out of service. A three-phase to ground fault is introduced to the system to test the controller validity. It's often seen as more severe than single-phase to ground faults and the three-phase to ground fault introduced more disturbance than single-phase fault because of the larger fault current. This onerous fault would lead to the tripping of one transmission line, changing the topology of the power system. Thus, it's worthy to test the effectiveness of the controllers under the system modal uncertainties.

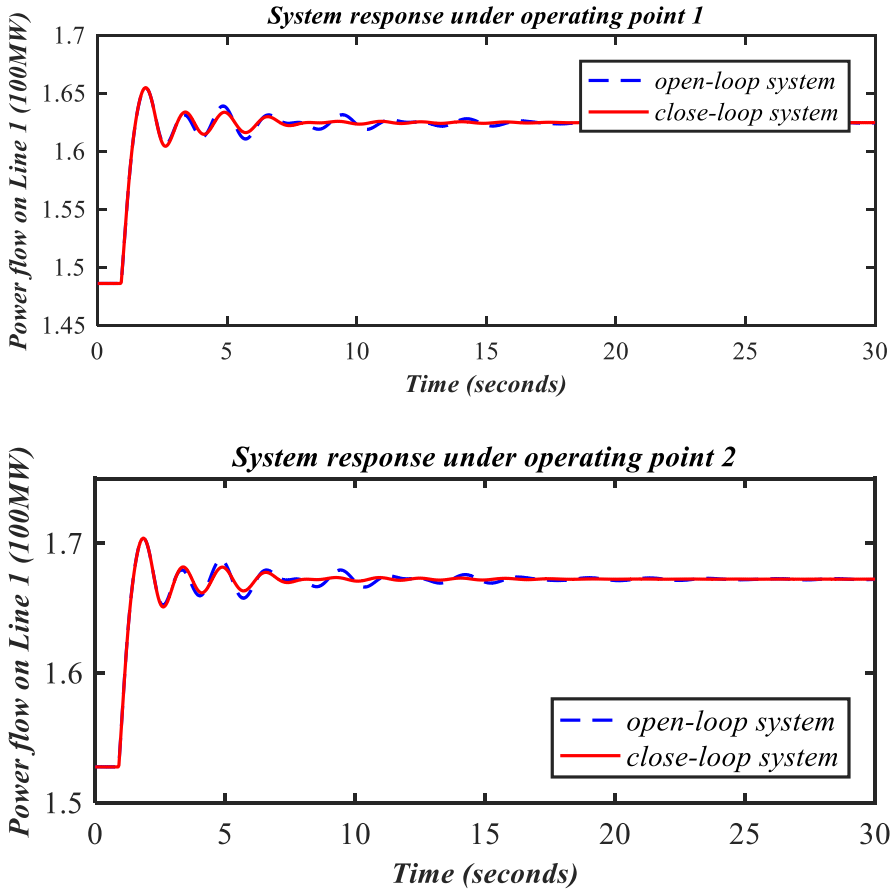

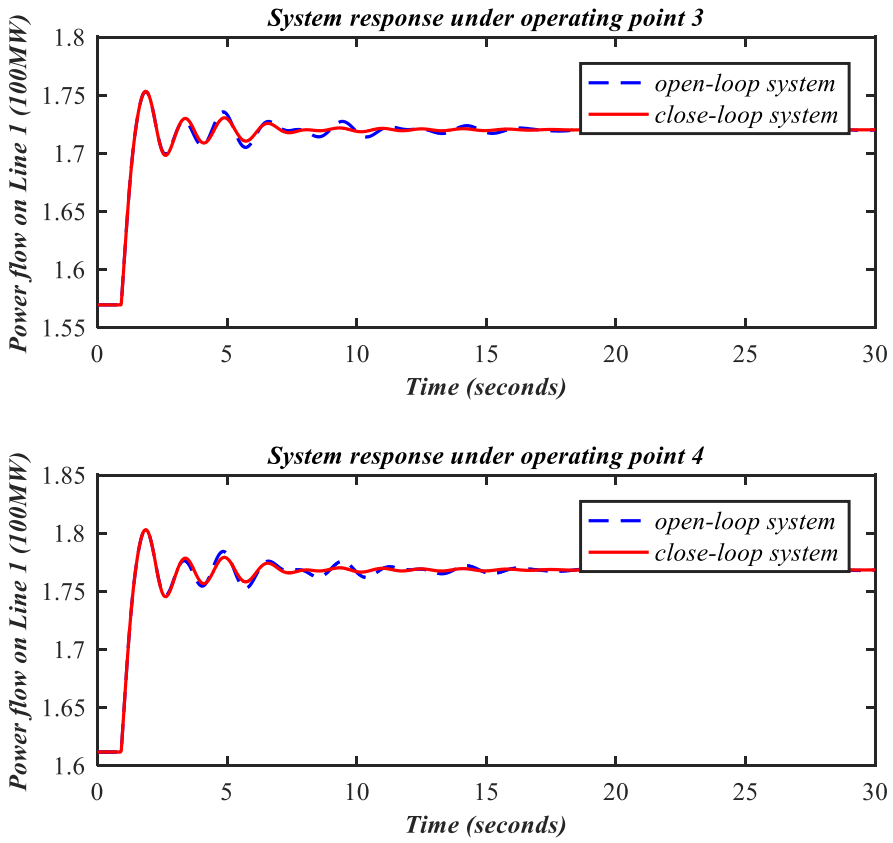

Figure 4.16 System response to line outage on power flow of Line 1

The system response is shown in Figure 4.16. To maintain the amount of active power transfer between these two systems, an increase of active power on Line 1 can be observed. The results show the oscillation ripples die down faster than the open-loop system, which indicates increased damping ratio of the previously identified weakly damped modes. The supplementary damping provided by the controllers is thus tested to be effective.

Discussion:

The common phenomenon from the simulation results is that the decrease period of settling time after the disturbances/faults. Compared to the open-loop system, the rate of decay of the inter-area oscillatory modes is much faster for the close-loop system with the installation of both damping controllers. By actively regulation of the references of the ac voltage of the

VSC-MTDC, the damping controllers has provided effective supplementary damping efforts for the power system. In each case, the controllers can suppress the oscillations within 20 seconds and also exhibit robustness against alterations of system operating points as well as the disturbance type, corroborating the numerical results obtained from the eigenvalue analysis of linear system performance. The real-time simulation in RTDS has included the other types of dynamics that is not include in the design stage, such as load, transmission line, governors, and the electromagnetic transients. In the designed system model, such details are not considered and this can potentially result in the difference of simulation results. As the controller is designed based on linearized power system, it's functionality may be underrated in the complicated power system with non-linear properties. Nevertheless, the RTDS simulations has brought the more complex power system into consideration and can indicate the key elements for future research.

4.4 Summary

This chapter implemented the coordinated robust damping control methodology introduced in Chapter 3 onto two of the three terminals of a VSC-MTDC. The device was embedded in the 5-area 16-machine 68-bus reduced equivalent NYPS-NETS power system which is a benchmark model for small signal analysis and control theory implementation. The multi-machine characteristic of the test system and the exhibition of multiple inter-area oscillatory modes rendered it suitable for damping control design. The control objective was to improve the four identified weakly damped inter-plant modes into the desirable range of damping ratios, ideally more than 10%. The mode shapes gave key information of the contribution of individual generator or groups of generators to a particular mode. In addition to participation factor analysis, modal residue of each system output indicated the controllability and

observability to the weakly damped modes and it was used to select a proper feedback signal to effectively allocate the control effort to suppress inter-area oscillations. Therefore, two power flow signals Line 73 and 84 were chosen as the feedback signals for T2 and T3 VSC-MTDC respectively.

The synthesis control target of regional pole placement and control effort optimization was formed as a BMI-based multi-objective multi-model optimization problem and subsequently solved via the two-step approach proposed in Chapter 3. A couple of SISO controllers were obtained and installed in the Terminal 2 and 3 q-axis ac voltage control side to dynamically modulate ac voltage reference. The performance of the controllers was tested with linear system performance analysis and real-time digital simulations. Consistent results from two software packages, MATLAB and RSCAD, have validated the effectiveness of the controllers in improving system small-signal stability and the robustness of the controllers was confirmed by the overall performance under multiple system operating points as well as various types of disturbances. Furthermore, with the coordinated design, no adverse effect between these two controllers was observed, which has improved the safety of the operation of power system.

CHAPTER 5 ROBUST COORDINATED DAMPING CONTROL DESIGN OF VSC-MTDC AND FACTS

5.1 Introduction

The coordinated robust damping control design for VSC-MTDC presented in Chapter 4 mainly focused on the coordinated design of different terminals of a single device. For a practical power system with various types of electrical and electronic components, it's beneficial to consider coordination damping control incorporating other devices such as FACTS, so that they can provide supplementary damping to the power system in addition to their primary functions.

In this chapter, a series of SISO damping controllers for one terminal of VSC-MTDC and TCSC are designed sequentially with the control methodology introduced in Chapter 3 and also applied in Chapter 4. Multiple devices are utilized to cover all four modes of weakly damped inter-area oscillations of the test system which is the 5-area 16-machine 68-bus reduced equivalent NYPS-NETS power system. The sequential approach allows the design to be carried out without extra decoupling procedure like a MIMO controller and thus increases the reliability of the controllers, as when one input signal fails, it won't necessarily jeopardize the other signals so that the remainder controller could maintain operable and provide system

damping. Linear system performance analysis and real-time digital simulation are applied to examine the feasibility of the proposed design and test the validity of the damping controllers.

5.2 Robust Coordinated Damping Controller Design for VSC-MTDC and FACTS

5.2.1 Test System Small-Signal Modelling and Eigenvalue Analysis

The test system for controller design used in this chapter is the 5-area 16-machine 68-bus reduced equivalent NYPS-NETS power system introduced in Figure 4.2 and to establish system multi-model, a few typical operating conditions are incorporated in the design stage. By varying active power consumption of Load 18, operating points 1-4 can be obtained, shown in Table 5.1.

Operating Points	*Load 18(MW)*
1	2470
2	2570
3	2670
4	2770

Table 5.1 Operating points selection

Eigenvalue analysis of the system gives the following results under each operating point in Table 5.2, Table 5.3, Table 5.4 and Table 5.5. Inter-area oscillation frequencies around 0.4 Hz, 0.5Hz, 0.6Hz and 0.8Hz show lack of damping.

Table 5.2 Damping ratio, frequency and Eigenvalues of Mode 1

Operating points	*Mode 1*		
	ζ	f (Hz)	*Eigenvalue*
1	7.7%	0.358	-0.173601±2.247613i
2	7.7%	0.358	-0.174548±2.251230i
3	7.7%	0.359	-0.175096±2.254221i
4	7.8%	0.359	-0.175584±2.255911i

Table 5.3 Damping ratio, frequency and Eigenvalues of Mode 2

Operating points	*Mode 2*		
	ζ	f (Hz)	*Eigenvalue*
1	4.8%	0.544	-0.165008±3.419049i
2	4.9%	0.544	-0.166403±3.420535i
3	4.9%	0.544	-0.167392±3.420645i
4	4.9%	0.544	-0.168496±3.420216i

Table 5.4 Damping ratio, frequency and Eigenvalues of Mode 3

Operating points	*Mode 3*		
	ζ	f (Hz)	*Eigenvalue*
1	8.6%	0.637	-0.344483±4.002225i
2	8.6%	0.637	-0.344573±4.004608i
3	8.6%	0.638	-0.344766±4.007213i
4	8.6%	0.638	-0.344603±4.007145i

Table 5.5 Damping ratio, frequency and Eigenvalues of Mode 4

Operating points	*Mode 4*		
	ζ	f (Hz)	*Eigenvalue*
1	4.9%	0.798	-0.247114±5.015753i
2	4.9%	0.798	-0.246810±5.013406i
3	4.9%	0.798	-0.246776±5.013772i
4	4.9%	0.798	-0.246877±5.012599i

The Eigenplot of the open-loop system in Figure 5.1 presents the locations of the poles in the complex z-plane and relative positions to the 10% damping ratio line. The complex conjugate pairs of poles outside the conic area are considered to be weakly damped and observed to have a slower decay rate of the oscillation.

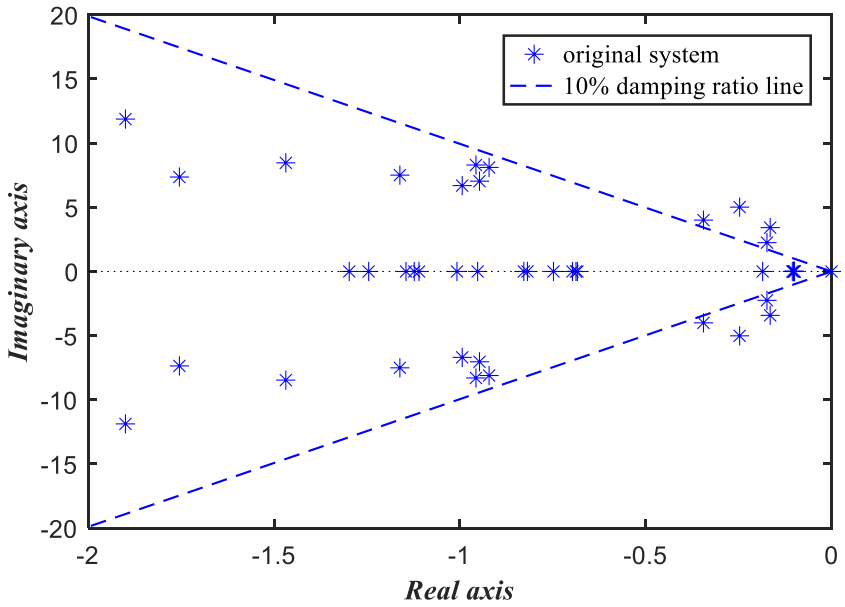

Figure 5.1 Eigenplot of the original open-loop system

VSC-MTDC and TCSC Installation Location and Control Mode

In this Chapter, VSC-MTDC and TCSC is considered for coordinated robust damping control study and the VSC-MTDC installation location is remained the same as Chapter 4: a 3-terminal VSC-HVDC with $V_{dc} - V_{ac}$ control mode is connected to Bus 18, Bus 50 and Bus 49 in radial formation. Hence the location of TCSC is to be determined. From the mode shape analysis, it can be observed that Area #3 equivalent generator 14 has great contribution regarding inter-area oscillatory modes 1, 2 and 4; therefore, it is proposed that the installation location of the TCSC is between Bus 41 and Bus 40 to increase power transfer capability and increase system damping. To cover all four poorly damped modes, damping controllers for Terminal 2 of the VSC-MTDC and TCSC are to be designed sequentially.

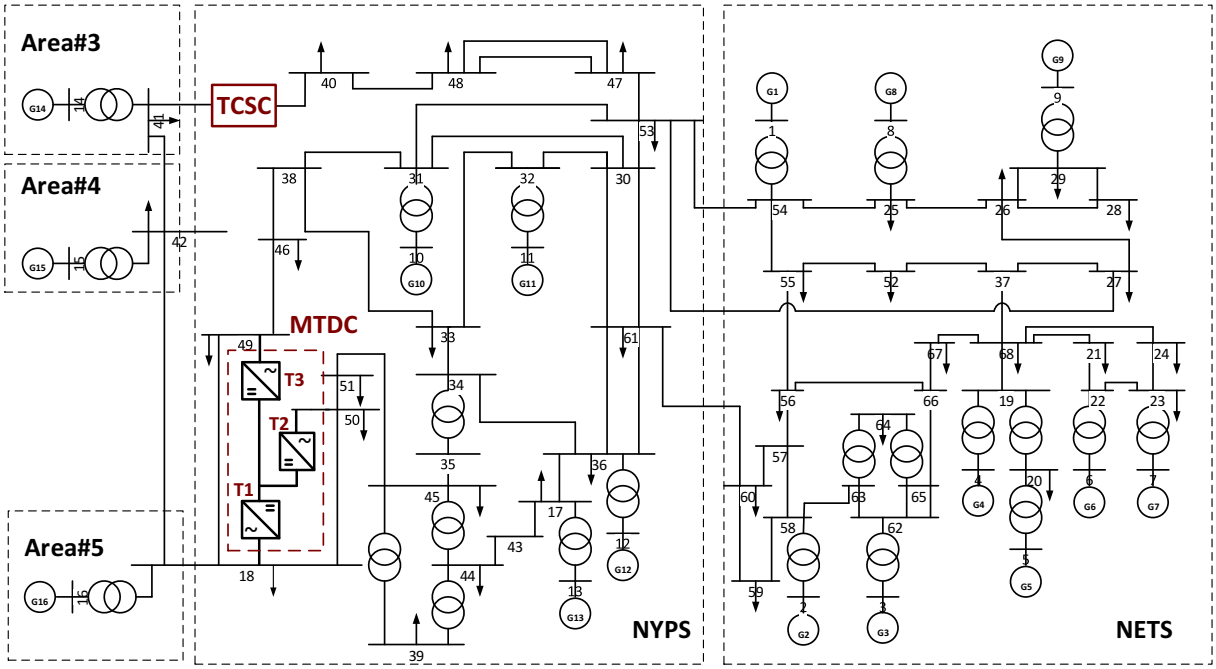

Figure 5.2 VSC-MTDC and TCSC installation location

5.2.2 Feedback Signal Selection

To select proper feedback signals for Terminal 2 of VSC-MTDC and TCSC, participation factor and modal residue analysis are adopted to assess power system output candidates as damping controller input.

Participation Factor

The participation factor analysis of generator states to the selected weakly damped oscillatory modes for the system with 3-terminal VSC-HVDC and TCSC is shown in Figure 5.3. For a small power system with only a few generators, participation factor can help choosing a synthesis signal from generator speed as the feedback signal for damping controllers. However, in a bulk power system, generator states alone cannot guarantee the level of observability to multiple inter-area oscillatory modes even with the highest participation

factor. Nevertheless, participation factor analysis is crucial to profile the inter-area oscillatory mode shapes. It can be observed from the graph that mode 1 is between generator groups in Area #1, 2 and single generator equivalent Areas#3, 4, 5; mode 2 is more asscociated with Area #3 and Area #5; mode 3 is between NYPS and NETS and mode 4 is between Area #3,5 and Area #4.

As generator 14, 15 and 16 are area equivalent generators, their linkage to the other areas as single or double circuits can be seen as weak ties. In addition, these generators have relatively high power output, which further increased their participation factors in the weakly damped inter-area oscillatory modes. Whereas the rest of the generators forms NYPS and NETS areas, they have relatively low participation factors.

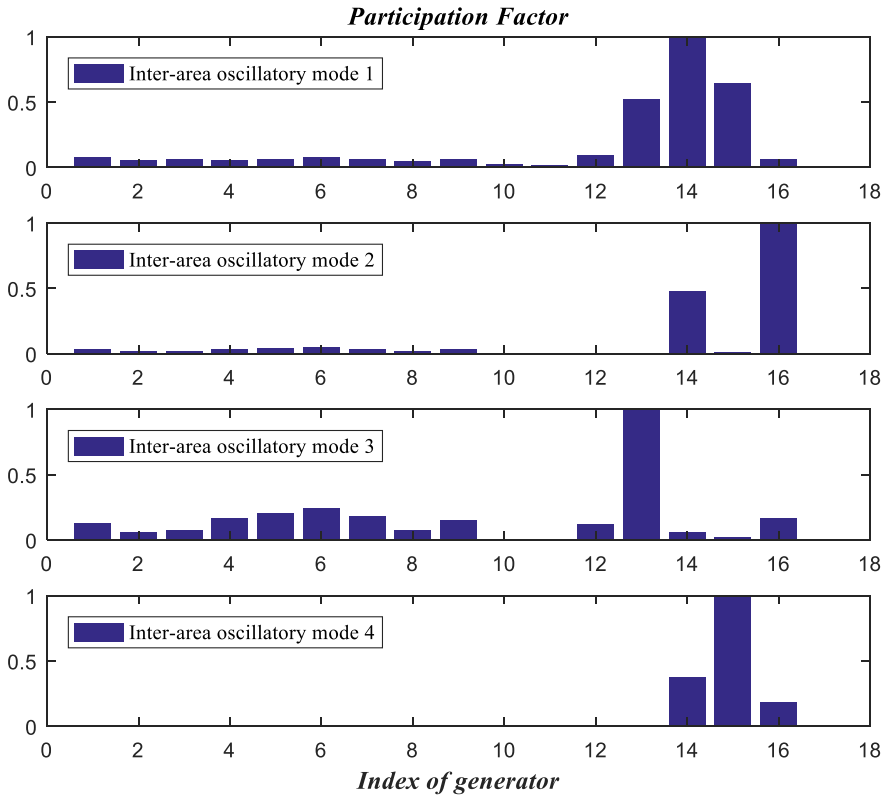

Figure 5.3 Participation factor analysis for weakly damped modes

Modal Residue Analysis

Active power flow on each transmission line is evaluated as feedback signal candidates with modal residue analysis. As HVDC and FACTS are already implemented in the designated locations, the modal controllability $w_i B$ is fixed and the modal residue exhibits the different observability to a particular mode from different system outputs. In the state space equations, the modal observability is determined by Cv_i, varied by different system output (controller input). Therefore, the modal residue for the particular damping controller design is determined by the observability of the various system outputs When calculating the scaled residues of different feedback signals, the comparison must be made within the same type of the signal and not against each other.

Absolute residues of 86 line power flows for four inter-area modes regarding Terminal 2 of VSC-MTDC damping controller is shown in Figure 5.4. In the modal residue analysis, the magnitude of residue R_i is the indicator for the amount of control effort needed for suppressing swing mode i with a certain feedback signal: the higher the magnitude means the lower the required control effort. For terminal 2 of VSC-HVDC system, it has relatively high residue in mode 1, 2 and 3. This is because terminal 2 is connected with Bus 50 and the HVDC transmission line is in parallel with the heavily loaded ac transmission Line 73 (Bus 18-50). Thus the selection of feedback signal is determined by the balanced control effort on residue values of mode 1, 2 and 3 and minimized residue on mode 4 to decrease its influence on the mode it's not responsible for [41].

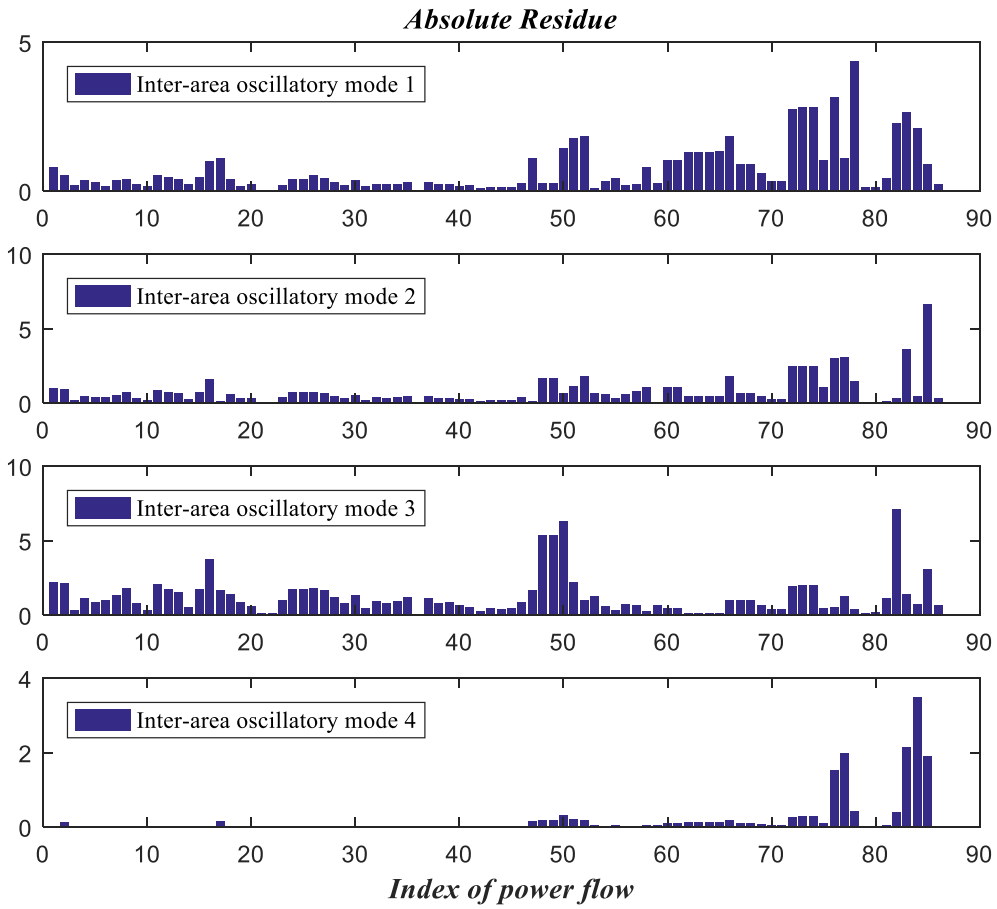

Figure 5.4 Absolute residue of different power flow for Terminal 2 of VSC-MTDC damping controller design

The modal residue of different feedback signals for TCSC is shown in Figure 5.5. As the TCSC is installed between Bus 40 and 41, which is the key transmission corridor from area 3 to the NYPS system. It has fairly high residues on mode 1, 2 and 4. The analysis of the results shows that a local control feedback signal with high residues on mode 1, 2 and 4 and low residue on swing mode 3 is the best candidate for the optimized control effort allocation.

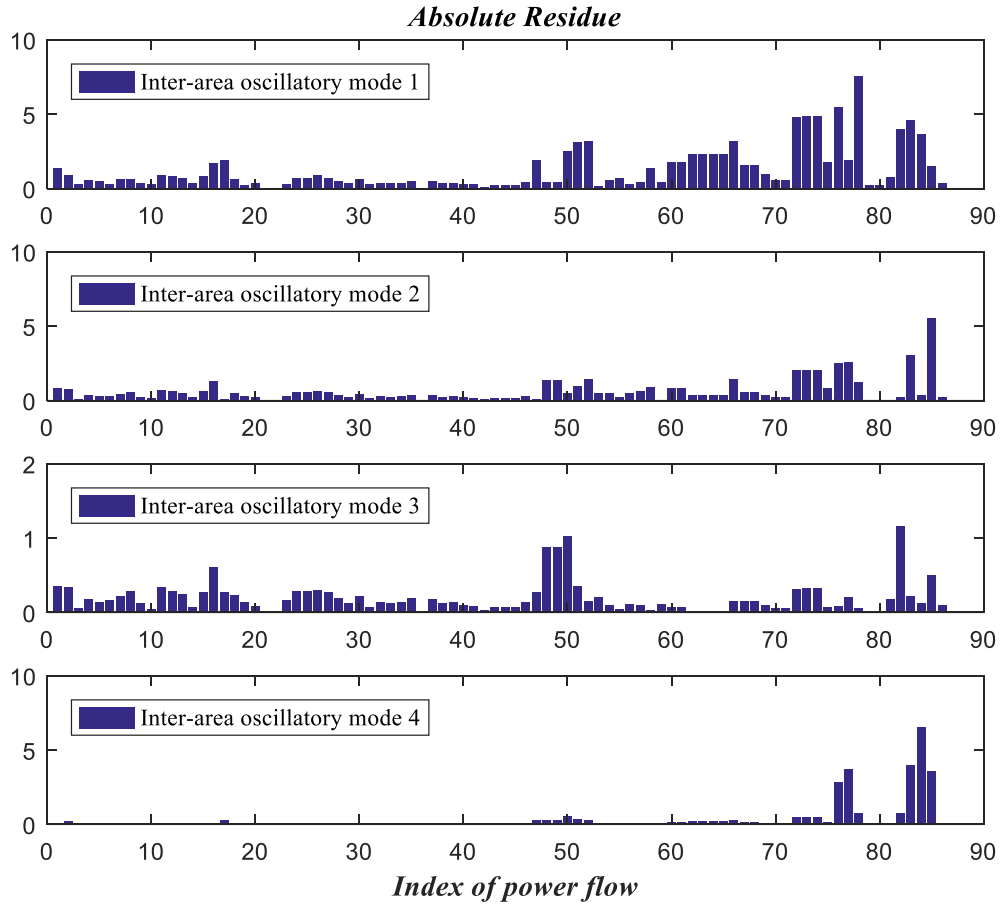

Figure 5.5 Absolute residue of different power flow for TCSC damping controller design

Beside the magnitude of modal residues, further criteria such as the phase angle and sensitivities to other modes [149] can also be introduced for a more comprehensive analysis of the feedback signal and control effort.

In addition to the modal residue analysis, the locations of the signals play an important part in the evaluation process. Remote signals can greatly expand the range of feedback signal candidates and it allows signals with high modal residues to be considered whereas local signals are more reliable as it does not require additional wide area measurement units. In this

case, feedback signal for Terminal 2 of VSC-MTDC damping controller is selected to be local active power flow on Line 18-50 and feedback signal for TCSC is selected to be active power on Line 14-40, shown in Figure 5.6.

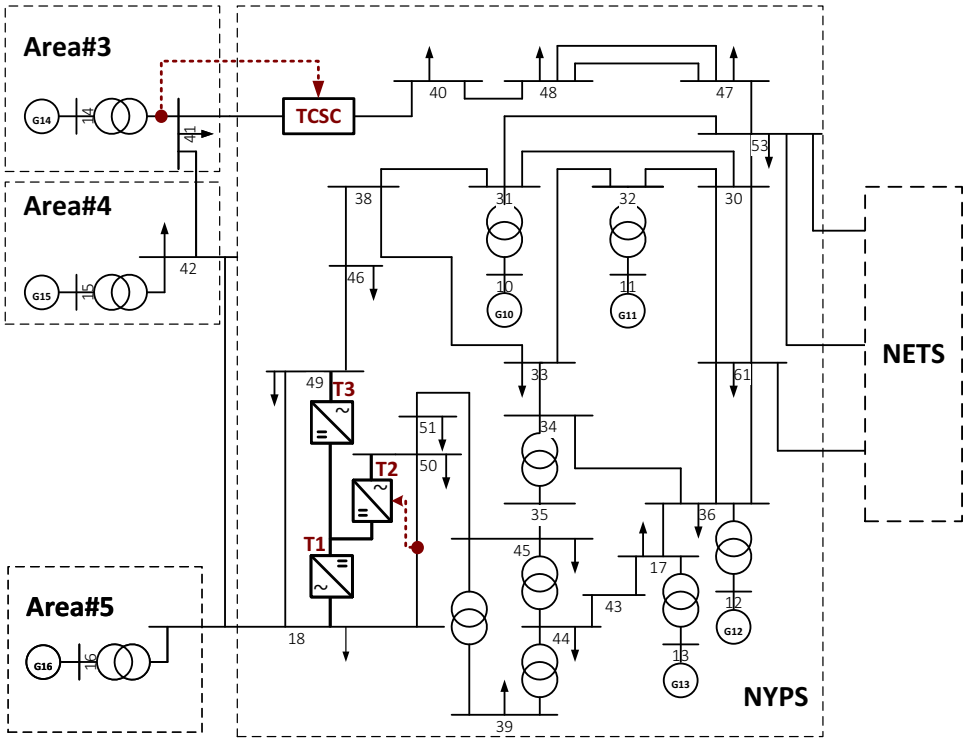

Figure 5.6 Feedback signal locations for Terminal 2 of VSC-MTDC and TCSC

5.2.3 Damping Controller Design for T2 of VSC-MTDC

Design methodology and steps introduced in Chapter 3 is applied to Terminal 2 of the VSC-MTDC.

System Order Reduction

The original open-loop system with VSC-MTDC and TCSC comes to 164th order and it is mandatory to reduce the order of the system to ease the controller design for practical implementation while maintaining key information in the frequency of interest. With balanced

truncation model approach, the reduced system becomes a 7th order system with 3 weakly damped modes, presented in Table 5.6. The eigenvalue analysis of the original full-order system is presented in Table 5.7.

Table 5.6 Eigenvalue analysis of reduced 7th order system

Mode Index	*Eigenvalues*	ζ	f *(Hz)*
1	-0.180778±2.251227i	8.0%	0.358
2	-0.177614±3.428311i	5.2%	0.546
3	-0.302110±3.936238i	7.7%	0.626
/	-16.168141	/	/

Table 5.7 Eigenvalue analysis of the original full-order system

Mode Index	*Eigenvalues*	ζ	f *(Hz)*
1	-0.174548±2.251230i	7.7%	0.358
2	-0.166403±3.420535i	4.9%	0.544
3	-0.344573±4.004608i	8.6%	0.637

Due to the low observability of mode 4 from the selected feedback signal, mode 1, 2 and 3 has been preserved in the reduced system for Terminal 2 damping controller design and mode 4 will be addressed in the subsequent damping controller design for TCSC.

The frequency response of the reduced system in comparison with the full-order system in Figure 5.7 shows great consistency with the original full-order system, maintaining crucial information of system damping characteristics in the frequency range of interest (0.2-0.8Hz). The information is retained by modal truncation reduction is the most significant states with high controllability and observability, thus the reduced system has the damping characteristics of the full-order system to carry out the controller design.

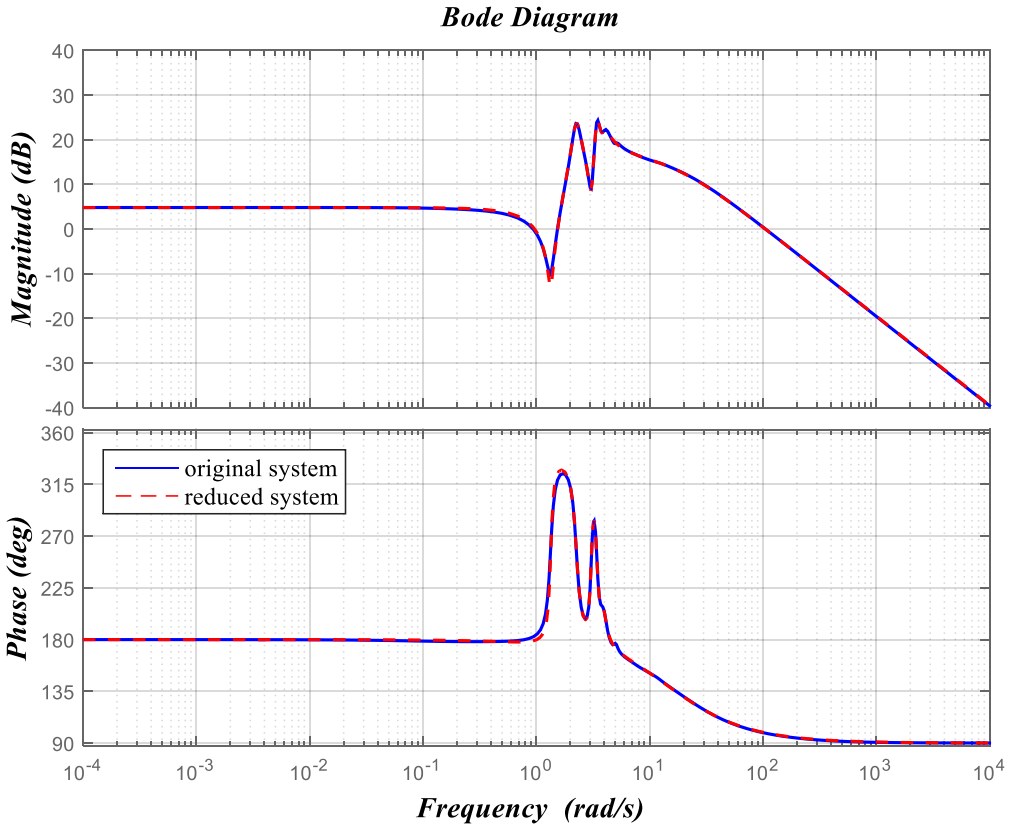

Figure 5.7 Bode diagram comparison

Controller State-Space Representation and Transfer Function

Terminal 2 damping controller is given in (5.1).

$$A_{T2} = \begin{bmatrix} -86.97 & -111.06 & 1937.3 & -1096.20 & -8696.4 & -4.79 & 10754.0 \\ 17.36 & 2.063 & 213.37 & -269.21 & -1470.6 & -2879.5 & -15705.2 \\ 3.53 & 4.105 & 83.12 & 35.55 & 446.30 & 20.00 & -43.84 \\ -1.225 & -0.137 & -16.23 & 19.13 & 82.48 & 202.47 & 1047.6 \\ -0.1805 & -0.227 & -4.92 & -2.94 & -36.53 & -14.53 & -57.12 \\ 0.0824 & 0.0045 & 1.18 & -1.35 & -3.94 & -13.66 & -67.36 \\ 0.0113 & 0.234 & 0.366 & 0.493 & 3.42 & 3.321 & 8.27 \end{bmatrix} \quad (5.1)$$

$$B_{T2} = \begin{bmatrix} -1.175 & 0.3902 & 0.0447 & -0.0278 & -0.0015 & 0.0018 & 3.66e-05 \end{bmatrix}$$

$$C_{T2} = \begin{bmatrix} -0.8186 & -14.2146 & -32.26 & -285.165 & -219.25 & -1172.1 & -28.558 \end{bmatrix}$$

And the transfer function is shown in (5.2).

$$T_{T2}(s) = \frac{0.079(s^2 + 22.494s + 54.257)(s^2 + 1.812s + 3.958)(s^2 + 0.831s + 2.432)}{(s + 21.56)(s^2 + 1.374s + 3.923)(s^2 + 0.868s + 2.962)(s^2 + 0.785s + 1.314)} \quad (5.2)$$

5.2.4 Damping Controller Design for TCSC

The first close-loop system of 171st order is formed by the damping controller for Terminal 2 of VSC-MTDC and the design for TCSC damping controller is subsequently dependent on the close-loop system and treats it as an open-loop system for modal reduction and optimization problem formulation. The 171st order system is to be reduced to 7th order simplified model in the following steps.

System Order Reduction

The reduced system preserves 3 inter-area modes, shown in Table 5.8, and it shows mode 1 and 2 has been successfully improved to adequately damping region with damping ratios more than 10%. Mode 4 which has not been considered in the previous design for Terminal 2 damping controller is observed with the selected feedback signal and will be addressed in the TCSC damping control design. Comparing to the eigenvalue characteristics before system reduction in Table 5.9, the reduced system has maintained the vital information for damping control design. Besides, with the properly selected feedback signal, the reduced model does not influence the swing mode it's not designed for, minimizing negative interactions between controllers.

Table 5.8 Eigenvalue analysis of reduced 7th order system

Mode Index	*Eigenvalues*	ζ	f *(Hz)*
1	-0.233778±2.251550i	10.3%	0.358
2	-0.341059±3.253072i	10.4%	0.518
4	-0.252480±5.007903i	5.0%	0.797
/	-20.138427	/	/

Table 5.9 Eigenvalue analysis of the original full-order system

Mode Index	*Eigenvalues*	ζ	f *(Hz)*
1	-0.232367±2.247103i	10.3%	0.358
2	-0.356357±3.388278i	10.5%	0.539
4	-0.253382±5.014782i	5.0%	0.798

Bode diagram in Figure 5.8 confirms the validity of the reduced system as it has the same frequency response in the frequency range of our interest (0.2 - 0.8 Hz). The information is retained by modal truncation reduction is the most significant states with high controllability and observability, thus the reduced system has the damping characteristics of the full-order system to carry out the controller design. Similar to the previous control objective specifications, 10% damping ratio is set as the pole placement region.

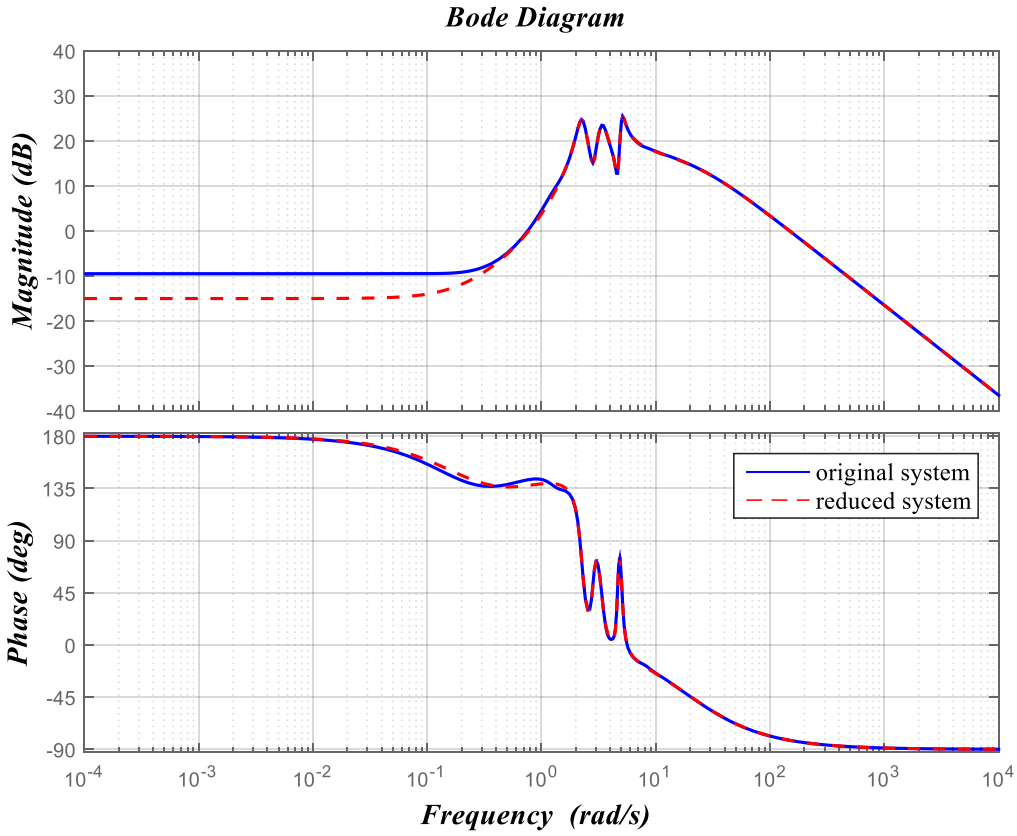

Figure 5.8 Bode diagram comparison

Controller State-Space Representation and Transfer Function

The TCSC damping controller is given in (5.3).

$$A_{TCSC} = \begin{bmatrix} -156.533 & -256.337 & -3701.2 & -4068.9 & -5119.41 & -8105.26 & 109740 \\ 6.5549 & 9.375 & 85.039 & 136.593 & -939.724 & 45.796 & -9424.75 \\ 1.900 & 3.264 & 44.893 & 37.732 & 61.665 & 57.317 & -1336.63 \\ -0.229 & -0.373 & -3.406 & -6.092 & 17.638 & -8.514 & 287.200 \\ -0.047 & -0.0533 & -1.231 & 0.0456 & -4.104 & -2.031 & 20.960 \\ 0.0030 & 0.0053 & 0.1547 & 0.173 & 3.018 & 1.012 & 6.944 \\ -0.0029 & -0.0023 & -0.1141 & -0.068 & -1.151 & 0.641 & -3.037 \end{bmatrix} \quad (5.3)$$

$$B_{TCSC} = \begin{bmatrix} 1.473 & -0.0758 & -0.0183 & 0.0027 & 4.0612e-04 & 9.8820e-06 & 7.2489e-06 \end{bmatrix}$$

$$C_{TCSC} = \begin{bmatrix} -0.8214 & -17.495 & -33.380 & -292.192 & -199.036 & 0.001023 & 15.1070 \end{bmatrix}$$

And the corresponding transfer function is shown in (5.4).

$$T_{TCSC}(s) = \frac{0.154(s^2 + 0.884s + 3.249)(s^2 - 8.033s + 27.584)(s^2 + 0.598s + 2.288)}{(s + 106.50)(s^2 + 1.784s + 4.213)(s^2 + 0.815s + 2.924)(s^2 + 5.390s + 1.891)} \quad (5.4)$$

5.2.5 Linear Eigenvalue Evaluations

The close-loop system performance is examined with eigenvalue analysis in Table 5.10-Table 5.12. The system performance of the close-loop system with 3 forms of formulation is improved in different patterns.

Firstly, the 7th order damping controller of Terminal 2 VSC-MTDC is installed to the original 164th order open-loop system, forming a close-loop system of 171st order. Its eigenvalue characteristic is presented in Table 5.10, where improvements of damping ratios of mode 1, 2 and 3 can be seen under all operating points and as mode 4 is not considered in the design stage, its damping ratio remains unchanged.

Table 5.10 System linear performance with T2 VSC-MTDC damping controller

Operating points	*Mode 1*		*Mode 2*		*Mode 3*		*Mode 4*	
	ζ	f (Hz)	ζ	f (Hz)	ζ	f (Hz)	ζ	f (Hz)
1	**10.4%**	0.357	**10.8%**	0.539	**10.8%**	0.654	5.1%	0.799
2	**10.3%**	0.358	**10.4%**	0.540	**10.7%**	0.654	5.0%	0.798
3	**10.2%**	0.358	**10.0%**	0.540	**10.6%**	0.653	5.0%	0.798
4	**10.1%**	0.358	**10.1%**	0.540	**10.5%**	0.652	5.0%	0.799

Secondly the 7th order damping controller of TCSC is implemented with the original 164th order open-loop system. This forms another close-loop system with dominant inter-area oscillatory modes and their damping ratios shown in Table 5.11. Since the TCSC damping controller is designed based on the close-loop system with Terminal 2 damping controller, its control effort focuses on mode 4 alone and it shows great improvement from the previous

under damped behaviour.

Table 5.11 System linear performance with TCSC damping controller

Operating points	*Mode 1*		*Mode 2*		*Mode 3*		*Mode 4*	
	ζ	f (Hz)	ζ	f (Hz)	ζ	f (Hz)	ζ	f (Hz)
1	8.8%	0.357	5.7%	0.534	8.8%	0.636	**15.0%**	0.802
2	8.8%	0.357	5.7%	0.534	8.8%	0.636	**15.3%**	0.803
3	8.8%	0.358	5.8%	0.534	8.8%	0.636	**15.0%**	0.800
4	8.8%	0.358	5.8%	0.534	8.8%	0.636	**15.4%**	0.804

Finally, both controllers are sequentially put into practice with the original system. The synthesis control effort from both controllers has effectively meliorated the damping characteristics across all four modes. A minimum 10% damping ratio is guaranteed in all operating points, indicating a successful coordinated robust design.

Table 5.12 System linear performance with T2 VSC-MTDC and TCSC damping controller

Operating points	*Mode 1*		*Mode 2*		*Mode 3*		*Mode 4*	
	ζ	f (Hz)	ζ	f (Hz)	ζ	f (Hz)	ζ	f (Hz)
1	**10.9%**	0.357	**12.0%**	0.534	**11.0%**	0.650	**14.9%**	0.802
2	**10.8%**	0.357	**11.6%**	0.534	**10.9%**	0.650	**15.2%**	0.803
3	**10.7%**	0.358	**11.1%**	0.534	**10.8%**	0.649	**14.9%**	0.800
4	**10.7%**	0.358	**10.8%**	0.534	**10.7%**	0.649	**15.3%**	0.804

The eigenvalue plot in Figure 5.9 shows the positions of poles in the complex plane under all four operating points. All the weakly damped poles that had less than 10% damping ratio are moved to the designated conic area with sufficient damping ratios. This effort is achieved by the regional pole placement control objective defined in Control Objectives section in Chapter 3. And the robustness of the controllers is ensured by the multi-model approach by introducing multiple operating conditions in the establishment of linearized system model. Sequential design of the two damping controllers minimized the coupling effect of the controller input signals and the two controllers can provide effective damping when working individually as well as together. The concurrent results prove the feasibility of the damping

control design in a robust and coordinated manner without negative interactions between the two controllers, showing great adaptability to various operating scenarios.

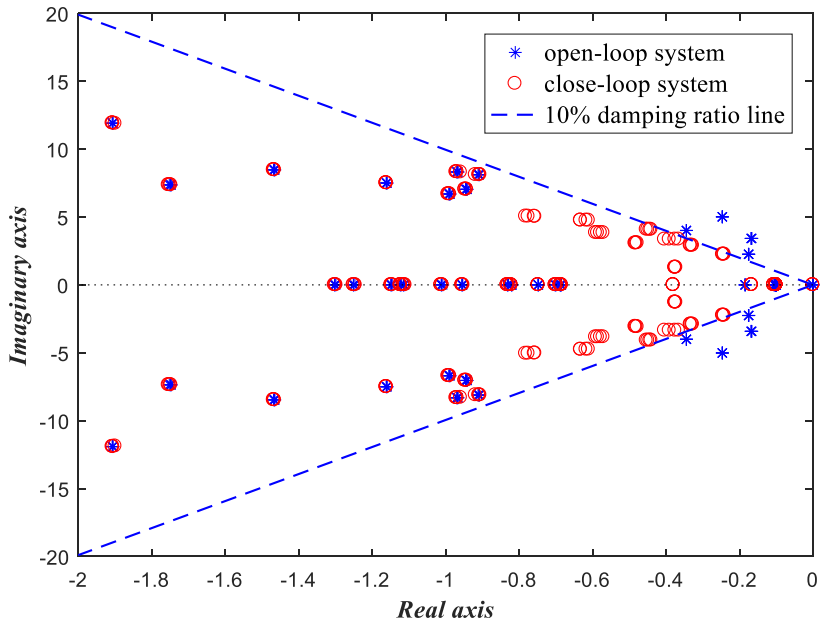

Figure 5.9 Eigenvalue plot under all operating points

5.2.6 Real-Time Simulation Case Studies

To fully examine the system performance, non-linear real-time digital simulations offer great insight in addition to the eigenvalue analysis. Terminal 2 of VSC-MTDC and TCSC damping controllers are installed in the test system and tested for the effectiveness and robustness under various disturbances and operating conditions. Three types of disturbances are introduced in the following case study: excitation system disturbance, load variation and line outage.

Excitation System Disturbance

In the first case study, excitation system disturbance is caused by a step change of excitation

system reference voltage for small time duration. The reference voltage V_{ref} for generator 14 endures a step change of 0.02 p.u. for 500ms and the system responses on active power of Line 73 (Bus 18-50) under operating points 1-4 are presented in Figure 5.10. As the damping controllers has improved the damping ratios of the poorly damped modes and the rate of decay is determined by the magnitude of the damping ratio, the oscillations observed in Figure 5.10 show shorter settling time compared to the original open-loop system without damping controllers.

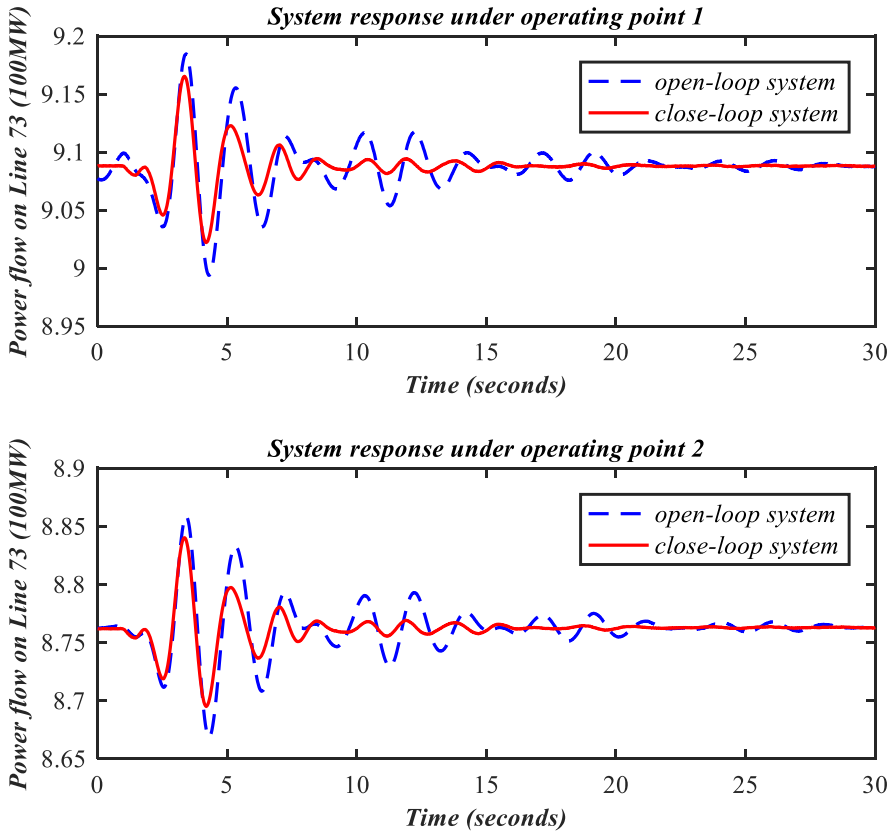

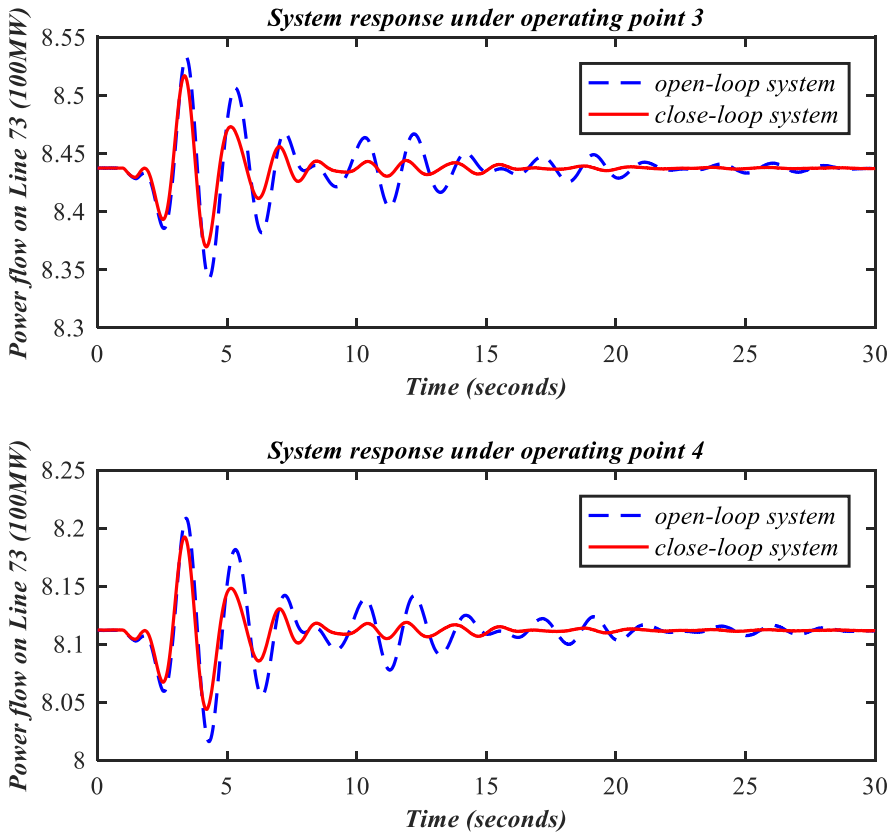

Figure 5.10 System response to excitation system disturbance on power flow of Line 73

Load Variation

Unlike the small variation given to the voltage reference in the previous scenario, Load 41 experiences a permanent step down from 1000MW to 800MW, resulting power fluctuation of the active power on Line 78 (Bus 41 to 40) where TCSC is installed, presented in Figure 5.11. Although load variation with such scale is not considered to be a small disturbance and does not fall into the small signal stability scope, it's fruitful to consider this type of disturbance in a small-signal stability study as it's essentially changing the operating points of the system and a great way to test the controller robustness. It's worthy to mention that although changing the load characteristics of the system lead to system model change, it's essential to test the controller's robustness under this varied system operating condition which is not included in the design stage. The purpose of the test is to check if the controllers can perform

their functionality to improve system damping in the situations that are not previously defined in the modelling stage.

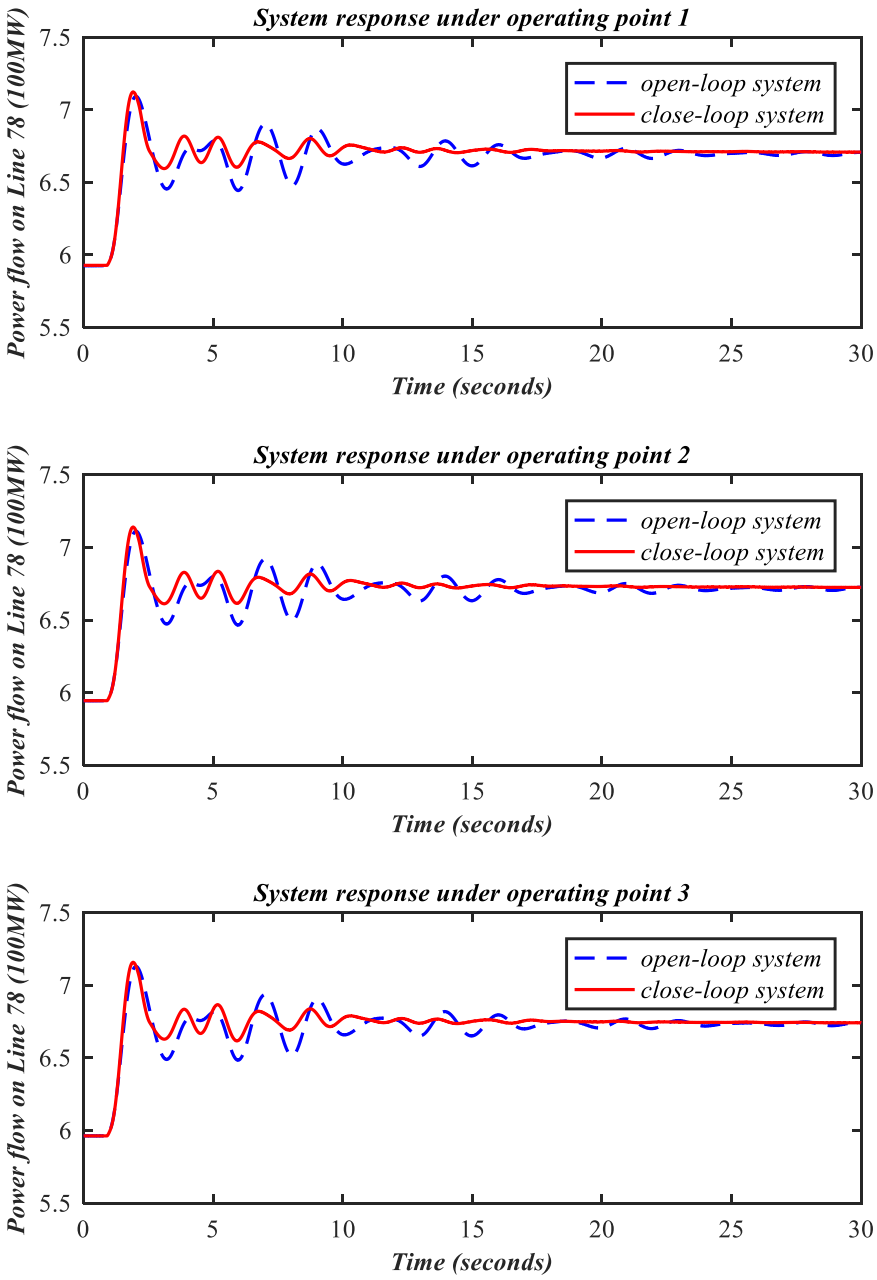

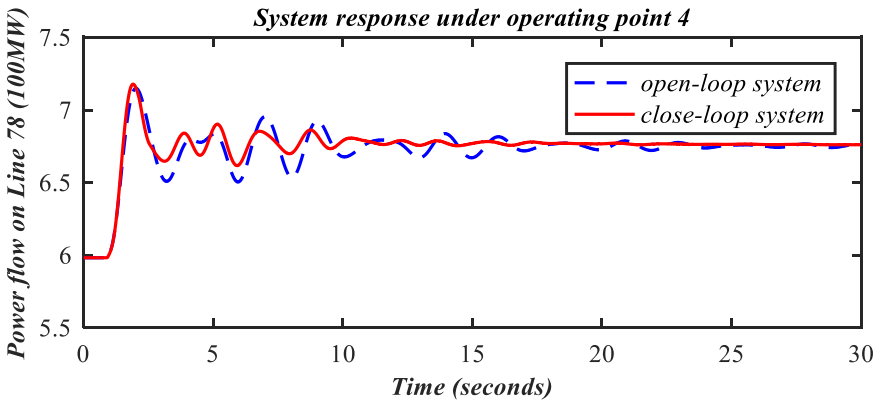

Figure 5.11 System response load variation on power flow of Line 78

Line Outage

One of the most severe faults that could stimulate system inter-area oscillation is the disturbance on the key transmission corridors connecting two large-scale areas. A three-phase to ground fault occurs on Line 86 (Bus 27-53), one of the transmission corridors between the NYPS and NETS. This line is subsequently tripped and stays out of service. The system response of another transmission corridor Line 1 (Bus 54-53) is shown in Figure 5.12. To maintain the amount of active power transfer between these two systems, an increase of active power on Line 1 can be observed. The results show the oscillation ripples die down faster than the open-loop system, which indicates increased damping ratio of the previously identified weakly damped modes. The supplementary damping provided by the controllers is thus tested to be effective.

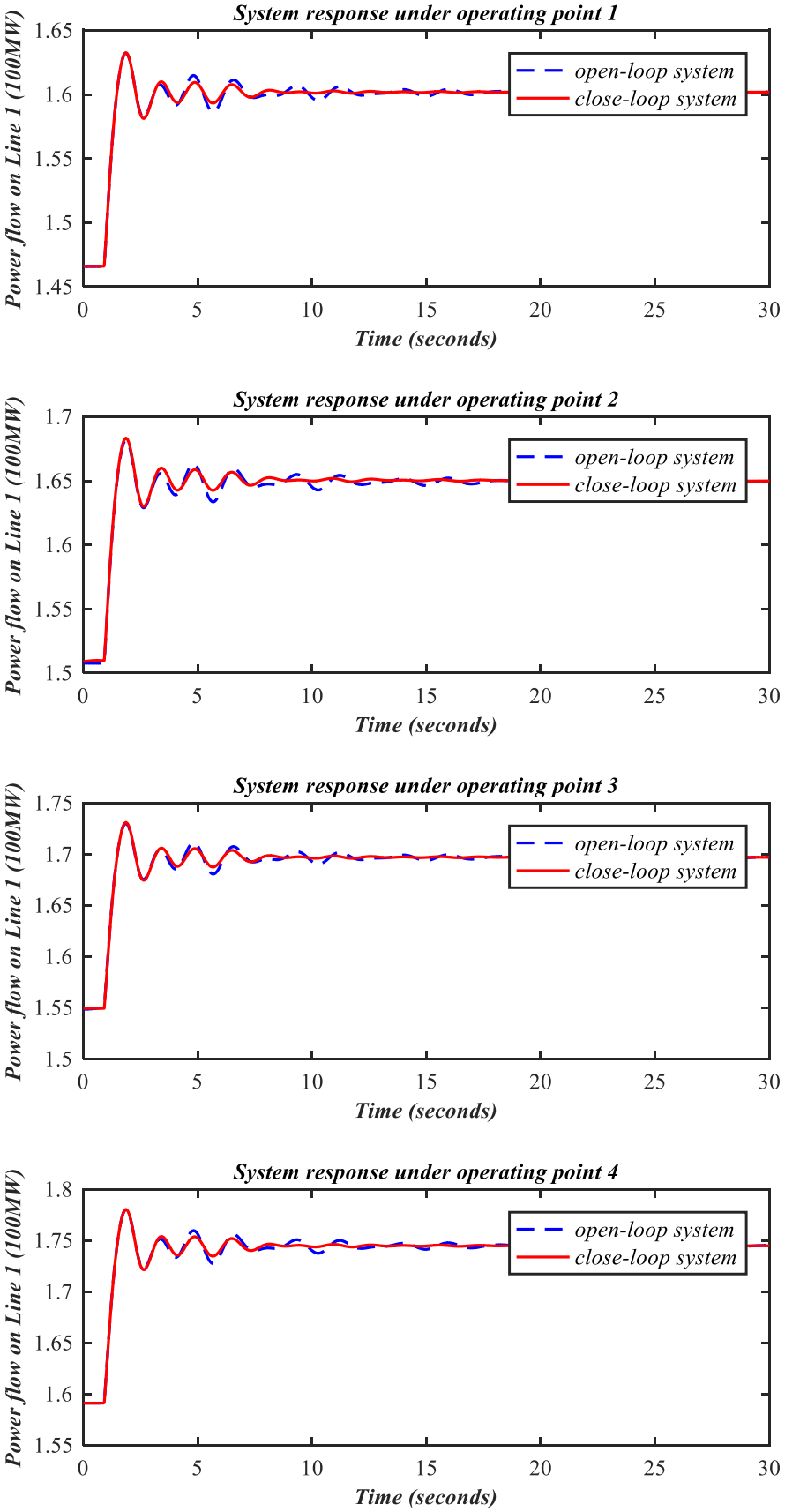

Figure 5.12 System response to line outage on power flow of Line 1

Discussion

The non-linear simulation results in Figure 5.10, Figure 5.11 and Figure 5.12 clearly demonstrated the damping effort of the supplementary controllers of Terminal 2 VSC-MTDC and TCSC. By actively regulation of the references of the ac voltage of the VSC-MTDC, the damping controllers has provided effective supplementary damping efforts for the power system. And the TCSC damping controller modulates the reactance reference of TCSC, the active power on the transmission line is responding to the oscillation and actively suppressing the inter-area swing from different generator groups. The settling time of system undergoing disturbances has been significantly shortened to less than 20s. Moreover, the damping controllers exhibit great robustness against different types of disturbances. The multi-model approach enables the controllers to be adaptive when system operating conditions are changed and provide effective damping to the inter-area oscillation modes. The real-time simulation in RTDS has included the other types of dynamics that is not include in the design stage, such as load, transmission line, governors, and the electromagnetic transients. In the designed system model, such details are not considered and this may reflect on the difference of simulation results. As the controller is designed based on linearized power system, it's functionality may be underrated in the complicated power system with non-linear properties. Nevertheless, the RTDS simulations has brought the more complex power system into consideration and can indicate the key elements for future research.

5.3 Summary

This chapter introduces damping control for two different devices: Terminal 2 of the VSC-MTDC and TCSC. In a pragmatic and interconnected power system, multiple inter-area

oscillatory modes with disparate mode shapes can be found especially in weakly connected transmission corridors. Under such circumstance, the capability of a single device to provide sufficient and effective damping towards all the oscillatory modes can be quite limited due to the installation location mostly decided by its primary functions. Therefore, the coordinated damping control of various types of devices such as HVDC and FACTS should be considered for satisfactory control effort in accordance with practical ratings. In this study, the sequential design resulted in a series of SISO damping controllers for multiple devices, instead of a centralized MIMO controller, to minimize the coupling effect and assure the robustness and potency of each controller.

The test benchmark system is the 5-area 16-generator 68-bus reduced equivalent NYPS-NETS power system. The 3-terminal VSC-MTDC was installed among Bus 18, 50 and 49 with radial connection and the TCSC was implemented between Bus 41 and 40. The supplementary damping controllers were formulated with BMI-based multi-objective multi-model optimization problem which was solved via a two-step method. The validity of the controllers was checked with linear system performance analysis for eigenvalue characteristics under all four operating points. It showed the controllers' control effort for specified modes and the improvement of damping ratios to a decent level. Furthermore, the real-time simulation in RTDS has demonstrated the robustness of the controllers regarding different operating conditions and disturbances.

CHAPTER 6 ASSESSMENT OF THE IMPACTS OF DIFFERENT CONTROL MODES ON DAMPING CONTROL PERFORMANCE OF VSC-MTDC

6.1 Introduction

In a VSC-MTDC system, the control mode for each terminal may vary depending on its location and the condition of the interconnected AC grid. The outer control loop tracks the reference value of specific signals given by the system level control strategy and usually falls into several categories: dc voltage control mode, ac voltage control mode, active power control mode and reactive power control mode. To maintain the active power balance, one VSC-MTDC terminal must adopt dc voltage control and other terminals can take up constant active power control of frequency control. When supplying a passive network with the VSC-MTDC, the terminal located in the passive network without sustainable power source often employs active power control mode for d-axis and ac voltage control mode for q-axis, meanwhile the terminal located in the main power grid adopts dc voltage control mode.

In Chapter 4 and Chapter 5, as the VSC-MTDC system is radially connected, the basic control modes for all three terminals are d-axis dc voltage control q-axis ac voltage control, which

essentially maintain dc voltage and regulate the active and reactive power injection from the grid. In this chapter, different d-axis control mode and its impact on the supplementary damping control design are investigated. Instead of dc voltage control, two of the three VSC-MTDC terminals take up constant active power control mode, fundamentally changing the small-signal modelling of the power system. Based on the small-signal model with active power control mode, damping controllers are designed with the methodology proposed in Chapter 3. Similar control design procedures will be undertaken to find the damping controller of a 3-terminal VSC-MTDC embedded in the test system and the validity and robustness of the controllers are evaluated with eigenvalue analysis for linear system performance as well as real-time simulations of system behaviour against various system disturbances under multiple operating points.

6.2 VSC-MTDC P-V_{ac} Control Mode Configuration

The detailed P-V_{ac} control mode configuration is illustrated in Figure 6.1. Different from the V_{dc}-V_{ac} control mode where d-axis reference signal is dc voltage, P-V_{ac} control mode sets the reference input signal of d-axis to active power P_{ref}, tracing the reference value and regulate the error through a PI control loop as the input of active-power current reference I_{cd_ref}. Supplementary control signals P_{damp} and V_{ac_damp} can be added to adjust the reference value dynamically for damping purposes, while it's not preferable to alter the dc voltage to provide system supplementary damping in the V_{dc}-V_{ac} control mode.

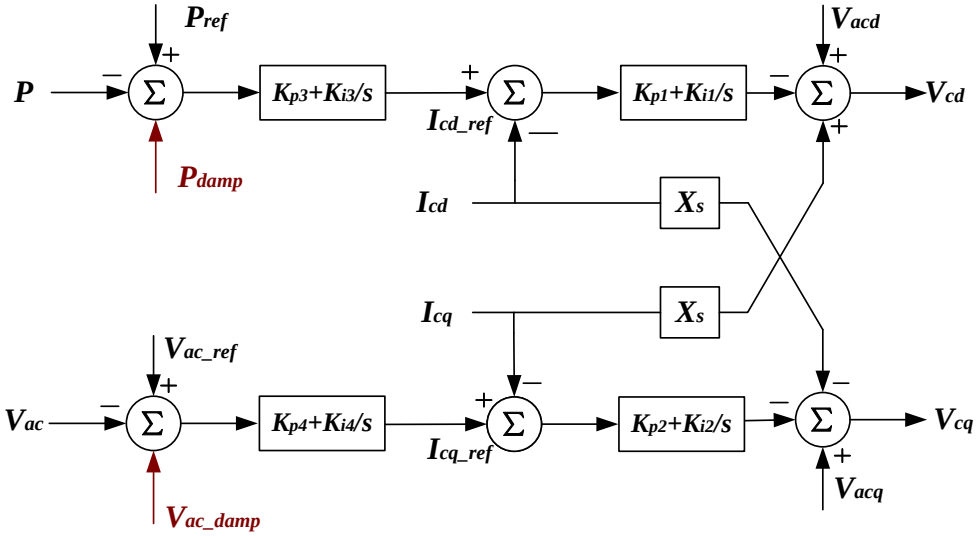

Figure 6.1 P-V_{ac} control mode configuration with supplementary damping signals

The mathematical representation of the above control mode can be expressed in (6.1)-(6.2)

d-axis active power control mode:

$$\begin{cases} \Delta P_{ref} - \Delta P = \Delta x_{c3} \\ K_{p3}\Delta x_{c3} + K_{i3}\Delta x_{c3} - \Delta I_{cd} = \Delta x_{c1} \\ -(K_{p1}\Delta x_{c1} + K_{i1}\Delta x_{c1}) + \Delta V_{acd} + X_s \Delta I_{cq} = \Delta V_{cd} \end{cases} \tag{6.1}$$

q-axis ac voltage control mode:

$$\begin{cases} \Delta V_{ac\_ref} - \Delta V_{ac} = \Delta x_{c4} \\ K_{p4}\Delta x_{c4} + K_{i4}\Delta x_{c4} - \Delta I_{cq} = \Delta x_{c2} \\ -(K_{p2}\Delta x_{c2} + K_{i2}\Delta x_{c2}) + V_{acq} - X_s \Delta I_d = \Delta V_{cq} \end{cases} \tag{6.2}$$

In this chapter, Terminal 1 remains V_{dc}-V_{ac} control mode and Terminal 2 and 3 has adopted the P-V_{ac} control mode, forming the state-space representation of the 3-terminal VSC-MTDC system in the following equations.

$$\Delta x_c = A_c \Delta x_c + B_c \Delta V + D_c \Delta U_c \tag{6.3}$$

where

Δx_c $\quad \left[\Delta x_{c1} \quad \Delta x_{c2} \quad \Delta x_{c3}\right]^T$

Δx_{c1} $\quad \left[\Delta V_{dc1} \quad \Delta x_{c11} \quad \Delta x_{c12} \quad \Delta x_{c13} \quad \Delta x_{c14}\right]^T$

Δx_{c2} $\quad \left[\Delta P_2 \quad \Delta x_{c21} \quad \Delta x_{c22} \quad \Delta x_{c23} \quad \Delta x_{c24}\right]^T$

Δx_{c3} $\quad \left[\Delta P_3 \quad \Delta x_{c31} \quad \Delta x_{c32} \quad \Delta x_{c33} \quad \Delta x_{c34}\right]^T$

ΔV_c $\quad \left[\Delta \theta_{s1} \quad \Delta V_{s1} \quad \Delta \theta_{s2} \quad \Delta V_{s2} \quad \Delta \theta_{s3} \quad \Delta V_{s3}\right]^T$

ΔU_c $\quad \left[\Delta V_{dc\_ref} \quad \Delta V_{ac1\_ref} \quad \Delta P_{i2\_ref} \quad \Delta V_{ac2\_ref} \quad \Delta P_{i3\_ref} \quad \Delta V_{ac3\_ref}\right]^T$

Note: $A_c \in 15\times15$, $B_c \in 15\times6$ and $D_c \in 15\times6$

6.3 Damping Controller Design for *P*-V_{ac} Control Mode

6.3.1 Test System Small-Signal Modelling and Eigenvalue Analysis

The 5-area 16-machine 68-bus system is adopted as the test benchmark system for small-signal analysis and damping controller design. Four operating points are selected for multi-model formulation, as listed in Table 6.1.

Table 6.1 Operating points selection

Operating Points	*Load 18(MW)*
1	2470
2	2570
3	2670
4	2770

Four weakly damped inter-area modes are identified under these operating points, shown in Table 6.2, Table 6.3, Table 6.4 and Table 6.5.

Table 6.2 Damping ratio, frequency and Eigenvalues of Mode 1

Operating points	*Mode 1*		
	ζ	f (Hz)	*Eigenvalue*
1	6.0%	0.397	-0.150879±2.492948i
2	6.1%	0.398	-0.152712±2.500643i
3	6.2%	0.399	-0.154762±2.509338i
4	6.2%	0.401	-0.156551±2.517735i

Table 6.3 Damping ratio, frequency and Eigenvalues of Mode 2

Operating points	*Mode 2*		
	ζ	f (Hz)	*Eigenvalue*
1	4.9%	0.551	-0.170632±3.459963i
2	5.0%	0.551	-0.172195±3.462931i
3	5.0%	0.552	-0.173858±3.467339i
4	5.0%	0.552	-0.175041±3.470096i

Table 6.4 Damping ratio, frequency and Eigenvalues of Mode 3

Operating points	*Mode 3*		
	ζ	f (Hz)	*Eigenvalue*
1	8.7%	0.634	-0.346233±3.984684i
2	8.6%	0.635	-0.346190±3.988800i
3	8.6%	0.635	-0.345979±3.992258i
4	8.6%	0.636	-0.345860±3.996748i

Table 6.5 Damping ratio, frequency and Eigenvalues of Mode 4

Operating points	*Mode 4*		
	ζ	f (Hz)	*Eigenvalue*
1	5.1%	0.803	-0.256995±5.047306i
2	5.1%	0.803	-0.256940±5.047070i
3	5.1%	0.803	-0.256855±5.047307i
4	5.1%	0.803	-0.256809±5.045741i

This corresponds with the eigenvalue plot of the original open-loop system shown in Figure 6.2. Four pairs of the complex conjugate poles are located outside the 10% damping ratio line, which shows lack of damping and causes longer period of settling time after system disturbance. Therefore, one of the control objectives is to shift the poles to the designated

adequately damped areas.

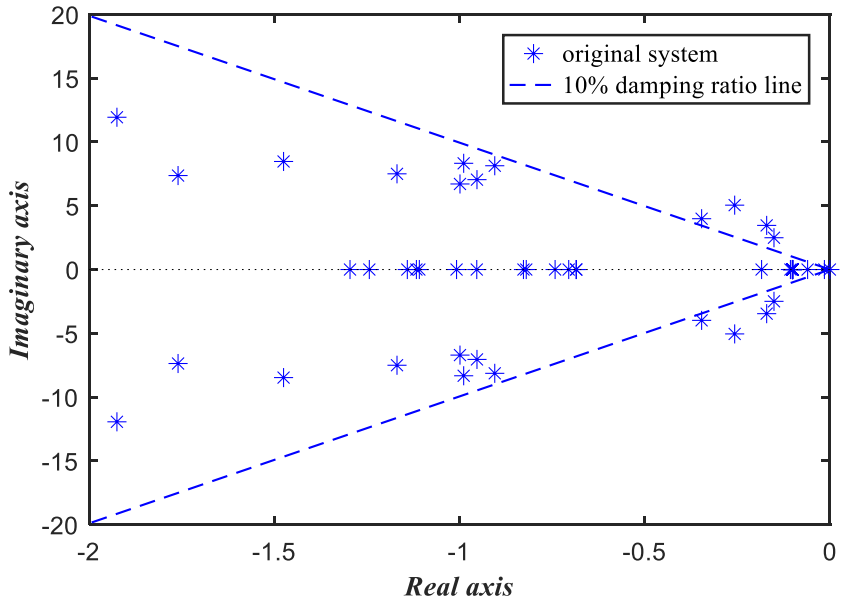

Figure 6.2 Eigenplot of the original open-loop system

VSC-MTDC Installation Location and Control Mode

The 3-terminal VSC-MTDC is installed in the exact location determined in Chapter 4: Terminal 1 is connected to Bus 18; Terminal 2 to Bus 50 and Terminal 3 to Bus 49. The detailed control mode configuration is illustrated in Figure 6.3.

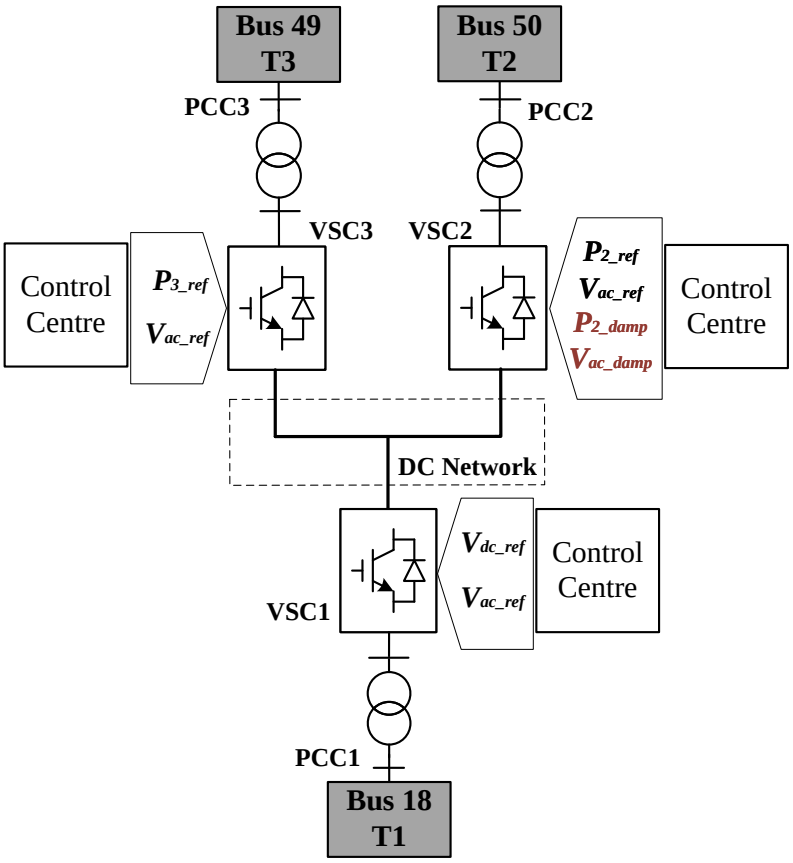

Figure 6.3 Detailed 3-terminal VSC-HVDC damping cotroller design in test system

The design objective is to find supplementary damping controllers for Terminal 2 d-axis active power control P_{damp} and q-axis ac voltage control V_{ac_damp} so that the weakly damped modes can be improved to a satisfactory level and at the same time optimal control effort is realized.

6.3.2 Feedback Signal Selection

Feedback damping control signal candidates should be scrupulously evaluated to ensure decent controllability and observability to the oscillatory modes. To this end, participation factor analysis of the contribution of generator states to certain modes and modal residue analysis of the sensitivity of system output to a particular oscillatory mode are executed

regarding the damping characteristics of the original open-loop system.

Participation factor

Figure 6.4 exhibits the normalized participation factor bar diagram of 16 generator states in respect to 4 weakly damped modes. This indicates the degree of involvement of each machine to each mode. It can be observed that all the generators including area equivalent generators 14-16 contributes to inter-area oscillatory mode 1; mode 2 can be seen as oscillation between generator 14 and generator 16; mode 3 is between NYPS and NETS; finally, mode 4 involves Generators 14, 15 and 16.

The participation factor analysis for the three different configurations of VSC-MTDC and TCSC implementations show similar results, as can be seen in Figure 4.7, Figure 5.3 and Figure 6.4. As the nature of the inter-area oscillation is generator or generator groups in different areas swings against each other, the identified weakly damped modes exhibit identical involvement from the generators. Thus, the reasons behind the patterns of the participation factors are similar as well: generator 14, 15 and 15 are area equivalent generators and interconnected with other areas with single or weak ties; heavy power flows are observed on these links which further contribute to the high participation factor of these generators.

However, participation factor cannot solely single out the ideal feedback signal as one local generator state may not provide the desired controllability and observability to inter-area oscillations. Therefore, the following modal residue analysis for system outputs effectively expands the range of feedback signal candidates and also evaluates their sensitivities.

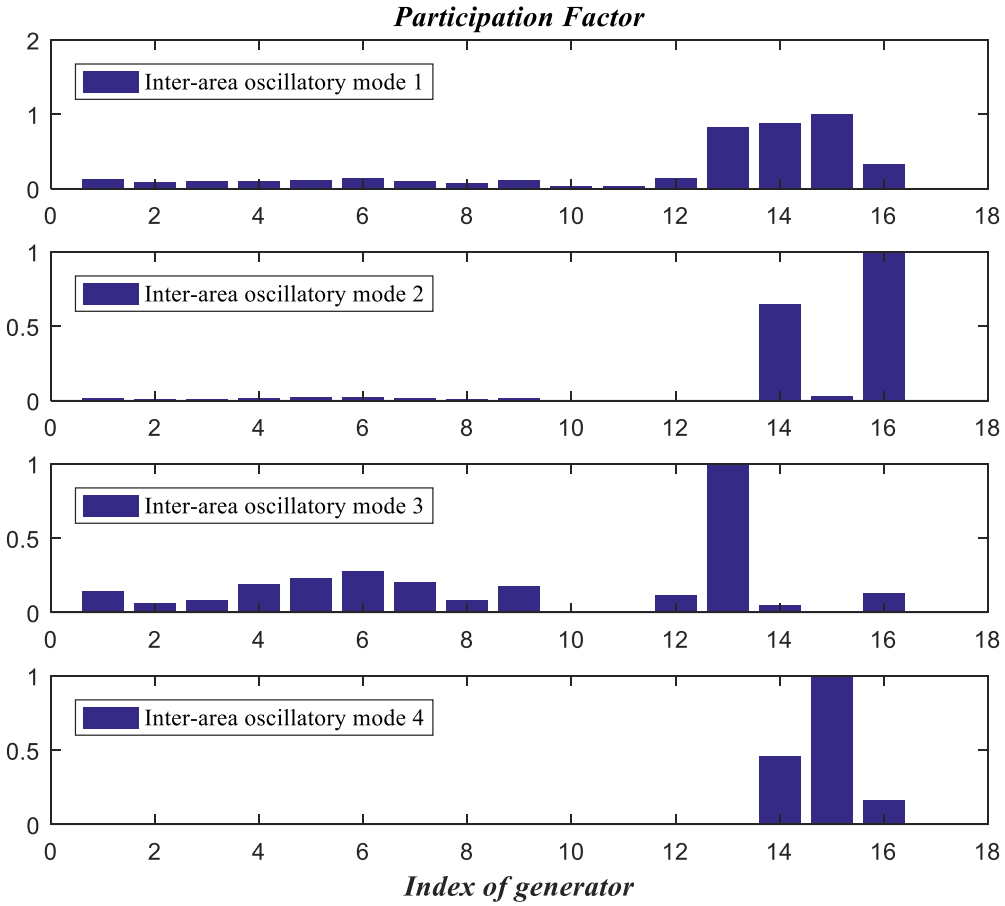

Figure 6.4 Participation factor analysis for weakly damped modes

Modal residue analysis

The modal residue R is known as the product of modal observability Cv and modal controllability wB. It contains vital information about the sensitivity to the swing mode of interest, in this case the poorly damped inter-area oscillatory modes. Active power flow on each line in the test system is assessed for its modal residue. The magnitude of the absolute residue for d-axis active power control of terminal 2 of the VSC-MTDC is shown in Figure 6.5. The outer loop control of the Terminal 2 and Terminal 3 of VSC-MTDC in this chapter is

active power and ac voltage control, which fundamentally changes the state-space equations of the system model and results in different controllability of the signals.

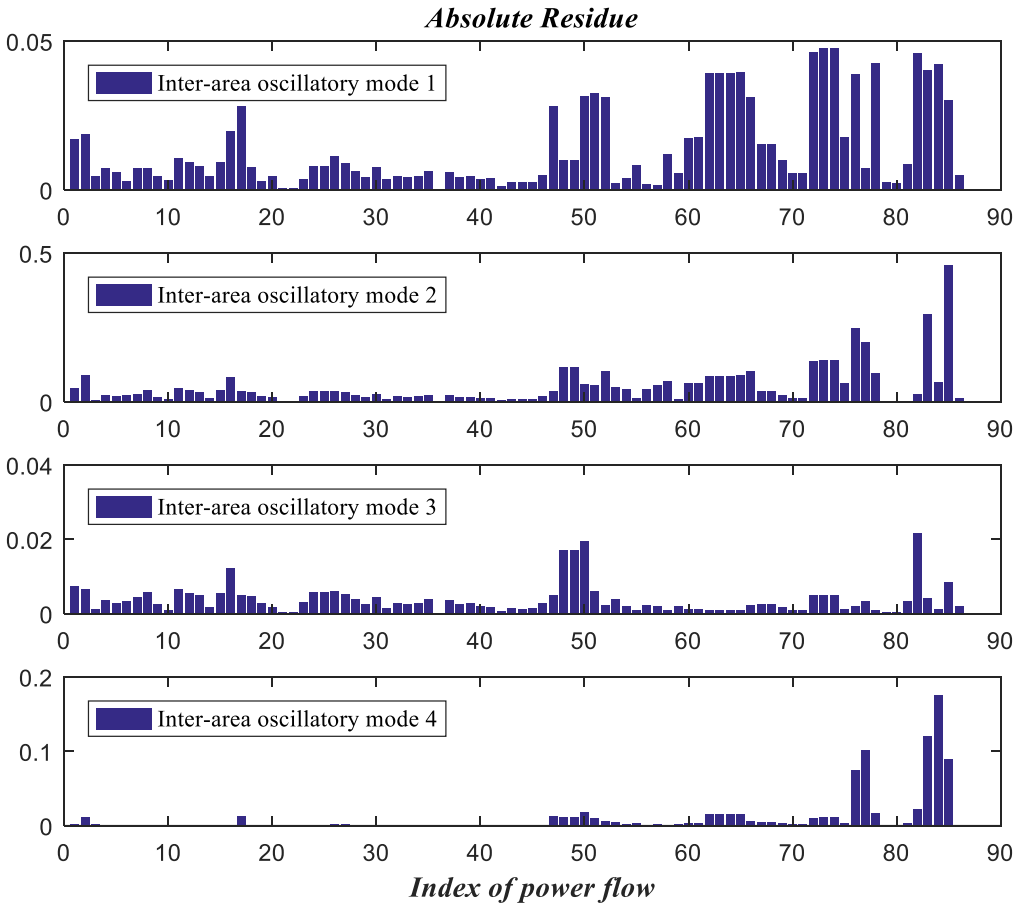

Figure 6.5 Absolute residue of different power flow for d-axis active power control of T2 VSC-MTDC

The absolute residue of q-axis ac voltage control is shown in Figure 6.6. The absolute residue analysis carried out in this study is mainly by assessing the magnitude of the modal reside. Further analysis can be done to introduce more criteria into consideration such as the phase angle for a more comprehensive feedback signal analysis [149].

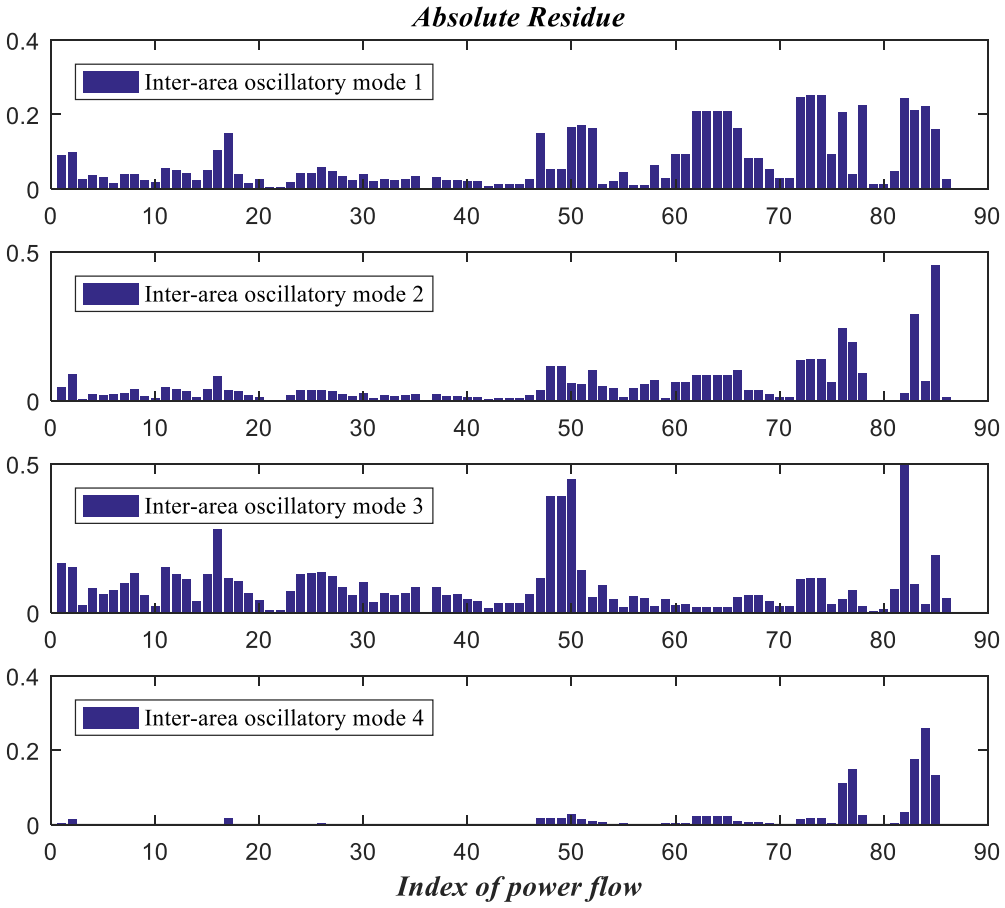

Figure 6.6 Absolute residue of different power flow for q-axis ac voltage control of T2 VSC-MTDC

The absolute residue for damping controller design of the d-axis active power control helps identify a suitable feedback signal. Considering mode 1, 2 and 4, a common signal which holds high modal residue across these three modes is considered as the better candidate. Power flow 83 (Bus14-41) is chosen from system output candidates as the feedback signal for d-axis active power supplementary damping controller. Similarly, power flow 82 (Bus 13-17) is chosen as the feedback signal for q-axis ac voltage supplementary damping controller design.

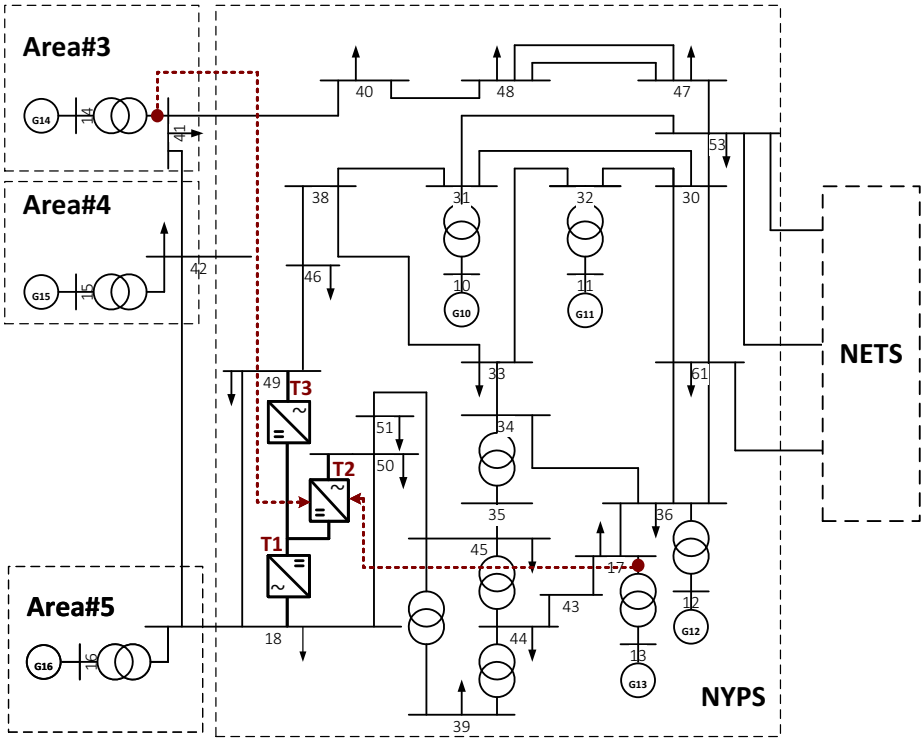

Figure 6.7 Feedback signal locations for d-axis and q-axis supplementary damping control of T2 VSC-MTDC

6.3.3 Damping controller design for d-axis active power control of T2 VSC-MTDC

The first step of the proposed sequential design is to apply the control methodology on the d-axis active power control of T2 VSC-MTDC. Necessary system order reduction is carried out for the original full-order open-loop system.

System Order Reduction

The obtained 7^{th} order reduced system from modal truncation reduction preserves 3 inter-area oscillatory modes, corresponding to the observability of the selected feedback signal. Table 6.6 shows most of the key information concerning the selected mode is kept up for the damping controller design at a later stage. For comparison, eigenvalues of the weakly damped modes of the original full-order system are listed in Table 6.7.

Table 6.6 Eigenvalue analysis of reduced 7th order system

Mode Index	*Eigenvalues*	ζ	f *(Hz)*
1	-0.162860±2.515650i	6.5%	0.400
2	-0.168045±3.460947i	4.8%	0.551
4	-0.269102±5.032828i	5.3%	0.801
/	-0.045898	/	/

Table 6.7 Eigenvalue analysis of the original full-order system

Mode Index	*Eigenvalues*	ζ	f *(Hz)*
1	-0.152712±2.500643i	6.1%	0.398
2	-0.172195±3.462931i	5.0%	0.551
4	-0.256940±5.047070i	5.1%	0.803

Figure 6.8 is the comparison of the frequency responses of the original system and reduced system. In the frequency range of interest, both responses exhibit identical magnitude and phase, allowing the reduced system to be a valid substitute of the original system for the ease of damping control design.

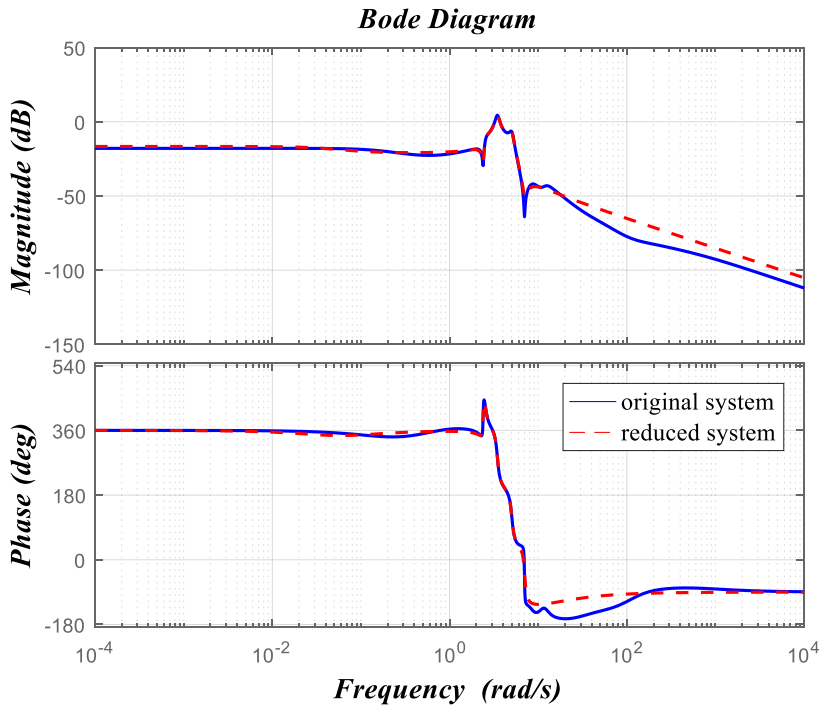

Figure 6.8 Bode diagram comparison

Controller State-Space Representation and Transfer Function

By solving the optimization problem through the two-step approach, controller state-space representation is given with the following matrices:

$$A_P = \begin{bmatrix} -0.2594 & -42.3958 & -2.0497 & -398.6017 & -52.4671 & -1255.0 & -30.0106 \\ 1.1776 & 1.3887 & 9.6035 & 114.2782 & 60.7347 & 585.4363 & 45.2141 \\ -0.1415 & 0.8814 & -3.9400 & -6.1555 & -19.3844 & -20.9220 & -2.4418 \\ 0.0200 & -0.0429 & 1.2718 & -7.5739 & 0.5328 & -41.9598 & -3.2473 \\ 0.0155 & 0.0060 & 0.4099 & 1.2052 & 1.8915 & -0.1161 & 0.1157 \\ -0.0052 & -8.819e-4 & -0.1206 & 0.7002 & 0.4722 & 4.2078 & 0.3246 \\ -0.0022 & -6.626e-4 & -0.0568 & -0.0166 & 1.0773 & 1.0773 & -0.0130 \end{bmatrix} \quad (6.4)$$

$$B_P = \begin{bmatrix} -5.2613 & -3.5959 & 0.2817 & 0.2596 & -0.0221 & -0.0259 & 0.0030 \end{bmatrix}$$

$$C_P = \begin{bmatrix} -1.1070 & -1.2128 & -29.6409 & -15.0849 & -162.6589 & -1.7430 & 0.2613 \end{bmatrix}$$

Transfer function $T_P(s)$ for d-axis active power control of Terminal 2 controller is

$$T_P(s) = \frac{34.972(s^2 - 5.381s - 0.249)(s^2 - 0.686s + 3.421)(s^2 + 1.494s + 3.174)}{(s + 0.04457)(s^2 + 1.912s + 5.259)(s^2 + 1.360s + 3.391)(s^2 + 0.981s + 2.442)} \quad (6.5)$$

6.3.4 Damping controller design for q-axis ac voltage control of T2 VSC-MTDC

With the damping controller obtained from the previous equations, first loop closure is achieved and thus the system order is increased to 170. The close-loop system is then seen as the new open-loop system for q-axis ac voltage damping controller design. Similarly system order reduction is mandatory for the practicality of the damping controllers.

System Order Reduction

The inter-area oscillatory modes remained in the reduced system are mode 1 and 3, shown in Table 6.8. From the implementation of active power supplementary damping controller, the damping ratio of mode 1 has been improved slightly and there's still room for further improvement. Mode 3 which is ignored in the previous step will be focused in this design stage. For comparison, eigenvalues of the weakly damped modes of the original full-order system are listed in Table 6.9.

Table 6.8 Eigenvalue analysis of reduced 7^{th} order system

Mode Index	*Eigenvalues*	ζ	f *(Hz)*
1	-0.215746±2.491722i	8.6%	0.397
3	-0.308224±3.965776i	7.7%	0.631
/	-0.835183±7.067955i	11.7%	1.125
/	-12.146205	/	/

Table 6.9 Eigenvalue analysis of the original full-order system

Mode Index	*Eigenvalues*	ζ	f *(Hz)*
1	-0.238032±2.442365i	9.7%	0.389
3	-0.342625±3.997213i	8.5%	0.636

The frequency response, in Figure 6.9, for reduced system shows great coherence with the new open-loop system in frequency range 0.2-1Hz and further control problem formulation and resolution can be carried out.

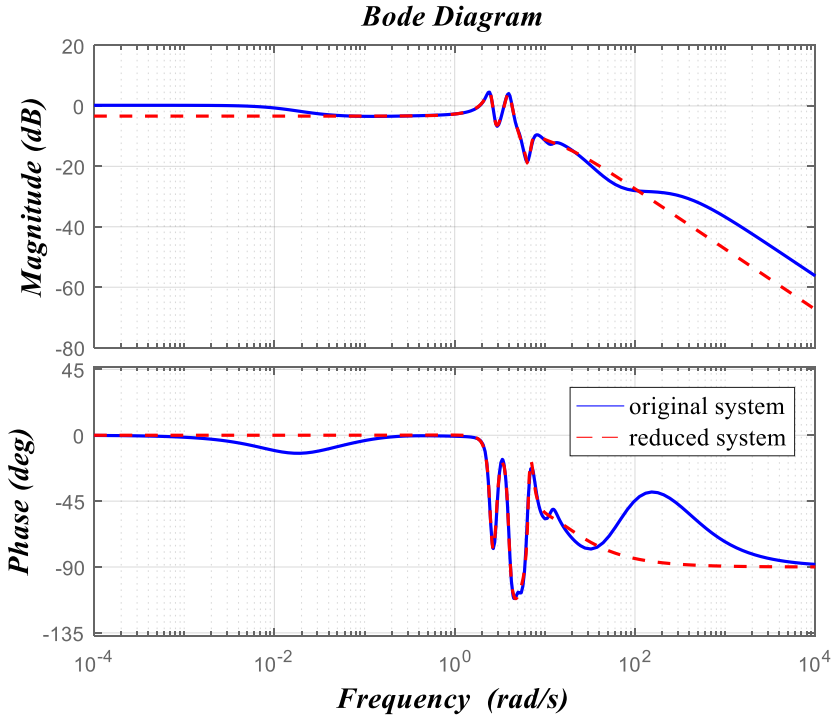

Figure 6.9 Bode diagram comparison

Controller State-Space Representation and Transfer Function

Through the two-step approach, the 7th order damping controller for the ac voltage control can be expressed in the following matrices:

$$A_V = \begin{bmatrix} -9.5699 & -94.0304 & -579.1290 & -1863.0 & -6435.1 & -8299.4 & -11950 \\ 0.7307 & -0.8271 & -21.5850 & -36.1659 & -387.2056 & -278.2770 & -1585.8 \\ 0.0556 & 1.2537 & 4.6127 & 12.1659 & 91.0253 & 96.3199 & 410.3938 \\ -0.083 & -0.0392 & 0.2672 & -2.0630 & -18.6172 & -17.2927 & -105.3593 \\ 5.75e-4 & -0.0041 & -0.0411 & 0.8138 & -0.4433 & -1.2512 & -0.4919 \\ 3.84e-4 & 0.0033 & 0.0350 & 0.1723 & 1.8507 & 1.3204 & 4.5856 \\ 1.19e-5 & -2.57e-4 & -0.0023 & -0.0164 & -0.1169 & 0.8522 & -0.8379 \end{bmatrix} \quad (6.6)$$

$$B_V = \begin{bmatrix} -0.7887 & -0.0021 & -0.0052 & 0.0027 & -1.23e-5 & -1.4723e-4 & 3.3288e-5 \end{bmatrix}$$

$$C_V = \begin{bmatrix} -0.4482 & -6.3394 & -39.1041 & -343.3987 & -463.6164 & -2617.7 & 46.1319 \end{bmatrix}$$

Transfer function $T_V(s)$ for q-axis ac voltage control of Terminal 2 controller is

$$T_V(s) = \frac{0.0363(s^2 + 41.577s + 150.330)(s^2 + 1.545s + 7.014)(s^2 + 1.214s + 3.031)}{(s + 4.277)(s^2 + 1.478s + 7.184)(s^2 + 1.229s + 3.953)(s^2 + 0.823s + 2.455)} \quad (6.7)$$

6.3.5 Linear Eigenvalue Evaluations

With the two damping controllers $T_p(s)$ and $T_V(s)$ obtained from the previous sections, linear close-loop system performance is examined with eigenvalue analysis. The first close-loop is formed by system plant dynamics $G_{sys}(s)$ and d-axis active power damping controller $T_p(s)$. The improved damping ratios of interested inter-area oscillatory modes identified in the original open-loop system are shown in Table 6.10. As the feedback signal selection mainly focuses on mode 1, 2 and 4, the damping control effort has significantly increased the damping ratios of these modes. It's notable that there's still room for improvement for mode 1.

Table 6.10 System performance with d-axis active power control of T2 VSC-MTDC damping controller

Operating points	*Mode 1*		***Mode 2***		*Mode 3*		***Mode 4***	
	ζ	f (Hz)	ζ	f (Hz)	ζ	f (Hz)	ζ	f (Hz)
1	8.8%	0.389	**12.9%**	0.564	8.6%	0.635	**10.3%**	0.810
2	9.6%	0.388	**12.5%**	0.571	8.5%	0.636	**10.3%**	0.813
3	9.3%	0.392	**12.5%**	0.566	8.5%	0.635	**10.2%**	0.811
4	9.5%	0.389	**12.5%**	0.575	8.6%	0.638	**10.5%**	0.815

The second close-loop is formed by the original system plant $G_{sys}(s)$ and supplementary damping controller $T_V(s)$ designed for the q-axis ac voltage control mode. As stated in Table 6.11, the damping controller alone shows great control effort applied on mode 1 and 3 which experience a considerable uplift of damping ratios. A minimum 10% of damping ratio is guaranteed in both modes.

Table 6.11 System performance with q-axis ac voltage control of T2 VSC-MTDC damping controller

Operating points	*Mode 1*		*Mode 2*		*Mode 3*		*Mode 4*	
	ζ	f (Hz)	ζ	f (Hz)	ζ	f (Hz)	ζ	f (Hz)
1	**10.4%**	0.399	4.8%	0.551	**11.7%**	0.657	5.1%	0.804
2	**10.2%**	0.400	5.0%	0.551	**11.6%**	0.657	5.1%	0.803
3	**10.0%**	0.401	5.0%	0.552	**11.6%**	0.657	5.1%	0.803
4	**10.0%**	0.402	5.0%	0.552	**11.5%**	0.656	5.1%	0.803

Finally, close-loop system with both damping controllers installed are analysed in Table 6.12. The combined control effort ameliorates the weakly damped modes from the original system, especially mode 1 which is provided with the synthetic control effort from both controllers. Besides, no adverse interaction is shown in these investigations, enabling the controllers to function well on its own or together.

Table 6.12 System performance with both T2 VSC-MTDC damping controllers

Operating points	*Mode 1*		*Mode 2*		*Mode 3*		*Mode 4*	
	ζ	f (Hz)	ζ	f (Hz)	ζ	f (Hz)	ζ	f (Hz)
1	**15.5%**	0.390	**12.5%**	0.564	**11.6%**	0.657	**10.3%**	0.811
2	**15.4%**	0.390	**12.1%**	0.571	**11.4%**	0.657	**10.3%**	0.814
3	**15.9%**	0.389	**12.0%**	0.566	**11.4%**	0.656	**10.4%**	0.812
4	**15.3%**	0.390	**12.1%**	0.575	**11.3%**	0.658	**10.5%**	0.816

The above analysis concludes the effectiveness and robustness of the damping controllers. Figure 6.10 shows the pole positions of the close-loop system with both damping controllers installed. It's clear to see that all of the poles that are outside the conic area have been shifted within the 10% damping ratio line, fulfilling the regional pole placement and control effort optimization control objectives. This effort is achieved by the regional pole placement control objective defined in Control Objectives section in Chapter 3. And the robustness of the controllers is ensured by the multi-model approach by introducing multiple operating conditions in the establishment of linearized system model. Sequential design of the two damping controllers minimized the coupling effect of the controller input signals and the two

controllers can provide effective damping when working individually as well as together.

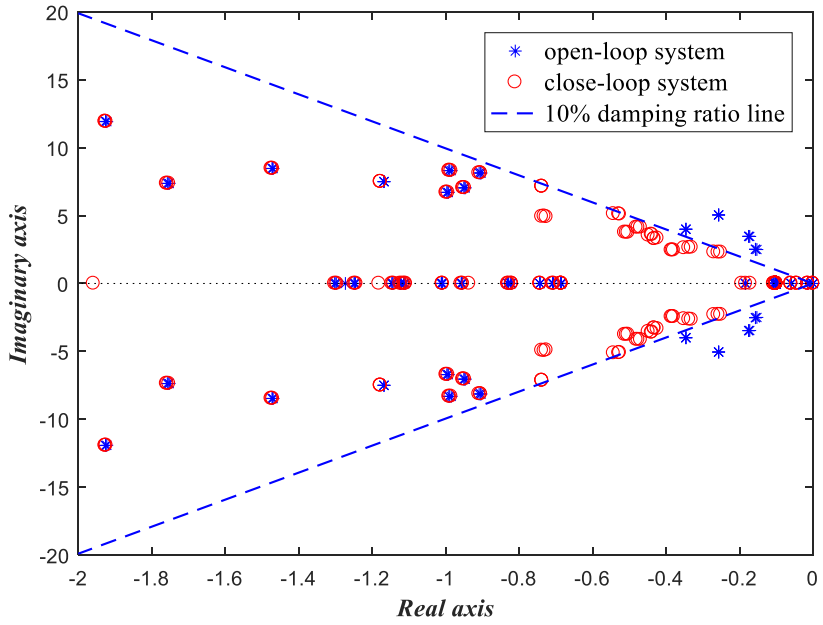

Figure 6.10 Eigenplot under all operating points

6.3.6 Real-Time Simulation Case Studies

The robust control objective is to have a damping controller that's adaptive to changes of system operating conditions and also capable of rejecting various types of disturbances. The real-time system simulation can reflect the approximate performance and behaviour of a practical power system and confirm the results obtained from linear system analysis to further validate the feasibility of the supplementary damping controllers. Besides, when designing multiple damping controllers, it's vital to stress the coordinated performance of these controllers and ensure there're no negative interactions as they are simultaneously employed in the power system. Several operating points are selected to simulate different system working conditions and the disturbances introduced to the system. To better compare the effectiveness of the damping controllers from $V_{dc}-V_{ac}$ control mode in Chapter 4 and the $P-V_{ac}$ control mode presented in this chapter, the same type of disturbances are introduced

and kept at the same severity. Detailed plots of the responses of the original system and close-loop system with both controllers implemented are shown in the following sections.

Excitation System Disturbance

The voltage reference at excitation system of G14 endures a 50ms disturbance from its original value 1.01pu to 1.03pu. Power flow on line 73 (Bus 18-50) which connects Area 5 and NYPS shows the system response after the disturbance under four operating conditions in Figure 6.11. As the damping controllers have improved the damping ratios of the poorly damped modes and the rate of decay is determined by the magnitude of the damping ratio, the oscillations observed in Figure 6.11 show shorter settling time compared to the original open-loop system without damping controllers.

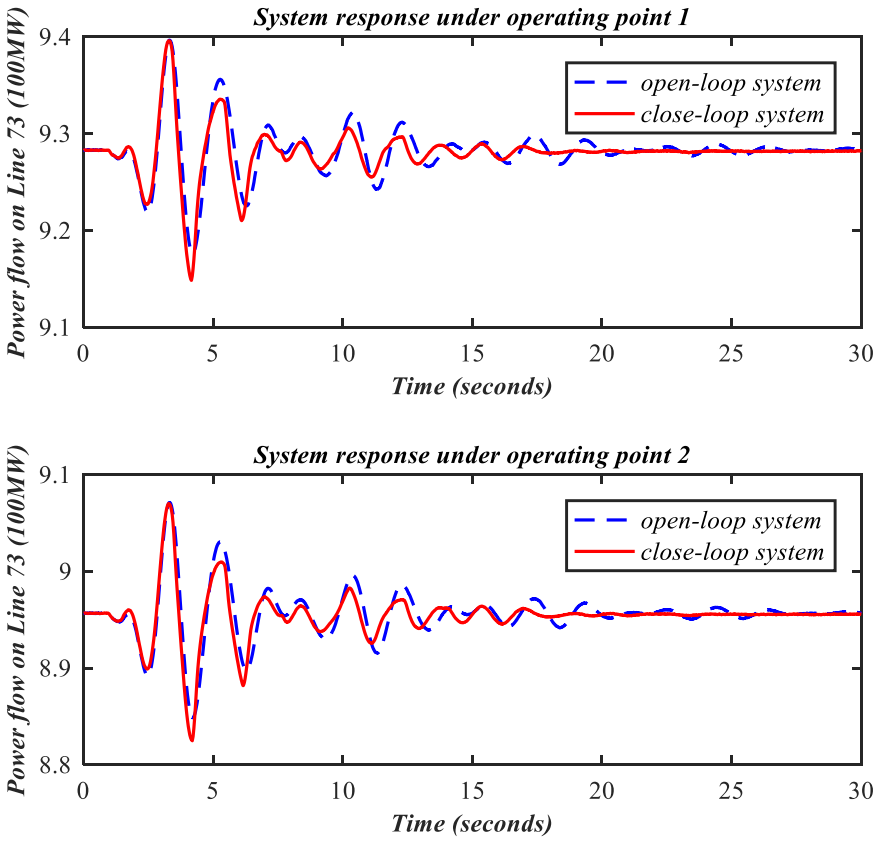

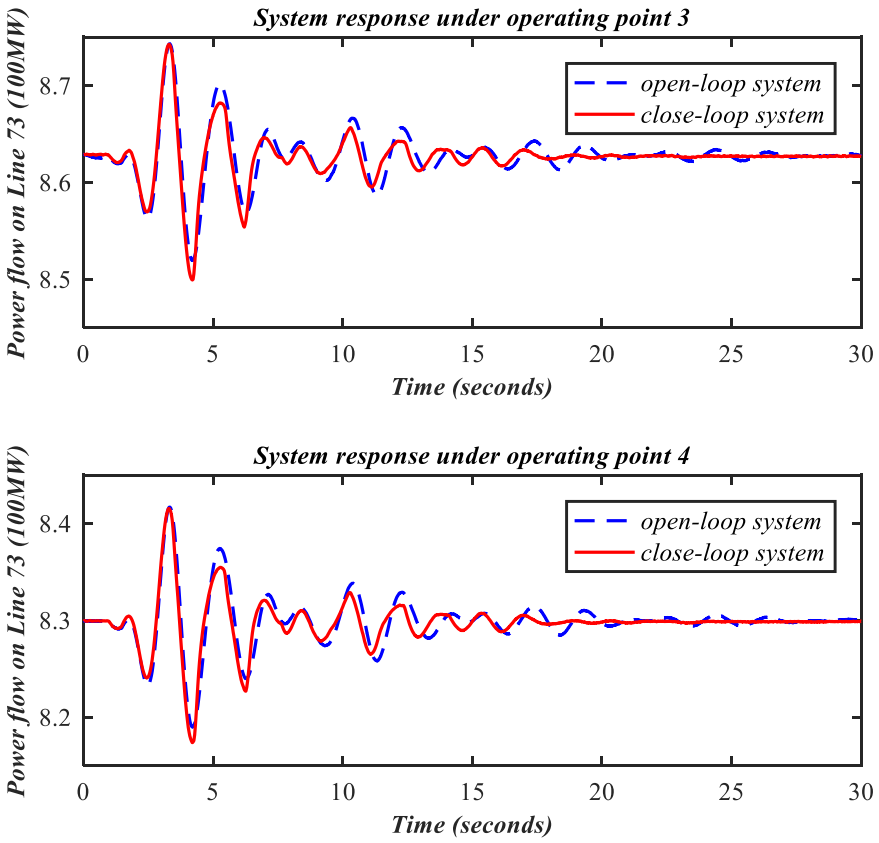

Figure 6.11 System response to excitation system disturbance on power flow of Line 73

Load Variation

A step change of Load 41 is set to shift from its original value 1000MW to 800MW at $t = 1s$ and the power flow on line 78 (Bus 41-40) reflects the system response after the disturbance. The load variation introduced in the simulation test of the controllers' effectiveness is considered as changing the system operating points which is not considered in the design stage. The merits of such examination is to ensure that the controllers can perform the supplementary damping functions and exhibit the robustness in various of system conditions.

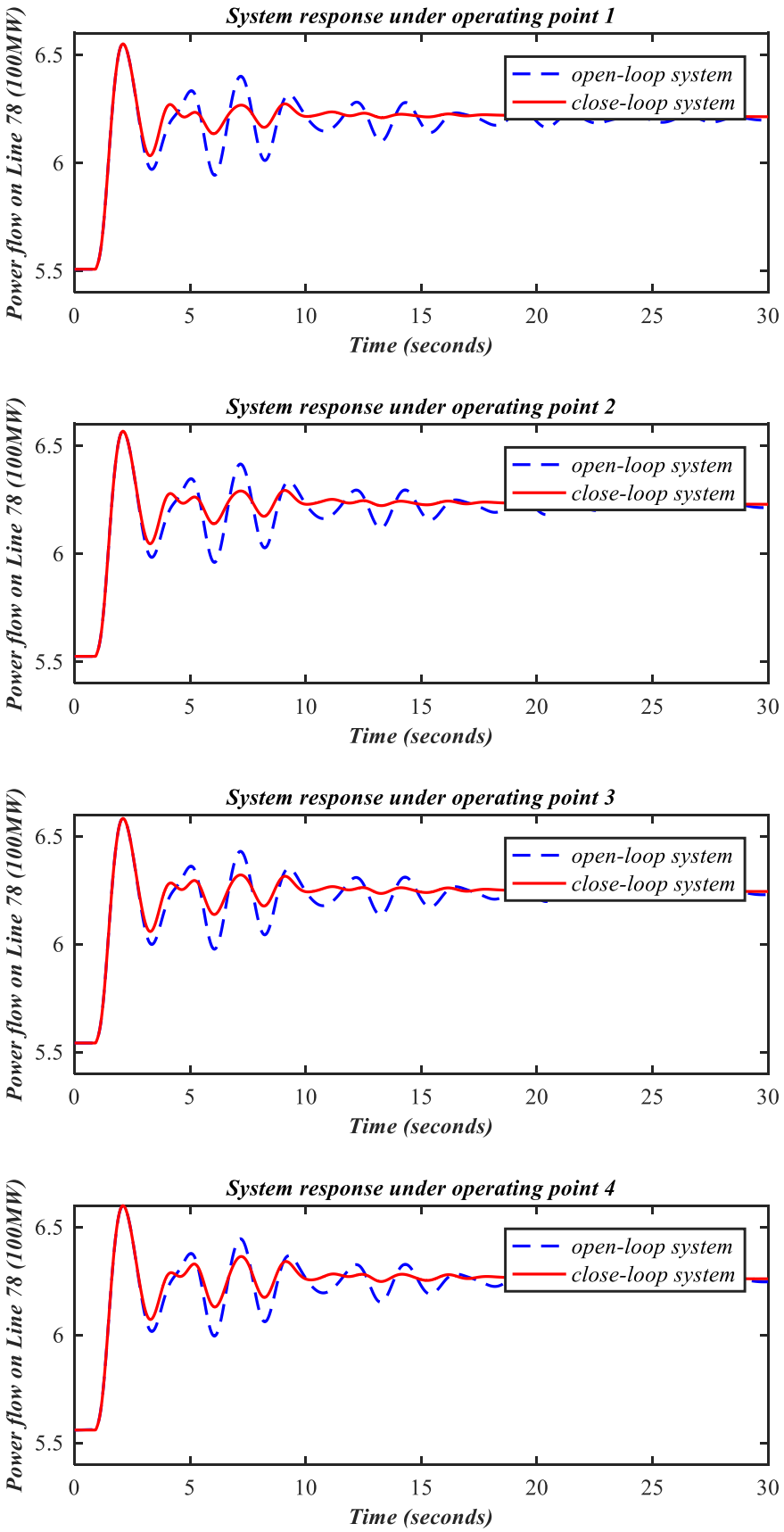

Figure 6.12 System response load variation on power flow of Line 78

Line Outage

A line outage occurs on Line 86 (Bus 27-53) which is one of the three transmission corridors connecting NYPS and NETS. The change of power flow on its neighbouring transmission line-Line 1 (Bus 54-53) is monitored to investigate the effects on damping controllers when the system experiences a major topology alteration.

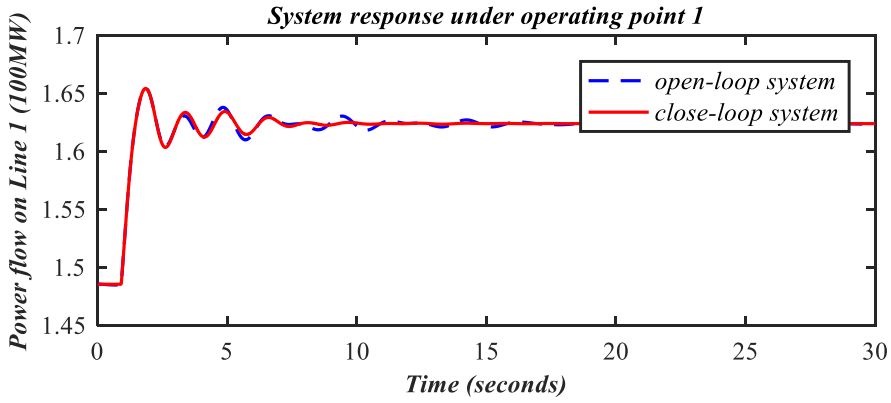

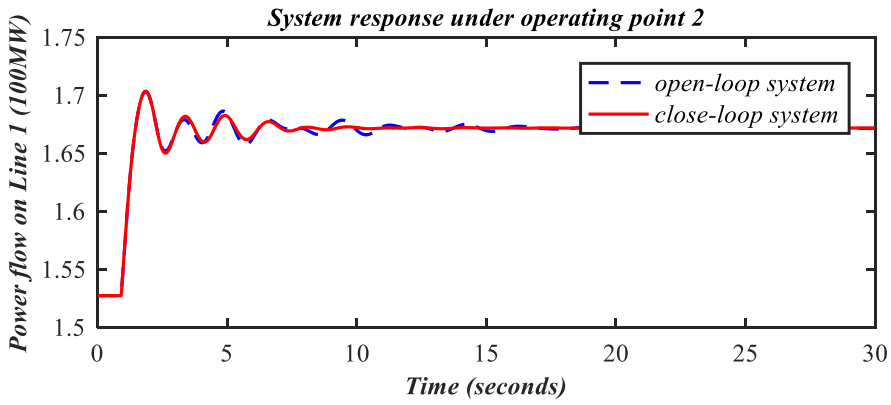

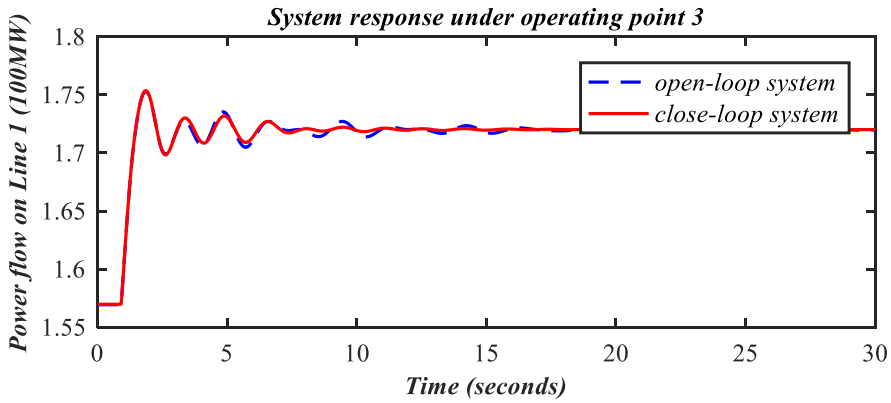

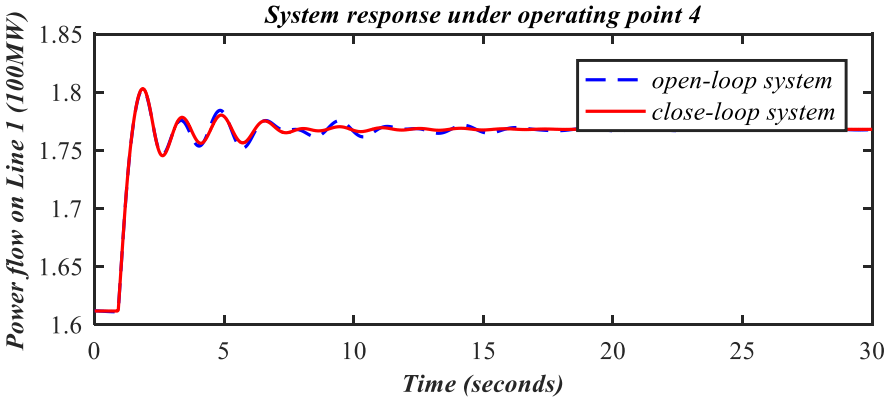

Figure 6.13 System response to line outage on power flow of Line 1

Discussion

It can be clearly observed from the simulation results in Figure 6.11, Figure 6.12 Figure 6.13 that the damping controllers designed for T2 d-axis active power control and q-axis ac voltage control prove to be effective under all the disturbances. The rate of decay in these scenarios has been increased, decreasing the settling time needed for a new point of equilibrium. In each case, the controllers are able to settle the oscillations in less than 20s, corresponding to the linear system performance from eigenvalue analysis. The results show the oscillation ripples die down faster than the open-loop system, which indicates increased damping ratio of the previously identified weakly damped modes. The supplementary damping provided by the controllers is thus tested to be effective. However, due to the differences of linear system model established in the design stage and the non-linear dynamic system used for real-time simulations, the increased level of complexity of system models brings in more uncertainties that aren't considered before, which may lead to differences of linear system performance and real-time simulations.

The robust control objective is met by various fault types and also the post-fault conditions. The multi-model approach shows its advantage in dealing with different operating conditions

and guarantees the effectiveness in a wide scope of possible scenarios. The combined control effort has covered all four weakly damped modes and the overall improvement of system damping is achieved without any negative interactions between these controllers. Besides, remote signals are adopted for each controllers and it shows good compatibility with the wide-area measurements.

6.4 Controller Assessment and Discussions

In this chapter, the d-q decoupled control modes for Terminal 2 and 3 of the VSC-MTDC differ from that presented in Chapter 3. Instead of regulating dc voltage, the d-axis active power control mode directly sets the reference of the desired transfer power from the ac grid to the converter station. As it's primarily important to maintain balanced and stable dc voltage in the dc network, the supplementary damping control action should not actively compromise the dc voltage stability in an interconnected network. Besides, from the modal residue analysis in $V_{dc} - V_{ac}$ control mode, the controllability and observability of controller output signal V_{dc} is considerably lower than that of output signal V_{ac}, thus limiting the number of controllable output candidates. However, in the case of $P - V_{ac}$ control mode, both signals from the d-q axis can provide more flexible choices for damping controller design. Both designs are tested with eigenvalue analysis on linear system models and also non-linear real-time simulations of post-fault/disturbance situations. The results have proven their feasibility and robustness in improving system damping characteristics.

6.5 Summary

This chapter has presented the coordinated robust supplementary damping controller design for Terminal 2 of VSC-MTDC with active power and ac voltage control mode. The d-q axis outer loop control configuration of the converter stations is varied from that presented in Chapter 4 and Chapter 5, where the measured and reference values of dc voltage and ac voltage are used as the input of the outer control loop as the basic control mode. The control methodology is similarly applied onto the $P-V_{ac}$ control mode with properly selected feedback signals as controller inputs. Two supplementary damping controllers are subsequently designed by solving the BMI-based multi-objective multi-model control problem. With participation factor analysis and modal residue analysis, the sensitivity of power flow on all 86 lines as feedback signal candidates to the four weakly damped modes are examined with care and an ideal feedback signal is selected when its modal residue is relatively high on the designated modes. As the $P-V_{ac}$ control mode offers more controller output candidates, the modal controllability also plays an important role in determining the optimal feedback signal. Therefore, from the results obtained by designing the d-axis active power supplementary damping controller, it's clear to see that the observable modes in active power control differ from that in ac voltage control. Besides the expanded controller outputs for more flexible design, the linear system performance analysis and real-time simulation results validated the robustness and effectiveness of these controllers under system disturbances in various operating conditions. Both designs have proven to be great improvement to the system damping and provided good solutions to the enhancement of the system small-signal stability.

CHAPTER 7 CONCLUSIONS AND FUTURE WORK

7.1 Conclusions

Renewable energy integration, high voltage power transmission over long distance and connecting power grids with different operating frequencies are some of the key features of a HVDC transmission system. Along with the transformation of electric power generation structure and the low-carbon roadmap target, stability issues arise and threaten the secure and safe operation of electrical power system with more complex interconnections. Low frequency oscillation often poses great challenge to the meshed ac/dc transmission system pushing toward its limits as demands continue to grow. Therefore, the small-signal stability enhancement through fast-controllable devices such as VSC-HVDC and FACTS is exceedingly significant to system design, planning and operation.

This thesis has discussed the coordinated and robust supplementary damping controller design for multi-terminal VSC-HVDC and FACTS devices. A model of the ac power system embedded with VSC-MTDC and FACTS device laid the foundation of further damping control design and improved the validity and practicality of the approach. BMI-based multiple control objective approach has been developed based on a multi-model incorporating several operating points. The supplementary damping control effort of these components has been fully exploited to avoid costly construction of new infrastructures. The main work and contributions presented in this thesis are listed as follows:

1. The new synthetic BMI-based multi-objective multi-model robust damping control design approach was proposed in this thesis. The robustness of the controllers is proved to be effective with the examination of system performance by introducing excitation system disturbance, load variation and line outage. The supplementary damping controllers has ameliorated the damping characteristics of the system. The coordinated control effort has allowed the controllers to function without negative interactions with one another. The robust damping control objectives are expressed as shifting the underdamped inter-area oscillatory poles into the desired region on the complex z-plane to effectively increase their damping ratio and the damping controllers is robust enough in the event of potential system modal uncertainties and additive disturbances. To meet the two criteria listed above, a BMI-based approach was introduced incorporating multiple control objectives on the multi-model system. Regional pole placement was considered to find a matrix to ensure the state matrix was stable and had all the eigenvalues in a particular region and it was formulated as a set of BMI constraints based on the generalized Lyapunov criterion. The pole placement control objective ensured the close-loop system stability and a minimum damping ratio level of the targeted modes. Besides the requirement for the damping ratio region, other control objectives needed to be considered simultaneously. The robust design should be resilient enough for system uncertainties, both structured and unstructured. Disturbance rejection was portrayed by optimizing the worst-case scenario and control effort optimization avoided over-design by minimizing the norm-bounded sensitivities, represented by H_∞ and H_2 performance. The synthesis BMI constraints were replicated regarding different linear system models as the structured uncertainties. The resulted optimization problem, with its multi-model based nature, cannot be solved directly with parameterization Lyapunov matrix, therefore a two-step method was utilized to find a common solution for the set of BMI matrices.

2. A comprehensive model with detailed dynamics of ac system components as well as VSC-MTDC and FACTS was derived for linear small-signal stability analysis. As the basis for damping control design, system model with six-order subtransient level representation of synchronous generators and electromechanical transient dynamics of VSC-MTDC and FACTS was expressed in linear time invariant state-space equations. The interface and transformation between d-q decoupled axis of ac system and converter stations were solved with parameter conversion for the integrated ac/dc system. Power injection models were used to represent the impact of HVDC and FACTS devices. Finally the linearization of the system dynamics was carried out around several independent operating points, forming a multi-model system for a robust damping control design.

3. The coordinated sequential design of multiple decentralized SISO damping controllers was investigated on the strength of the robust damping control approach. Having several SISO controller in the place of a MIMO controller for all devices can improve the reliability of the damping effort by minimizing the cross-coupling effects among the input signals. The sequential design allowed the damping controller for one device to be designed in the first stage and first loop closure was achieved. Then the first close-loop system was regarded as an open-loop system for the design of the damping controller for the next device.

4. The robust and coordinated design approach considering multiple control objectives and multi-model system optimization was applied to Terminal 2 and Terminal 3 of a three-terminal VSC-MTDC of $V_{dc} - V_{ac}$ d-q decoupled control mode. The VSC-MTDC was embedded in a benchmark small-signal stability study system: reduced equivalent 5-area 16-machine 68-bus NYPS-NETS power system. Several operating points were simultaneously considered when linear state-space representation of the system model was formed.

Eigenvalue analysis of the linear system models identified the frequency and damping ratios of the weakly damped modes and participation factor analysis was applied to evaluate the contribution of each generator state and also indicated the involved areas to individual mode. To select proper feedback signals for each controller so that it had high impact on the designated modes and low impact on other unrelated swing modes, modal residue analysis took system outputs into consideration and remarkably extended the scope of feedback signal candidates. Transmission line power with higher modal residues on particular modes was selected for each controller. As the product of modal observability and controllability, modal residue of higher magnitude meant less control efforts were needed. Since the controller outputs were selected as q-axis ac voltage control signal, the controllability was fixed and the variation of the modal residue came from different level of observability of the system outputs/controller inputs. System order reduction was carried out for each open-loop system to ease the design and reduce computational complexity. The BMI-based optimization control technique was applied onto the reduced system, so the order of the damping controllers maintained the same order as the reduced order system.

The controller performance was examined by eigenvalue analysis for each operating point to compare the damping characteristics before and after the design. A significant increase of the damping ratios from under damped state to adequately damped state. All four modes were covered by the two damping controllers, unlike a single device that might not have the necessary capacity and sensitivity to all modes. In addition to the linear analysis in MATLAB, real-time simulations in RTDS had the capability of introducing various types of disturbances and faults to check system responses in different working conditions with and without damping controllers. The results showed the effectiveness of the damping controllers in reducing the settling time of the inter-area oscillations and the improvement of system small-

signal stability.

5. The coordinated and robust damping controller design was subsequently extended to Terminal 2 of VSC-MTDC and a TCSC. Since the implementation of FACTS devices as transmission infrastructure reinforcement has been reported in many practical projects around the globe, it's wise to apply the coordinated damping control onto different types of devices for more flexible design. The advantage of employing multiple devices into the design was that it greatly expanded the controllability and observability of the controller outputs and provided more effective feedback signal candidates. To produce better comparative results, the 3-terminal VSC-MTDC was installed at the same location in the 5-area 16-machine test system as that in Chapter 4 and the location of the TCSC was determined by the mode shape analysis.

The coordinated sequential design procedure based on BMI optimization of a multi-mode system with multiple control objectives were undertaken to design the decentralized SISO damping controllers of Terminal 2 of VSC-MTDC and TCSC. Modal residue analysis evaluated the sensitivity of local and remote feedback signals to the underdamped swing modes. To ensure a coordinated design, proper selection of feedback signals was one of the key steps among the overall design procedure. The ideal feedback signal should bear high level of modal residues on the modes designated for control effort to a particular controller and considerably lower level of sensitivity for other swing modes to reduce the adverse effect between the controllers.

To assess the feasibility of the obtained supplementary damping controllers, eigenvalue analysis was carried out for the original open-loop system and two close-loop systems formed with each controller subsequently. It showed the individual and combined control effort in

improving the damping ratios of the identified swing modes. The 10% least damping ratio criterion was met for all four modes in the close-loop system with both controllers installed against the structured system uncertainties of operating condition change. Real-time simulations were carried out to further examine the effectiveness and robustness of the obtained linear damping controllers on a non-linear dynamic power system. Detailed and precise modelling platform was built in RSCAD and various types of disturbances were introduced in the system operating in steady state. Under disturbances, the damping controllers exhibited great resilience against the contingencies and were able to stabilize the system within 20 seconds.

6. The assessment of different damping controller design in respect to variation of internal d-q decoupled control modes of VSC converter stations was presented. Compared to $V_{dc}-V_{ac}$ control where dc and ac voltage references were regulated through d-q axis, $P-V_{ac}$ control modulated the active power to be transferred through converter station and grid connection point ac voltage. These two modulation signals could both be accommodated into the damping controller design, which expanded the selection of controller outputs. The $P-V_{ac}$ control formation effectively changed the state-space representation of the overall system, so the modal controllability was subject to alteration depending on the selection of controller outputs, leaving a degree of freedom when allocating target controllable modes for each controller. The eigenvalue analysis and real-time simulation results demonstrated the effectiveness of both designs with different patterns of improvement to certain modes.

7.2 Future Work

Upon the completion of the studies presented in this thesis, possible future research work can be extended in the following aspects:

1. In this study, a three-terminal radial-connected VSC-MTDC was considered in the case studies, not taking into account the meshed dc networks with more terminals. With the meshed design, it creates abundance in the dc network and raises the level of reliability as more dc links between the converter stations are constructed. As there're practical projects such as the 5-terminal VSC-HVDC system in China [29] that have been completed and put into operation, the modelling and stability analysis of a system with similar scale and complexity are essential for the ac/dc interconnected power system. Besides, reflecting on one of the main applications of VSC-MTDC-integrating wind farms into the ac grid, it's valuable to investigate the impact of wind farms on the small-signal stability of the whole network and also the design of supplementary damping controller of the wind farm converter stations.

2. The two types of d-q decoupled control modes in this thesis are $V_{dc}-V_{ac}$ control and $P-V_{ac}$ control. The supplementary damping control design can also be applied to q-axis reactive power control mode and the experiments on $V_{dc}-Q$ and $P-Q$ control modes can fully complete the investigations on the assessments of the impact of different control mode configuration on the feasibility and robustness of the damping controllers. The application of damping controller design for wind farms with $P-Q$ control mode can be less effective compared to grid connected VSC converter stations due to its capacity limitations. As mentioned in Chapter 6, the modelling of disparate internal control formulation greatly

influences the damping controller outputs and alters the modal residue characteristics of the feedback signals.

3. The converter model in this study was three-phase two-level six-pulse VSC converter and as the development of MMC becomes more popular and recognised with its lower switching losses and higher ratings than the traditional two-level and three-level VSC converters, exploiting the supplementary damping control of the MMC technology should be needed especially when integrating offshore wind farms that are prone to disturbances. Some of the advantages of MMC include high reliability and availability and with similar upper control configuration to the two-level VSC converter, it can be fruitful to develop new functionalities like small-signal stability improvement to a meshed ac/dc power system.

4. In Chapter 5 where the damping control of VSC-MTDC and a TCSC is simultaneously considered, other types of FACTS devices particularly with IGBT based apparatus can be introduced to the damping control design. Parallel connected devices, SVC and STATCOM, are built in power systems for reactive power compensation and maintaining voltage stability and have been investigated in many literatures for their supplementary damping performance with various approaches. It could be a valuable extension of the current work to these devices as they bring intricate dynamics and interactions with VSC-MTDC as well as the main power grid.

APPENDIX A

Five-area system data

A.1 Generator Parameters

	Rated MVA	X_{Li}	R_{si}	X_{di}	X'_{di}	X''_{di}	T'_{doi}	T''_{doi}	X_{qi}	X'_{qi}	X''_{qi}	T'_{qoi}	T''_{qoi}	H_i
G1	2200	0.0125	0	1.8	0.56	0.45	10.20	0.05	1.24	0.50	0.45	1.50	0.035	2.33
G2	800	0.035	0	1.8	0.43	0.31	6.56	0.05	1.72	0.37	0.31	1.50	0.035	4.95
G3	800	0.0304	0	1.8	0.38	0.32	5.70	0.05	1.71	0.36	0.32	1.50	0.035	4.96
G4	800	0.0295	0	1.8	0.30	0.24	5.69	0.05	1.77	0.27	0.24	1.50	0.035	4.16
G5	700	0.027	0	1.8	0.36	0.27	5.40	0.05	1.69	0.33	0.27	0.44	0.035	4.77
G6	900	0.0224	0	1.8	0.35	0.28	7.30	0.05	1.71	0.32	0.28	0.40	0.035	4.91
G7	800	0.0322	0	1.8	0.30	0.24	5.66	0.05	1.78	0.27	0.24	1.50	0.035	4.33
G8	800	0.028	0	1.8	0.35	0.28	6.70	0.05	1.74	0.31	0.28	0.41	0.035	3.92
G9	1000	0.0298	0	1.8	0.49	0.38	4.79	0.05	1.75	0.43	0.38	1.96	0.035	4.04
G10	1200	0.0199	0	1.8	0.49	0.43	9.37	0.05	1.22	0.48	0.43	1.50	0.035	2.91
G11	1600	0.0103	0	1.8	0.25	0.17	4.10	0.05	1.73	0.21	0.17	1.50	0.035	2.01
G12	1900	0.022	0	1.8	0.55	0.45	7.40	0.05	1.69	0.50	0.45	1.50	0.035	5.18
G13	12000	0.003	0	1.8	0.33	0.24	5.90	0.05	1.74	0.30	0.24	1.50	0.035	4.08
G14	10000	0.0017	0	1.8	0.29	0.23	4.10	0.05	1.73	0.25	0.23	1.50	0.035	3.00
G15	10000	0.0017	0	1.8	0.29	0.23	4.10	0.05	1.73	0.25	0.23	1.50	0.035	3.00
G16	11000	0.0041	0	1.8	0.36	0.28	7.80	0.05	1.69	0.30	0.28	1.50	0.035	4.45

A.2 Static AC Exciter and PSS Parameters

Static AC exciter								
	G1	G2	G3	G4	G5	G6	G7	G8

K_{Ai}	100	100	100	100	100	100	100	100
T_{Ai}	0.01	0.01	0.01	0.01	0.01	0.01	0.01	0.01
	G9	G10	G11	G12	G13	G14	G15	G16
K_{Ai}	100	100	100	100	100	100	100	100
T_{Ai}	0.01	0.01	0.01	0.01	0.01	0.01	0.01	0.01

PSS												
	G1	G2	G3	G4	G5	G6	G7	G8	G9	G10	G11	G12
K_{pss}	10	10	10	10	10	10	10	10	10	10	5	11
T_w	10	10	10	10	10	10	10	10	10	10	10	10
T_a	0.1	0.08	0.08	0.08	0.08	0.1	0.08	0.08	0.08	0.1	0.08	0.10
T_b	0.02	0.02	0.02	0.02	0.02	0.02	0.02	0.02	0.02	0.02	0.03	0.02
T_c	0.08	0.08	0.08	0.08	0.08	0.1	0.08	0.08	0.05	0.1	0.05	0.10
T_d	0.02	0.02	0.02	0.02	0.02	0.02	0.02	0.02	0.01	0.02	0.01	0.02

A.3 Transmission Line Parameters

Line index	From bus	To bus	Resistance (p.u.)	Reactance (p.u.)	line charging (p.u.)	Tap ratio
1	53	54	0.007	0.0822	0.3493	
2	53	30	0.0008	0.0074	0.48	
3	54	55	0.0013	0.0151	0.2572	
4	54	25	0.007	0.0086	0.146	
5	54	1	0	0.0181	0	1.025
6	55	56	0.0013	0.0213	0.2214	
7	55	52	0.0011	0.0133	0.2138	
8	56	57	0.0008	0.0128	0.1342	
9	56	66	0.0008	0.0129	0.1382	
10	57	58	0.0002	0.0026	0.0434	
11	57	60	0.0008	0.0112	0.1476	
12	58	59	0.0006	0.0092	0.113	
13	58	63	0.0007	0.0082	0.1389	
14	58	2	0	0.025	0	1.070
15	59	60	0.0004	0.0046	0.078	
16	60	61	0.0023	0.0363	0.3804	
17	61	30	0.0019	0.0183	0.29	

18	62	63	0.0004	0.0043	0.0729	
19	62	65	0.0004	0.0043	0.0729	
20	62	3	0	0.02	0	1.070
21	64	63	0.0016	0.0435	0	1.060
22	64	65	0.0016	0.0435	0	1.060
23	65	66	0.0009	0.0101	0.1723	
24	66	67	0.0018	0.0217	0.366	
25	67	68	0.0009	0.0094	0.171	
26	68	37	0	0	0	
27	68	19	0	0	0	
28	68	21	0.0008	0.0135	0.2548	
29	68	24	0.0003	0.0059	0.068	
30	37	52	0.0007	0.0082	0.1319	
31	37	27	0.0013	0.0173	0.3216	
32	19	20	0.0007	0.0138	0	1.060
33	19	4	0.0007	0.0142	0	1.070
34	20	5	0.0009	0.018	0	1.009
35	21	22	0.0008	0.014	0.2565	
36	22	23	0.0006	0.0096	0.1846	
37	22	6	0	0.0143	0	1.025
38	23	24	0.0022	0.035	0.361	
39	23	7	0.0005	0.0272	0	
40	25	26	0.0032	0.0323	0.531	
41	25	8	0.0006	0.0232	0	1.025
42	26	27	0.0014	0.0147	0.2396	
43	26	28	0.0043	0.0474	0.7802	
44	26	29	0.0057	0.0625	1.029	
45	28	29	0.0014	0.0151	0.249	
46	29	9	0.0008	0.0156	0	1.025
47	61	30	0.0019	0.0183	0.29	
48	61	36	0.0022	0.0196	0.34	
49	61	36	0.0022	0.0196	0.34	
50	36	17	0.0005	0.0045	0.32	
51	34	36	0.0033	0.0111	1.45	
52	35	34	0.0001	0.0074	0	0.946
53	33	34	0.0011	0.0157	0.202	
54	32	33	0.0008	0.0099	0.168	
55	30	31	0.0013	0.0187	0.333	
56	30	32	0.0024	0.0288	0.488	
57	53	31	0.0016	0.0163	0.25	
58	31	38	0.0011	0.0147	0.247	
59	33	38	0.0036	0.0444	0.693	
60	38	46	0.0022	0.0284	0.43	

61	46	49	0.0018	0.0274	0.27	
62	53	47	0.0013	0.0188	1.31	
63	47	48	0.0025	0.0268	0.4	
64	47	48	0.0025	0.0268	0.4	
65	48	40	0.002	0.022	1.28	
66	35	45	0.0007	0.0175	1.39	
67	17	43	0.0005	0.0276	0	
68	43	44	0.0001	0.0011	0	
69	44	45	0.0025	0.073	0	
70	39	44	0	0.0411	0	
71	39	45	0	0.0839	0	
72	45	51	0.0004	0.0105	0.72	
73	50	18	0.0012	0.0288	2.06	
74	50	51	0.0009	0.0221	1.62	
75	49	18	0.0076	0.1141	1.16	
76	18	42	0.004	0.06	2.25	
77	42	41	0.004	0.06	2.25	
78	41	40	0.006	0.084	3.15	
79	31	10	0	0.026	0	1.040
80	32	11	0	0.013	0	1.040
81	36	12	0	0.0075	0	1.040
82	17	13	0	0.0033	0	1.040
83	41	14	0	0.0015	0	1.000
84	42	15	0	0.0015	0	1.000
85	18	16	0	0.003	0	1.000
86	53	27	0.032	0.32	0.41	1.000

A.4 Generation Parameters

Generator index	Active power (MW)	Reactive power (Mvar)
G1	250	77.04
G2	545	192.74
G3	650	212.11
G4	632	132.33
G5	505	174.01
G6	700	256.30
G7	560	121.38
G8	540	22.40
G9	800	22.31
G10	500	-0.42
G11	1000	40.31

G12	1350	117.65
G13	4051	862.04
G14	1785	-38.27
G15	1000	68.79
G16	4000	143.55

A.5 Load Parameters

Bus index	Active power (MW)	Reactive power (Mvar)
17	6000.00	300.00
18	2470.00	123.00
20	680.00	103.00
21	174.00	115.00
23	148.00	85.00
25	224.00	47.00
26	139.00	17.00
27	281.00	76.00
28	206.00	28.00
29	284.00	27.00
39	267.00	12.60
40	65.63	23.53
41	1000.00	250.00
42	1150.00	250.00
44	267.55	4.84
45	208.00	21.00
46	150.70	28.50
47	203.12	32.59
48	241.20	2.20
49	164.00	29.00
52	158.00	30.00
53	252.70	118.56
55	322.00	2.00
56	500.00	184.00
59	234.00	84.00
60	522.00	177.00
61	104.00	125.00
64	9.00	88.00
67	320.00	153.00
68	329.00	32.00

LIST OF PUBLICATIONS

[1] Can Li, Jingchao Deng and Xiao-Ping Zhang, "Robust Coordination damping control of multi-model system with FACTS devices via sequential approach," *11th IET International Conference on AC and DC Power Transmission (ACDC 2015)*, 10-12 February 2015.

[2] Can Li, Dechao Kong, Ying Xue, Rui Guan, Andrew Taylor, Ray Zhang, Xiao-Ping Zhang, Dilan Jayaweera, "Enhancement of Power System Small-Signal Stability by Coordinated Damping Control of Multiple FACTS Devices," *The 13th. IET International Conference on. AC and DC Power Transmission (ACDC 2017)*, 14 – 16 February 2017.

[3] Can Li, Ying Xue, Rui Guan, Xiao-Ping Zhang, Dilan Jayaweera, "Coordinated Design and Application of Robust Damping Controllers for Multiple FACTS Devices to Enhance Small-Signal Stability of Large Scale Power System," *CSEE Journal of Power and Energy Systems (Abstract Submitted).*

[4] J. Deng, X.-P. Zhang and C. Li, "Coordinated Design of Multiple Robust FACTS Damping Controllers: A BMI-based Sequential Approach for Multi-Model Systems," *IEEE Transactions on Power Systems*, 2015, Digital Object Identifier: 10.1109/TPWRS.2015.2392153.

LIST OF REFERENCES

[1] Y. Qiu, C. Dai, and R. Jin, "Impact of power electronic device development on power grids," in *2016 28th International Symposium on Power Semiconductor Devices and ICs (ISPSD)*, 2016, pp. 9-14.

[2] O. E. Oni, I. E. Davidson, and K. N. I. Mbangula, "A review of LCC-HVDC and VSC-HVDC technologies and applications," in *2016 IEEE 16th International Conference on Environment and Electrical Engineering (EEEIC)*, 2016, pp. 1-7.

[3] S. K. Kerahroudi, G. A. Taylor, M. Bradley, and A. F. Zobaa, "A framework for coordinated stability control in the future GB transmission system using HVDC and power flow controller devices," in *AC and DC Power Transmission (ACDC 2012), 10th IET International Conference on*, 2012, pp. 1-6.

[4] Y. Pipelzadeh, B. Chaudhuri, T. C. Green, and R. Adapa, "Role of western HVDC link in stability of future Great Britain (GB) transmission system," in *2015 IEEE Power & Energy Society General Meeting*, 2015, pp. 1-5.

[5] T. M. L. Assis, S. Kuenzel, and B. C. Pal, "Impact of Multi-Terminal HVDC Grids on Enhancing Dynamic Power Transfer Capability," *IEEE Transactions on Power Systems*, vol. PP, no. 99, pp. 1-1, 2016.

[6] H. Huang, J. Chen, Z. Gao, C. Gao, W. Huang, and W. Zhen, "Research and development of multivariable coordinated automatic voltage control system for Guizhou power grid," in *2011 International Conference on Advanced Power System Automation and Protection*, 2011, vol. 1, pp. 677-682.

[7] P. Cruchon, S. Sabeg, Y. Coatanea, and N. Baumier-Duphil, "Power quality regulation and standardisation — The French example," in *CIRED 2005 - 18th International Conference and Exhibition on Electricity Distribution*, 2005, pp. 1-4.

[8] Y. Lei, W. Fan, and Q. Wei, "The study of the control system of Composite Power quality Regulation Device," in *2014 China International Conference on Electricity Distribution (CICED)*, 2014, pp. 232-235.

[9] S. Chen, J. Wang, and T. T. Lie, "A Conceptual View of Power Quality Regulation Using Market-Driven Mechanism," in *2006 International Conference on Power System Technology*, 2006, pp. 1-6.

[10] L. Xu, L. Yao, and C. Sasse, "Grid Integration of Large DFIG-Based Wind Farms Using VSC Transmission," *IEEE Transactions on Power Systems*, vol. 22, no. 3, pp. 976-984, 2007.

[11] R. Melicio, V. M. F. Mendes, and J. P. S. Catalao, "Electrical grid integration and power quality studies of a variable-speed wind energy conversion system," in *2009 IEEE Bucharest PowerTech*, 2009, pp. 1-6.

[12] S. Heier, "Wind Power [a review of Grid Integration of Wind Energy Conversion Systems (S. Heier; 2006); book review]," *IEEE Power and Energy Magazine,* vol. 6, no. 3, pp. 95-97, 2008.

[13] J. Sardi, N. Mithulananthan, and D. Q. Hung, "A comprehensive community energy storage planning strategy based on a cost-benefit analysis," in *2016 Australasian Universities Power Engineering Conference (AUPEC)*, 2016, pp. 1-6.

[14] B. Young, N. Ertugrul, and H. G. Chew, "Overview of optimal energy management for nanogrids (end-users with renewables and storage)," in *2016 Australasian Universities Power Engineering Conference (AUPEC)*, 2016, pp. 1-6.

[15] B. N. Abramovich, Y. A. Sychev, and A. A. Belsky, "Intelligent power system on the base of active-adaptive control and interaction between elements," in *2015 International Siberian Conference on Control and Communications (SIBCON)*, 2015, pp. 1-6.

[16] N. G. Interconnectors, "Getting more connected: The opportunity from greater electricity interconnection," 2014.

[17] Poyry, "Costs and benefits of GB interconnection," 2016.

[18] N. Grid, "Electrical Ten Year Statement (ETYS)," 2015.

[19] N. Flourentzou, V. G. Agelidis, and G. D. Demetriades, "VSC-Based HVDC Power Transmission Systems: An Overview," *IEEE Transactions on Power Electronics,* vol. 24, no. 3, pp. 592-602, 2009.

[20] S. Shah, R. Hassan, and J. Sun, "HVDC transmission system architectures and control - A review," in *2013 IEEE 14th Workshop on Control and Modeling for Power Electronics (COMPEL)*, 2013, pp. 1-8.

[21] B. V. Eeckhout, "The Economic Value of VSC-HVDC Compared to HVAC for Offshore Wind Farms," Master Thesis 2008.

[22] P. Wang, X. P. Zhang, P. F. Coventry, and R. Zhang, "Start-Up Control of an Offshore Integrated MMC Multi-Terminal HVDC System With Reduced DC Voltage," *IEEE Transactions on Power Systems,* vol. 31, no. 4, pp. 2740-2751, 2016.

[23] D. Kong, "Advanced HVDC systems for renewable energy integration and power transmission: modelling and control for power system transient stability," Dissertation 2013.

[24] R. Ruderval, J. P. Charpentier, and R. Sharma, "High Voltage Direct Current (HVDC)Transmission Systems Technology Review Paper."

[25] Y. Xue, X. P. Zhang, and C. Yang, "Elimination of Commutation Failures of LCC HVDC System with Controllable Capacitors," *IEEE Transactions on Power Systems,* vol. 31, no. 4, pp. 3289-3299, 2016.

[26] Y. Xue and X. P. Zhang, "Reactive Power and AC Voltage Control of LCC HVDC System With Controllable Capacitors," *IEEE Transactions on Power Systems,* vol. 32, no. 1, pp. 753-764, 2017.

[27] A. M. Abbas and P. W. Lehn, "PWM based VSC-HVDC systems — A review," in *2009 IEEE Power & Energy Society General Meeting*, 2009, pp. 1-9.

[28] A. M. Alsseid, D. Jovcic, and A. Starkey, "Small signal modelling and stability analysis of multiterminal VSC-HVDC," in *Power Electronics and Applications (EPE 2011), Proceedings of the 2011-14th European Conference on*, 2011, pp. 1-10.

[29] L. Chuanyue, H. Xiaobo, J. Guo, and J. Liang, "The DC grid reliability and cost evaluation with Zhoushan five-terminal HVDC case study," in *2015 50th International Universities Power Engineering Conference (UPEC)*, 2015, pp. 1-6.

[30] G. Bathurst and P. Bordignan, "Delivery of the Nan'ao multi-terminal VSC-HVDC system," in *11th IET International Conference on AC and DC Power Transmission*, 2015, pp. 1-6.

[31] H. Rao, "Architecture of Nan'ao multi-terminal VSC-HVDC system and its multi-functional control," *CSEE Journal of Power and Energy Systems,* vol. 1, no. 1, pp. 9-18, 2015.

[32] D. Ingemansson, J. D. Wheeler, N. M. MacLeod, F. Gallon, and O. Ruiton, "The South West scheme: A new HVAC and HVDC transmission system in Sweden," in *10th IET International Conference on AC and DC Power Transmission (ACDC 2012)*, 2012, pp. 1-5.

[33] A. Albakkar and O. P. Malik, "Intelligent FACTS controller based on ANFI architecture," in *2011 IEEE Power and Energy Society General Meeting*, 2011, pp. 1-7.

[34] P. Farhadi, M. Ziaei, M. Bayati, E. Ramezani, and T. Sojoudi, "Fuzzy control performance on unified power flow controller to increase power system stability," in

Power Engineering, Energy and Electrical Drives (POWERENG), 2013 Fourth International Conference on, 2013, pp. 1421-1426.

[35] E. V. Larsen, J. J. Sanchez-Gasca, and J. H. Chow, "Concepts for design of FACTS controllers to damp power swings," *IEEE Transactions on Power Systems*, vol. 10, no. 2, pp. 948-956, 1995.

[36] X.-P. Zhang, C. Rehtanz, and B. Pal, *Flexible AC Transmission Systems: Modelling and Control*. Springer, 2006.

[37] N. Grid, "National Electricity Transmission System Security and Quality of Supply Standard," 2017.

[38] ENSG, "Our Electricity Transmission Network: A Vision For 2020," The Electricity Networks Strategy Group2012.

[39] S. Bruno, G. D. Carne, and M. L. Scala, "Transmission Grid Control Through TCSC Dynamic Series Compensation," *IEEE Transactions on Power Systems*, vol. 31, no. 4, pp. 3202-3211, 2016.

[40] P. M. Aston, G. A. Taylor, and A. M. Carter, "Future wide area monitoring requirements for the GB transmission system," in *10th IET International Conference on AC and DC Power Transmission (ACDC 2012)*, 2012, pp. 1-6.

[41] B. Pal and B. Chaudhuri, *Robust Control in Power Systems*. Springer, 2005.

[42] K. Prasertwong, N. Mithulananthan, and D. Thakur, "Understanding low-frequency oscillation in power systems," *International Journal of Electrical Engineering Education*, vol. 47, no. 3, pp. 248-262, 2010.

[43] S. Golshannavaz, M. Farsadi, and D. Nazarpour, "Low frequency oscillations damping by static synchronous series compensator equipped with an auxiliary fuzzy logic controller," in *2011 19th Iranian Conference on Electrical Engineering*, 2011, pp. 1-6.

[44] S. M. H. Hosseini, J. Olamaee, and H. Samadzadeh, "Power oscillations damping by Static Var Compensator using an Adaptive Neuro-Fuzzy controller," in *Electrical and Electronics Engineering (ELECO), 2011 7th International Conference on*, 2011, pp. I-80-I-84.

[45] S. V. Khatami, H. Soleymani, and S. Afsharnia, "Adaptive neuro-fuzzy damping controller design for a power system installed with UPFC," in *IPEC, 2010 Conference Proceedings*, 2010, pp. 1046-1051.

[46] S. Wivutbudsiri, K. Hongesombut, and J. Rungrangpitayagon, "Wide-area power system control using Thyristor Controlled Series Capacitor based fuzzy logic

controller designed by observed signals," in *Electrical Engineering Congress (iEECON), 2014 International*, 2014, pp. 1-4.

[47] N. G. Hingorani and L. Gyugyi, *Understanding FACTS: Concepts and Technology of Flexible AC Transmission Systems*. Wiley, 2000.

[48] P. W. Sauer and A. Pai, *Power System Dynamics and Stability*. Prentice Hall, 1998.

[49] P. Kundur, N. J. Balu, and M. G. Lauby, *Power System Stability and Control*. McGraw-hill, 1994.

[50] S. Arabi, H. Hamadanizadeh, and B. Fardanesh, "Convertible static compensator performance studies on the NY State transmission system," in *2002 IEEE Power Engineering Society Summer Meeting*, 2002, vol. 1, p. 232

[51] H. U. Banna, A. Luna, P. Rodriguez, A. Cabrera, H. Ghorbani, and S. Ying, "Performance analysis of conventional PSS and fuzzy controller for damping power system oscillations," in *Renewable Energy Research and Application (ICRERA), 2014 International Conference on*, 2014, pp. 229-234.

[52] L. Weixing and O. Boon-Teck, "Optimal acquisition and aggregation of offshore wind power by multiterminal voltage-source HVDC," *IEEE Transactions on Power Delivery*, vol. 18, no. 1, pp. 201-206, 2003.

[53] J. Hongbo and A. Ekstrom, "Multiterminal HVDC systems in urban areas of large cities," *IEEE Transactions on Power Delivery*, vol. 13, no. 4, pp. 1278-1284, 1998.

[54] a. B. R. A. L. Xu, "Grid Connection of Large Offshore Wind Farms using HVDC," *Wind Energy*, vol. 9, no. 4, pp. 371-382, 2006.

[55] N. M. Kirby, M. J. Luckett, L. Xu, and W. Siepmann, "HVDC transmission for large offshore windfarms," in *AC-DC Power Transmission, 2001. Seventh International Conference on (Conf. Publ. No. 485)*, 2001, pp. 162-168.

[56] L. Weixing and O. Boon Teck, "Multiterminal LVDC system for optimal acquisition of power in wind-farm using induction generators," *IEEE Transactions on Power Electronics*, vol. 17, no. 4, pp. 558-563, 2002.

[57] L. Weixing and O. Boon-Teck, "Premium quality power park based on multi-terminal HVDC," *IEEE Transactions on Power Delivery*, vol. 20, no. 2, pp. 978-983, 2005.

[58] L. Xu, L. Yao, M. Bazargan, and Y. Wang, "The Role of Multiterminal HVDC for Wind Power Transmission and AC Network Support," in *2010 Asia-Pacific Power and Energy Engineering Conference*, 2010, pp. 1-4.

[59] X. Chen *et al.*, "Integrating wind farm to the grid using hybrid multi-terminal HVDC technology," in *2010 IEEE Industrial and Commercial Power Systems Technical Conference - Conference Record*, 2010, pp. 1-6.

[60] O. Kotb, M. Ghandhari, R. Eriksson, and V. K. Sood, "A study on the control of a hybrid MTDC system supplying a passive network," in *Power System Technology (POWERCON), 2014 International Conference on*, 2014, pp. 2427-2432.

[61] X. F. Fuan and C. Shijie, "Performance analysis of a hybrid multi-terminal HVDC system," in *2005 International Conference on Electrical Machines and Systems*, 2005, vol. 3, pp. 2169-2174 Vol. 3.

[62] E. Lannoye, "Renewable energy integration: practical management of variability, uncertainty, and flexibility in power grids [book reviews]," *IEEE Power and Energy Magazine*, vol. 13, no. 6, pp. 106-107, 2015.

[63] R. Grondin, I. Kamwa, L. Soulieres, J. Potvin, and R. Champagne, "An approach to PSS design for transient stability improvement through supplementary damping of the common low-frequency," *IEEE Transactions on Power Systems*, vol. 8, no. 3, pp. 954-963, 1993.

[64] C. Y. Chung, C. T. Tse, A. K. David, and A. B. Rad, "A new H∞ based PSS design using numerator – denominator perturbation representation," *Electric Power Systems Research*, vol. 52, no. 1, pp. 37-42, 10/1/ 1999.

[65] E. V. Larsen and D. A. Swann, "Applying Power System Stabilizers Part I: General Concepts," *IEEE Transactions on Power Apparatus and Systems*, vol. PAS-100, no. 6, pp. 3017-3024, 1981.

[66] Y.-N. Yu and Q.-h. Li, "Pole-placement power system stabilizers design of an unstable nine-machine system," *IEEE Transactions on Power Systems*, vol. 5, no. 2, pp. 353-358, 1990.

[67] Y. Zhang, O. P. Malik, and G. P. Chen, "Artificial neural network power system stabilizers in multi-machine power system environment," *IEEE Transactions on Energy Conversion*, vol. 10, no. 1, pp. 147-155, 1995.

[68] H. Quinot, H. Bourles, and T. Margotin, "Robust coordinated AVR+PSS for damping large scale power systems," *IEEE Transactions on Power Systems*, vol. 14, no. 4, pp. 1446-1451, 1999.

[69] M. Parsa and J. Toyoda, "Implementation of a hybrid power system stabilizer," *IEEE Transactions on Power Systems*, vol. 4, no. 4, pp. 1463-1469, 1989.

[70] C. F. Xue, X. P. Zhang, and K. R. Godfrey, "Design of STATCOM damping control with multiple operating points: a multimodel LMI approach," *IEE Proceedings: Generation, Transmission and Distribution*, vol. 153, no. 4, pp. 375-382, 2006.

[71] J. Deng and X. P. Zhang, "Robust Damping Control of Power Systems With TCSC: A Multi-Model BMI Approach With H_2 Performance," *IEEE Transactions on Power Systems*, vol. PP, no. 99, pp. 1-10, 2014.

[72] C. Li, J. Deng, and X. p. Zhang, "Robust coordination damping control of multi-model system with FACTS devices via sequential approach," in *AC and DC Power Transmission, 11th IET International Conference on*, 2015, pp. 1-6.

[73] J. Deng, C. Li, and X. P. Zhang, "Coordinated Design of Multiple Robust FACTS Damping Controllers: A BMI-Based Sequential Approach With Multi-Model Systems," *IEEE Transactions on Power Systems*, vol. 30, no. 6, pp. 3150-3159, 2015.

[74] R. Preece, A. M. Almutairi, O. Marjanovic, J. V. Milanovi, and x, "Damping of electromechanical oscillations by VSC-HVDC active power modulation with supplementary wams based modal LQG controller," in *2011 IEEE Power and Energy Society General Meeting*, 2011, pp. 1-7.

[75] L. Yong, C. Rehtanz, S. Ruberg, L. Longfu, and C. Yijia, "Wide-Area Robust Coordination Approach of HVDC and FACTS Controllers for Damping Multiple Interarea Oscillations," *IEEE Transactions on Power Delivery*, vol. 27, no. 3, pp. 1096-1105, 2012.

[76] N. R. Chaudhuri, R. Majumder, B. Chaudhuri, and J. Pan, "Stability Analysis of VSC MTDC Grids Connected to Multimachine AC Systems," *IEEE Transactions on Power Delivery*, vol. 26, no. 4, pp. 2774-2784, 2011.

[77] N. R. Chaudhuri, R. Majumder, B. Chaudhuri, J. Pan, and R. Nuqui, "Modeling and stability analysis of MTDC grids for offshore wind farms: A case study on the North Sea benchmark system," in *2011 IEEE Power and Energy Society General Meeting*, 2011, pp. 1-7.

[78] M. Amin, M. Zadeh, J. A. Suul, E. Tedeschi, M. Molinas, and O. B. Fosso, "Stability analysis of interconnected AC power systems with multi-terminal DC grids based on the Cigre DC grid test system," in *Renewable Power Generation Conference (RPG 2014), 3rd*, 2014, pp. 1-6.

[79] G. O. Kalcon, G. P. Adam, O. Anaya-Lara, S. Lo, and K. Uhlen, "Small-Signal Stability Analysis of Multi-Terminal VSC-Based DC Transmission Systems," *IEEE Transactions on Power Systems*, vol. 27, no. 4, pp. 1818-1830, 2012.

[80] S. Y. Ruan, G. J. Li, T. T. Lie, and S. S. Choi, "Improving power system damping by utilizing VSC-HVDC," in *2012 IEEE Power and Energy Society General Meeting*, 2012, pp. 1-6.

[81] S. D. Arco, J. A. Suul, and M. Molinas, "Implementation and analysis of a control scheme for damping of oscillations in VSC-based HVDC grids," in *Power Electronics and Motion Control Conference and Exposition (PEMC), 2014 16th International*, 2014, pp. 586-593.

[82] H. F. Latorre, M. Ghandhari, and L. Soder, "Use of local and remote information in POD control of a VSC-HVdc," in *PowerTech, 2009 IEEE Bucharest*, 2009, pp. 1-6.

[83] Y. Pipelzadeh, B. Chaudhuri, and T. C. Green, "Control Coordination Within a VSC HVDC Link for Power Oscillation Damping: A Robust Decentralized Approach Using Homotopy," *IEEE Transactions on Control Systems Technology*, vol. 21, no. 4, pp. 1270-1279, 2013.

[84] Y. Pipelzadeh, N. R. Chaudhuri, B. Chaudhuri, and T. C. Green, "Coordinated Control of Offshore Wind Farm and Onshore HVDC Converter for Effective Power Oscillation Damping," *IEEE Transactions on Power Systems*, vol. PP, no. 99, pp. 1-1, 2016.

[85] A. Fuchs, M. Imhof, T. Demiray, and M. Morari, "Stabilization of Large Power Systems Using VSC-HVDC and Model Predictive Control," *IEEE Transactions on Power Delivery*, vol. 29, no. 1, pp. 480-488, 2014.

[86] A. Fuchs, S. Mari, x00E, thoz, M. Larsson, and M. Morari, "Grid stabilization through VSC-HVDC using wide area measurements," in *PowerTech, 2011 IEEE Trondheim*, 2011, pp. 1-6.

[87] Z. Chen, C. Mao, D. Wang, J. Lu, and Y. Zhou, "Design and Implementation of Voltage Source Converter Excitation System to Improve Power System Stability," *IEEE Transactions on Industry Applications*, vol. 52, no. 4, pp. 2778-2788, 2016.

[88] R. Eriksson, "Coordinated Control of Multiterminal DC Grid Power Injections for Improved Rotor-Angle Stability Based on Lyapunov Theory," *IEEE Transactions on Power Delivery*, vol. 29, no. 4, pp. 1789-1797, 2014.

[89] R. Preece, J. V. Milanovic, A. M. Almutairi, and O. Marjanovic, "Probabilistic Evaluation of Damping Controller in Networks With Multiple VSC-HVDC Lines," *IEEE Transactions on Power Systems*, vol. 28, no. 1, pp. 367-376, 2013.

[90] R. Preece, J. V. Milanovi, and x, "Tuning of a Damping Controller for Multiterminal VSC-HVDC Grids Using the Probabilistic Collocation Method," *IEEE Transactions on Power Delivery*, vol. 29, no. 1, pp. 318-326, 2014.

[91] C. A. B. Karim and M. A. Zamee, "Design and analysis of pole-placement controller for dynamic stability improvement of VSC-HVDC based power system," in *Strategic Technology (IFOST), 2014 9th International Forum on*, 2014, pp. 272-275.

[92] C. Li, S. Li, F. Han, J. Shang, and E. Qiao, "A VSC-HVDC fuzzy controller to damp oscillation of AC/DC power system," in *2008 IEEE International Conference on Sustainable Energy Technologies*, 2008, pp. 816-819.

[93] S. Li, J. Zhang, G. Zhang, J. Shang, M. Zhou, and Y. Li, "Design of integrative fuzzy logic damping controller of VSC-HVDC," in *Power Systems Conference and Exposition, 2009. PSCE '09. IEEE/PES*, 2009, pp. 1-6.

[94] L. Guo-Jie, R. Siye, P. Lin, S. Yuanzhang, and L. Xiong, "A novel nonlinear control for stability improvement in HVDC light system," in *IEEE Power Engineering Society General Meeting, 2005*, 2005, pp. 837-845 Vol. 1.

[95] S. Y. Ruan, G. J. Li, and Y. Z. Sun, "Damping of power swing by the control of VSC-HVDC," in *2007 International Power Engineering Conference (IPEC 2007)*, 2007, pp. 614-618.

[96] J. Zhu, J. Liu, H. Wu, and L. Yuan, "Coordinated Damping Control of VSC-HVDC Controllers and Wide Area Controllers," in *2012 Asia-Pacific Power and Energy Engineering Conference*, 2012, pp. 1-4.

[97] Y. Pipelzadeh, N. R. Chaudhuri, B. Chaudhuri, and T. C. Green, "System stability improvement through optimal control allocation in voltage source converter-based high-voltage direct current links," *IET Generation, Transmission & Distribution*, vol. 6, no. 9, pp. 811-821, 2012.

[98] S. Y. Ruan, G. J. Li, B. T. Ooi, and Y. Z. Sun, "Power system damping from real and reactive power modulations of voltage-source-converter station," *IET Generation, Transmission & Distribution*, vol. 2, no. 3, pp. 311-320, 2008.

[99] A. Banerjee and N. R. Chaudhuri, "Robust Damping of Inter-Area Ocillations in AC-MTDC Grids using Hinf Mixed-sensitivity approach," in *2016 IEEE Power and Energy Society General Meeting (PESGM)*, 2016, pp. 1-5.

[100] F. O. Resende, M. H. Vasconcelos, and J. A. P. Lopes, "Simultaneous tuning of power system stabilizers installed in the VSC-based MTDC networks of large offshore wind farms," in *Power Systems Computation Conference (PSCC), 2014*, 2014, pp. 1-7.

[101] R. Eriksson, "A New Control Structure for Multiterminal DC Grids to Damp Interarea Oscillations," *IEEE Transactions on Power Delivery*, vol. 31, no. 3, pp. 990-998, 2016.

[102] R. L. Lee *et al.*, "Application of static VAr compensators for the dynamic performance of the Mead-Adelanto and Mead-Phoenix transmission projects," *IEEE Transactions on Power Delivery,* vol. 10, no. 1, pp. 459-466, 1995.

[103] C. Gama, "Brazilian North-South Interconnection control-application and operating experience with a TCSC," in *1999 IEEE Power Engineering Society Summer Meeting*, 1999, vol. 2, pp. 1103-1108

[104] A. M. Simoes, D. C. Savelli, P. C. Pellanda, N. Martins, and P. Apkarian, "Robust Design of a TCSC Oscillation Damping Controller in a Weak 500-kV Interconnection Considering Multiple Power Flow Scenarios and External Disturbances," *IEEE Transactions on Power Systems,* vol. 24, no. 1, pp. 226-236, 2009.

[105] L. Tain-Syh, H. Yuan-Yih, G. Tzong-Yih, L. Jiann-Tyng, and H. Chiung-Yi, "Application of thyristor-controlled series compensators to enhance oscillatory stability and transmission capability of a longitudinal power system," *IEEE Transactions on Power Systems,* vol. 14, no. 1, pp. 179-185, 1999.

[106] N. Yang, Q. Liu, and J. D. McCalley, "TCSC controller design for damping interarea oscillations," *IEEE Transactions on Power Systems,* vol. 13, no. 4, pp. 1304-1310, 1998.

[107] I. R. Petersen and R. Tempo, "Robust control of uncertain systems: Classical results and recent developments," *Automatica,* no. 0.

[108] G. Zames, "Feedback and optimal sensitivity: Model reference transformations, multiplicative seminorms, and approximate inverses," *IEEE Transactions on Automatic Control,* vol. 26, no. 2, pp. 301-320, 1981.

[109] H. Kwakernaak, "Robust control and H∞-optimization—Tutorial paper," *Automatica,* vol. 29, no. 2, pp. 255-273, 3// 1993.

[110] J. C. Doyle, K. Glover, P. P. Khargonekar, and B. A. Francis, "State-space solutions to standard H2 and Hinf control problems," *IEEE Transactions on Automatic Control,* vol. 34, no. 8, pp. 831-847, 1989.

[111] G. N. Taranto, J. K. Shiau, J. H. Chow, and H. A. Othman, "Robust decentralised design for multiple FACTS damping controllers," *IEE Proceedings: Generation, Transmission and Distribution,* vol. 144, no. 1, pp. 61-67, 1997.

[112] C. Scherer, "The Riccati inequality and state-space H∞-optimal control," *Univ. Wnrzburg, Germany,* 1990.

[113] B. Pal, "Robust damping of interarea oscillations with unified power-flow controller," *IEE Proceedings: Generation, Transmission and Distribution,* vol. 149, no. 6, pp. 733-738, 2002.

[114] B. Chaudhuri, B. C. Pal, A. C. Zolotas, I. M. Jaimoukha, and T. C. Green, "Mixed-sensitivity approach to Hinf control of power system oscillations employing multiple FACTS devices," *IEEE Transactions on Power Systems,* vol. 18, no. 3, pp. 1149-1156, 2003.

[115] B. Chaudhuri and B. C. Pal, "Robust damping of multiple swing modes employing global stabilizing signals with a TCSC," *IEEE Transactions on Power Systems,* vol. 19, no. 1, pp. 499-506, 2004.

[116] R. Majumder, B. C. Pal, C. Dufour, and P. Korba, "Design and real-time implementation of robust FACTS controller for damping inter-area oscillation," *IEEE Transactions on Power Systems,* vol. 21, no. 2, pp. 809-816, 2006.

[117] M. M. Farsangi, Y. H. Song, and M. Tan, "Multi-objective design of damping controllers of FACTS devices via mixed H2/H∞ with regional pole placement," *International Journal of Electrical Power & Energy Systems,* vol. 25, no. 5, pp. 339-346, 2003.

[118] D. McFarlane and K. Glover, "A loop-shaping design procedure using Hinf synthesis," *IEEE Transactions on Automatic Control,* vol. 37, no. 6, pp. 759-769, 1992.

[119] Z. Chuanjiang, M. Khammash, V. Vittal, and Q. Wenzheng, "Robust power system stabilizer design using Hinf loop shaping approach," *IEEE Transactions on Power Systems,* vol. 18, no. 2, pp. 810-818, 2003.

[120] R. Majumder, B. Chaudhuri, H. El-Zobaidi, B. C. Pal, and I. M. Jaimoukha, "LMI approach to normalised Hinf loop-shaping design of power system damping controllers," *IEE Proceedings: Generation, Transmission and Distribution,* vol. 152, no. 6, pp. 952-960, 2005.

[121] J. Kennedy and R. Eberhart, "Particle swarm optimization," in *1995 IEEE International Conference on Neural Networks,* 1995, vol. 4, pp. 1942-1948.

[122] B. Chaudhuri, S. Ray, and R. Majumder, "Robust low-order controller design for multi-modal power oscillation damping using flexible AC transmission systems devices," *IET Generation, Transmission & Distribution,* vol. 3, no. 5, pp. 448-459, 2009.

[123] D. P. Ke and C. Y. Chung, "An Inter-Area Mode Oriented Pole-Shifting Method With Coordination of Control Efforts for Robust Tuning of Power Oscillation Damping

Controllers," *IEEE Transactions on Power Systems,* vol. 27, no. 3, pp. 1422-1432, 2012.

[124] A. L. B. Do Bomfim, G. N. Taranto, and D. M. Falcao, "Simultaneous tuning of power system damping controllers using genetic algorithms," *IEEE Transactions on Power Systems,* vol. 15, no. 1, pp. 163-169, 2000.

[125] I. Kamwa, G. Trudel, and L. Gerin-lajoie, "Robust design and coordination of multiple damping controllers using nonlinear constrained optimization," *IEEE Transactions on Power Systems,* vol. 15, no. 3, pp. 1084-1092, 2000.

[126] Z. Wang, C. Y. Chung, K. P. Wong, and C. T. Tse, "Robust power system stabiliser design under multi-operating conditions using differential evolution," *IET Generation, Transmission & Distribution,* vol. 2, no. 5, pp. 690-700, 2008.

[127] R. A. Jabr, B. C. Pal, and N. Martins, "A Sequential Conic Programming Approach for the Coordinated and Robust Design of Power System Stabilizers," *IEEE Transactions on Power Systems,* vol. 25, no. 3, pp. 1627-1637, 2010.

[128] C. Li-Jun and I. Erlich, "Simultaneous coordinated tuning of PSS and FACTS damping controllers in large power systems," *IEEE Transactions on Power Systems,* vol. 20, no. 1, pp. 294-300, 2005.

[129] R. A. Ramos, L. F. C. Alberto, and N. G. Bretas, "A new methodology for the coordinated design of robust decentralized power system damping controllers," *IEEE Transactions on Power Systems,* vol. 19, no. 1, pp. 444-454, 2004.

[130] B. R. Barmish and E. Jury, "New tools for robustness of linear systems," *IEEE Transactions on Automatic Control,* vol. 39, no. 12, pp. 2525-2525, 1994.

[131] B. R. Barmish, "A generalization of Kharitonov's four-polynomial concept for robust stability problems with linearly dependent coefficient perturbations," *IEEE Transactions on Automatic Control,* vol. 34, no. 2, pp. 157-165, 1989.

[132] D. D. Simfukwe, B. C. Pal, R. A. Jabr, and N. Martins, "Robust and low-order design of flexible ac transmission systems and power system stabilisers for oscillation damping," *IET Generation, Transmission & Distribution,* vol. 6, no. 5, pp. 445-452, 2012.

[133] I. Kamwa, R. Grondin, and Y. Hebert, "Wide-area measurement based stabilizing control of large power systems-a decentralized/hierarchical approach," *Power Systems, IEEE Transactions on,* vol. 16, no. 1, pp. 136-153, 2001.

[134] G. T. Heydt, C. C. Liu, A. G. Phadke, and V. Vittal, "Solution for the crisis in electric power supply," *Computer Applications in Power, IEEE,* vol. 14, no. 3, pp. 22-30, 2001.

[135] A. C. Zolotas, B. Chaudhuri, I. M. Jaimoukha, and P. Korba, "A Study on LQG/LTR Control for Damping Inter-Area Oscillations in Power Systems," *IEEE Transactions on Control Systems Technology*, vol. 15, no. 1, pp. 151-160, 2007.

[136] Z. Xiao-Ping, "Multiterminal voltage-sourced converter-based HVDC models for power flow analysis," *IEEE Transactions on Power Systems*, vol. 19, no. 4, pp. 1877-1884, 2004.

[137] J. D. Rojas, D. Valverde-Méndez, V. M. Alfaro, O. Arrieta, and R. Vilanova, "Comparison of multi-objective optimization methods for PI controllers tuning," in *2015 IEEE 20th Conference on Emerging Technologies & Factory Automation (ETFA)*, 2015, pp. 1-8.

[138] C. H. Liu and Y. Y. Hsu, "Design of a Self-Tuning PI Controller for a STATCOM Using Particle Swarm Optimization," *IEEE Transactions on Industrial Electronics*, vol. 57, no. 2, pp. 702-715, 2010.

[139] Z. Yan, Y. Xue, and X. P. Zhang, "PI parameters determination in dq decoupling control of VSC terminals," in *13th IET International Conference on AC and DC Power Transmission (ACDC 2017)*, 2017, pp. 1-5.

[140] W. H. Schilders, van der Vorst, Henk A., Rommes, Joost (Eds.), "Model Order Reduction: Theory, Research Aspects and Applications."

[141] M. Chilali and P. Gahinet, "H∞ design with pole placement constraints: an LMI approach," *IEEE Transactions on Automatic Control*, vol. 41, no. 3, pp. 358-367, 1996.

[142] S. Kanev, C. Scherer, M. Verhaegen, and B. De Schutter, "Robust output-feedback controller design via local BMI optimization," *Automatica*, vol. 40, no. 7, pp. 1115-1127, 2004.

[143] M. Klein, G. J. Rogers, S. Moorty, and P. Kundur, "Analytical investigation of factors influencing power system stabilizers performance," *IEEE Transactions on Energy Conversion*, vol. 7, no. 3, pp. 382-390, 1992.

[144] M. Safonov and R. Chiang, "A Schur method for balanced-truncation model reduction," *IEEE Transactions on Automatic Control*, vol. 34, no. 7, pp. 729-733, 1989.

[145] R. C. Dorf, *Modern control systems*. Addison-Wesley Longman Publishing Co., Inc., 1995.

[146] *Real-time Digital Simulator*. Available: http://www.rtds.com/index/index.html

[147] R. Kuffel, J. Giesbrecht, T. Maguire, R. P. Wierckx, and P. McLaren, "RTDS-a fully digital power system simulator operating in real time," in *1995 IEEE Conference Proceedings on Communications, Power, and Computing, WESCANEX 95*, 1995, vol. 2, pp. 300-305 vol.2.

[148] C. Canizares *et al.*, "Benchmark Models for the Analysis and Control of Small-Signal Oscillatory Dynamics in Power Systems," *IEEE Transactions on Power Systems,* vol. PP, no. 99, pp. 1-1, 2016.

[149] L. P. Kunjumuhammed and B. C. Pal, "Selection of Feedback Signals for Controlling Dynamics in Future Power Transmission Networks," *IEEE Transactions on Smart Grid,* vol. 6, no. 3, pp. 1493-1501, 2015.

[150] H. F. Wang, "Selection of robust installing locations and feedback signals of FACTS-based stabilizers in multi-machine power systems," *IEEE Transactions on Power Systems,* vol. 14, no. 2, pp. 569-574, 1999.